行政院國家科學委員會專題研究計畫　成果報告

半導體異質結構一致和非一致自旋相依傳輸(3/3)

計畫類別： 個別型計畫
計畫編號： NSC93-2112-M-009-008-
執行期間： 93 年 08 月 01 日至 94 年 07 月 31 日
執行單位： 國立交通大學電子工程學系暨電子研究所

計畫主持人： 霍斯科
共同主持人： 李建平

報告類型： 完整報告

處理方式： 本計畫可公開查詢

中　華　民　國 94 年 10 月 24 日

摘要 (Abstract)

英文

Studies of spin-dependent confinement and transport phenomena in semiconductor nano-structures have been progressing significantly since spintronics became a focus of recent interest. The most promising application of spintronic devices can be found in the potential applications for quantum information processing, and, in particular, in the design of a spin-based quantum computer. For the recent years in our pioneering works we proposed to deploy the spin-orbit interaction in conventional non-magnetic III-V semiconductor nano-structures to build elements of spintronic devices. In III-V and II-VI semiconductors the spin-orbit interaction lifts the conduction state spin-degeneracy and has been used successfully to interpret experimental results in various semiconductor nano-structures: quantum wells, wires, nano-rings, and dots. The semiconductor approach has the advantage of being compatible with conventional semiconductor technology.

This report summarizes the major results obtained from the program of the “Coherent and non-coherent spin-dependent transport in semiconductor heterostructures” project. Three subjects are discussed in the following including: spin-dependent coherent transmission probability and tunneling time for all-semiconductor symmetric double barrier structures; spin-dependent scattering and the spin-dependent Hall effect in three-dimensional random arrays of small semiconductor quantum dots and from impurities in two-dimensional channels; magnetic properties of semiconductor multi-electron quantum dots and rings. In addition we investigated magneto-optical properties of semiconductor nano-structured meta-materials built from non-magnetic InAs/GaAs nano-rings. Those systems can exhibit simultaneously negative effective permittivity and permeability over a certain optical frequency range – the main condition for materials with negative refractive index.

Several publications were performed based on those results.

Keywords: Spintronics, Spin, Nanostructures, Semiconductor

中文

因為自旋電子學近來備受矚目，所以在半導體奈米結構中，電子自旋的侷限效應與傳輸現象的研究有很突破的進展。自旋電子元件中最具潛力與可行性的應用當屬量子資訊方面，特別是在自旋量子電腦的設計。近年來我們進行很多具有首創性的研究，研究傳統非磁性 III-V 族半導體奈米結構的自旋軌域的交互作用，以建立自旋電子元件的基本要素。在 III-V 族和 II-VI 族半導體中，自旋軌域的交互作用提升了傳導帶自旋能階簡併，這個結果成功的解釋了各種不同半導體奈米結構的實驗結果，例如：量子井、量子線、量子環與量子點。而且這個半導體理論具有可以跟傳統半導體科技相容的優點。

這份報告總結的主要結論都是從"半導體異質結構的同調與非同調自旋相依傳輸"的研究計劃歸納出來的。我們主要探討三個主題：在各種半導體中，對稱雙能障結構的自旋相依同調傳輸的機率與穿遂時間；分別探討三維隨機排列的半導體量子點與二維通道內的雜質，造成的自旋相依散射與自旋相依霍爾效應；具有多電子的半導體量子點與量子環，其磁性特性。另外，我們也研究由非磁性的砷化銦/砷化鎵奈米環組成的奈米結構半導體的磁性與光性。這個系統可以在一個特定的光之頻率範圍內，同時表現出負的有效介電常數與導磁率特性 (主要的條件是材料本身必須具有負的折射率)。

我們的研究成果已經有數個發表在期刊上。

關鍵詞：**自旋電子 學**；**自旋**；**奈米結構**；**半導體**

Contents

1. Introduction

In order to utilize spin in semiconductor nano-structures, one needs to be able to polarize, inject, transport, manipulate, store, and detect spin. That can make use in modern quantum information, quantum cryptography, and quantum computing.

All of the needs necessarily require comprehensive quantitative understanding of the physical processes controlling the electron spin in quantum semiconductor nano-structures. To manufacture spintronics applications a large number of investigations need to be performed:

- explore transport, optical and magnetic properties of semiconductor nano-structures with promising spin dependent properties;
- understand and control spin dependent interface effects and spin dependent transport across semiconductor interface and in multiple quantum well structures;
- explore issues in controlling spin optical, magnetic, magneto-optical, and magneto-transport effects in quantum dots, arrays of quantum dots, antidotes and quantum wells and wires as well.

Structures of interest

Semiconductor quantum nano-structures (quantum wells, dots, antidots, and rings) on the base of semiconductors with strong electron spin-orbit interaction InAs/GaAs, InAs/Si, InSb/(GaAs, InAs, GaSb, InP).

Phenomena, properties and characteristics of semiconductor quantum structures under investigation

1. Time dependent characteristics of tunneling and transport with quantum spin states within natural frequency scale given by spin splitting (GHz-THz). Spin dependent resonant tunneling and spin filtering in multi-layer semiconductor structures.
2. Spin dependent transport and characteristics of electron scattering in antidot arrays and impurities in semiconductor quantum wells.
3. Optical (infrared absorption and magneto photoluminescence) characteristics of semiconductor quantum nano-structures (quantum wells, dots, and rings).
4. Spin dependent transport and characteristics to implement the “spin field-effect transistor” or the “spin high electron mobility transistor”.
5. Magnetic characteristics (magnetization of single and multi-electron quantum dots and rings).
6. Magnetic and magneto-optics characteristics of quantum dot’s and ring’s arrays.

Theoretical problems must be solved

1. Spin dependent electron transport in semiconductor quantum nano-structures:
    - spin dependent tunnel and spin dependent quasi ballistic electron transport in multi-barrier structures;
    - spin dependent electron transport in arrays of quantum dots (antidots) with external electric and magnetic fields, and different mechanisms of the electron scattering in semiconductor quantum wells.
2. Spin dependent electron confinement in small semiconductor quantum dots and nano-rings:
    - electron spin state characteristics for various types of small quantum dots and rings of semiconductors with strong spin-orbit interaction;
    - electron spin states in small semiconductor quantum dots and rings in external magnetic fields;
    - magnetization of small magnetic semiconductor quantum dots and rings.

3. Spin dependent optical and magnetic phenomena in semiconductor quantum rings:
    - Magneto-optical and luminescence spectra of semiconductor quantum nano-rings;
    - effects of trapped magnetic flux interaction with electron spin in small quantum rings;
    - optical characteristics of two and three dimensional arrays of them.

Exactly like it is mentioned above we performed the program of theoretical research, which results we present in this report.

2. Spin-dependent coherent transmission in all-semiconductor symmetric double barrier structures

ELSEVIER

Superlattices and Microstructures 34 (2003) 547–552

Superlattices
and Microstructures

www.elsevier.com/locate/superlattices

Electron spin filtering in all-semiconductor tunneling structures

Leo Yu*, H.C. Huang, O. Voskoboynikov

National Chiao Tung University, 1001 Ta Hsueh Rd., Hsinchu 300, Taiwan, ROC

Available online 12 May 2004

Abstract

In this work we briefly review the present day perspectives for exploiting conventional non-magnetic semiconductor nano-technology to design high speed spin-filter devices. In recent theoretical investigations a high spin polarization has been predicted for the ballistic tunneling current in semiconductor single- and double-barrier asymmetric tunnel structures of III–V semiconductors with strong Rashba spin–orbit coupling. We show in this paper that the polarization in the tunneling can probability be sufficiently increased for producing realistic single-barrier structures by including of the Dresselhaus term into consideration.

PACS: 73.23.-b; 73.63.-b

Keywords: Nano-structures; Spin–orbit interaction; Tunneling

Recently a new branch of electronics, so-called spintronics, became a focus of interest (see for instance [1, 2]). For this reason the electronic spin polarization (filtering) in solid-state systems has attracted considerable attention. Many possible structures were investigated for achieving high level electronic spin filtering and injection. Most of them consist of magnetic material elements (see [1–5] for references). But in principle one can use the all-semiconductor approach utilizing multi-layered nano-systems to generate and detect the electron spin polarization [6]. The semiconductor approach has the advantage of being compatible with conventional semiconductor technology. From this point of view the most important property of semiconductors to be utilized in all semiconductor

* Corresponding address: Department of Electronics Engineering and Institute of Electronics, National Chiao Tung University, 1001 Ta Hsueh Rd., Hsinchu 300, Taiwan, ROC. Tel.: +886-03-5712121x83415; fax: +886-03-5724361.
E-mail address: leoyu.ee89@nctu.edu.tw (L. Yu).

0749-6036/$ - see front matter © 2004 Published by Elsevier Ltd
doi:10.1016/j.spmi.2004.03.056

spintronic nano-devices is the spin–orbit (SO) interaction [7–9]. The control of spin in semiconductors together with modern semiconductor technology can guarantee the future of the spintronics and result in valuable commercial interest.

The SO interaction comes from a relativistic correction to the electronic non-relativistic Hamiltonian and manifests the lack of inversion symmetry in semiconductor compounds. In the bulk of III–V and II–VI semiconductor materials the SO interaction lifts the spin degeneracy of the conduction states in the center of the Brillouin zone [7]. This part of the SO interaction is called of bulk inversion asymmetry (BIA) type and it is represented by the effective Dresselhaus Hamiltonian. Macroscopic effective electric fields in semiconductor nano-structures result in structural inversion asymmetry (SIA) and a linear (in the electron wavevector $\mathbf{k}$) term (or of Rashba type) of the SO interaction [8, 9]. Ample experimental evidence in recent years shows that the SO interaction becomes easy to detect in semiconductor heterostructures by measurements of the Shubnikov–de Haas oscillations [10], weak antilocalization [11], and electronic Raman scattering [12].

It has been found out recently that the Rashba spin–orbit coupling in conventional III–V semiconductor tunnel barrier structures can lead to the spin-dependent tunneling phenomenon [13–15]. The spin-polarization ratio in tunneling structures is defined as

$$P(E_z, \mathbf{k}) = \frac{T_+(E_z, \mathbf{k}) - T_-(E_z, \mathbf{k})}{T_+(E_z, \mathbf{k}) + T_-(E_z, \mathbf{k})}, \tag{1}$$

where $T_\pm(E_z, \mathbf{k})$ is the spin-up (spin-down) tunneling probability and E_z is the part of the electronic energy which corresponds to the motion perpendicular to the barrier (z-axis), and $\mathbf{k} = (k_x, k_y)$ is the component of the electronic wavevector parallel to the barrier. In resonant tunnel heterostructures (due to the strict resonant tunnel conditions) the spin-dependent asymmetry in the tunneling probability can gain a higher level. In symmetric structures with the exceptional Rashba interaction included we need to apply an external perpendicular electric field F_z to generate asymmetry of the tunneling probability. At the same time in asymmetric structures a difference between T_+ and T_- exists with zero external electric field and it is possible to reverse the polarization by means of adjusting the strength of the external electric field F_z.

The calculation results show considerable influence of the SO interaction on the tunneling transmission characteristics at zero external magnetic field and the dependence can be controlled by an external electric field. In addition the SO interaction can provide a big difference (a few orders of magnitude) between tunneling times of electrons of different spin polarizations without additional magnetic fields [16]. The polarization of the electronic current can gain about 40% for moderate electric fields.

The Dresselhaus coupling term can also lead to a dependence of the tunneling probability on the spin orientation even for symmetrical barrier structures [17]. Results from different authors suggest that the spin–orbit filtering for all-semiconductor tunnel devices can reach almost 100% polarization for more sophisticated designs of the devices [18, 19]. Recent investigations have shown that completely planar or linear designs of the tunnel transistors can be achieved with present day technology [20]. Such a design should have much better efficiency in spin filtering.

In this paper we further investigate the spin-dependent tunneling probability for realistic symmetric tunneling structures, with consideration of both the Rashba and

Dresselhaus couplings. Our calculation is performed for realistic semiconductor structures on the basis of the effective electronic one-band Hamiltonian, energy- and position-dependent electron effective mass approximation, and spin-dependent Ben Daniel–Duke boundary conditions. We consider the spin-dependent Hamiltonian for a single-barrier structure, which can be written as follows [13, 17, 21, 22]:

$$\hat{H} = \hat{H}_0 + \hat{H}_D + \hat{H}_R, \tag{2}$$

where

$$\hat{H}_0 = -\frac{\hbar^2}{2}\frac{\mathrm{d}}{\mathrm{d}z}\frac{1}{m(E,z)}\frac{\mathrm{d}}{\mathrm{d}z} + \frac{\hbar^2 k^2}{2m(E,z)} + E_c(z) + V(z),$$

and

$$\frac{1}{m(E,z)} = \frac{2P^2}{3\hbar^2}\left[\frac{2}{E - E_c(z) + E_g(z) + V(z)} + \frac{1}{E - E_c(z) + E_g(z) + \Delta(z) + V(z)}\right],$$

represents the energy- and position-dependent reciprocal effective mass. $E_c(z)$, $E_g(z)$, and $\Delta(z)$ stand for the position-dependent conduction-band edge, the band gap, and the spin–orbit splitting in the valence band, $V(z) = -eF_z z$ is the potential energy due to the external electric field in the barrier region (e is the electronic charge), and P is the momentum matrix element. In Eq. (2) the Rashba and Dresselhaus terms (when the kinetic energy of electrons is substantially smaller than the barrier height V_0) are correspondingly [13, 17, 21]

$$\hat{H}_R = (\hat{\sigma}_x k_y - \hat{\sigma}_y k_x) \cdot \frac{\mathrm{d}\beta(E,z)}{\mathrm{d}z},$$

and

$$\hat{H}_D = \gamma(\hat{\sigma}_x k_x - \hat{\sigma}_y k_y)\frac{\mathrm{d}^2}{\mathrm{d}z^2},$$

where $\hat{\boldsymbol{\sigma}} = \{\hat{\sigma}_x, \hat{\sigma}_y, \hat{\sigma}_z\}$ is the vector of the Pauli matrices,

$$\beta(E,z) = \frac{P^2}{3}\left[\frac{1}{E - E_c(z) + E_g(z) + V(z)} - \frac{1}{E - E_c(z) + E_g(z) + \Delta(z) + V(z)}\right]$$

is the Rashba spin-coupling parameter, and γ is a material constant.

The wavefunction of the electron can be written in the form

$$\Phi_{\pm}(x,y,z) = \chi_{\pm}\Psi_{\pm}(z)\exp[i(k_x x + k_y y)]$$

where $\chi_{\pm}$ are spinors, which correspond to electron spin states of opposite spin directions, and $\Psi_{\pm}$ satisfies the spin-dependent Ben Daniel–Duke boundary conditions in each

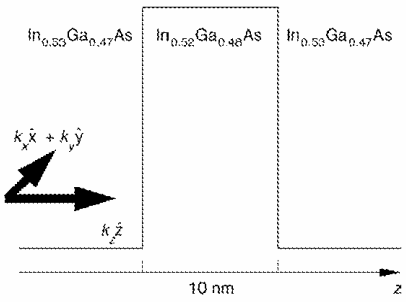

Fig. 1. A sketch of a realistic $In_{0.53}Ga_{0.47}As/In_{0.52}Al_{0.48}As/In_{0.53}Ga_{0.47}As$ symmetric single-barrier structure of width 10 nm.

interface of the structure:

$$\begin{cases} \Psi_{\pm}(z) \\ \left\{\left[\frac{\hbar^2}{2m} + \gamma(\hat{\sigma}_x k_x - \hat{\sigma}_y k_y)\right]\frac{\mathrm{d}}{\mathrm{d}z} + \beta(\hat{\sigma}_x k_y - \hat{\sigma}_y k_x)\right\} \Psi_{\pm}(z) \\ \quad \Rightarrow \text{continuous at the boundary.} \end{cases}$$

The standard solutions of the Schrödinger equation with the Hamiltonian (2) and the spin-dependent boundary conditions above allow us to calculate the spin-dependent tunneling probability and polarization ratio (1) for symmetric single-barrier tunneling structures [13, 23], as we demonstrate in Fig. 1. In Fig. 2 we present results of our calculation for a realistic $In_{0.53}Ga_{0.47}As/In_{0.52}Al_{0.48}As/In_{0.53}Ga_{0.47}As$ symmetric single-barrier structure of width 10 nm. The band structure parameters are chosen as follows: for $In_{0.53}Ga_{0.47}As$ $E_g = 0.937$ eV, $\Delta = 0.361$ eV, $m^*/m_0 = 0.04368$, $\gamma = 76.89$ eV A^3; for $In_{0.52}Al_{0.48}As$ $E_g = 1.289$ eV, $\Delta = 0.332$ eV, $m^*/m_0 = 0.0840$, $\gamma = 73.36$ eV A^3; band offset $V_0 = 0.278$ eV [24, 25]. Parameters for compound materials are calculated according to a linear interpolation formula. The polarization is quite significant even without an electric field (symmetric structure, only the Dresselhaus coupling is included). An additional possibility for manipulating the polarization ratio arises when an external electric field is applied (the Rashba term included). Fig. 2(b) and (c) show how one can manipulate with the polarization by means of the field.

To briefly conclude, in this paper we demonstrate that the transmission tunneling probability for a realistic symmetric single-barrier structure can gain a well-recognizable spin dependence for a not too large in-plane wavevector of the tunneling electrons. In addition, one can control the magnitude of the polarization ratio by means of an external electric field. The effect described can provide a basis for more advanced spin-filtering techniques at zero magnetic field. Our calculation results show that the interplay between the BIA and SIA interactions makes the spin-filtering processes richer and more controllable.

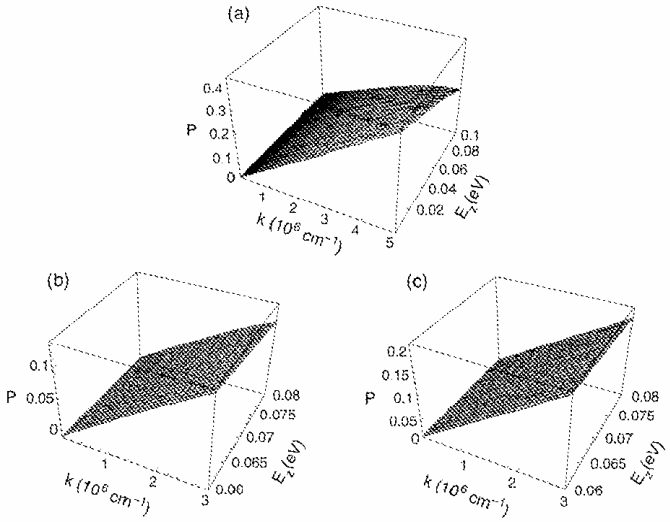

Fig. 2. (a) The polarization ratio for a $In_{0.53}Ga_{0.47}As/In_{0.52}Al_{0.48}As/In_{0.53}Ga_{0.47}As$ symmetric single-barrier structure without an external electric field; (b) the polarization ratio for the same structure with the external electric field $F_z = +5 \times 10^4$ V cm^{-1}; (c) the polarization ratio for the same structure with the external electric field $F_z = -5 \times 10^4$ V cm^{-1}.

Acknowledgement

This work was supported by the National Science Council of Taiwan under contract NSC-92-2212-M-009-015.

References

[1] G. Prinz, Science 282 (1998) 1660.
[2] J.M. Kikkawa, I.P. Smorchkova, N. Smamrth, D.D. Awschalom, Science 277 (1997) 1284.
[3] D.L. Smith, R.N. Silver, Phys. Rev. B 64 (2001) 045323.
[4] I. Žutic, J. Fabian, S. Das Sarma, Phys. Rev. B 64 (2001) 121201.
[5] J.F. Gregg, I. Petej, E. Jouquelet, C. Dennis, J. Phys. D 35 (2002) R121.
[6] O. Voskoboynikov, C.P. Lee, J. Supercond. 16 (2003) 361.
[7] G. Dresselhaus, Phys. Rev. 100 (1955) 580.
[8] Yu.A. Bychkov, E.I. Rashba, J. Phys. C 17 (1984) 6039.
[9] E.I. Rashba, J. Supercond. 15 (2002) 13.
[10] B. Jusserand, D. Richards, G. Allan, C. Priester, B. Etienne, Phys. Rev. B 51 (1995) 4707.
[11] T. Koga, J. Nitta, T. Akazaki, H. Takayanagi, Phys. Rev. Lett. 89 (2002) 046801.
[12] G. Engeles, J. Lange, Th. Schäpers, H. Lüth, Phys. Rev. B 55 (1997) R1958.
[13] A. Voskoboynikov, S.S. Liu, C.P. Lee, Phys. Rev. B 58 (1998) 15397; Phys. Rev. B 59 (1999) 12514.

[14] A. Voskoboynikov, S.S. Liu, C.P. Lee, O. Tretyak, J. Appl. Phys. 87 (2000) 387.
[15] E.A. de Andrada e Silva, G.C. La Rocca, Phys. Rev. B 59 (1999) R15583.
[16] O. Voskoboynikov, S.S. Liu, C.P. Lee, Solid State Commun. 115 (2000) 477.
[17] V.I. Perel', S.A. Tarasenko, I.N. Yassievich, S.D. Ganichev, V.V. Bel'kov, W. Prettl, Phys. Rev. B 67 (2003) 201304.
[18] T. Koga, J. Nitta, H. Takayanagi, S. Datta, Phys. Rev. Lett. 88 (2002) 126601.
[19] D.Z.-Y. Ting, X. Cartoixá, Appl. Phys. Lett. 81 (2002) 4198.
[20] M. Governale, D. Boese, U. Zülicke, C. Schroll, Phys. Rev. B 65 (2002) 140403.
[21] G. Bastard, Wave Mechanics Applied to Semiconductor Heterostructures, Les Edition de Physique, Les Ulis, 1990.
[22] E.A. de Andrada e Silva, G.C. La Rocca, F. Bassani, Phys. Rev. B 55 (1997) 16293.
[23] E.O. Kane, Tunneling Phenomenon in Solids, Plenum, New York, 1969.
[24] J.H. Davies, The Physics of Low-dimensional Semiconductors: An Introduction, Cambridge University Press, Cambridge, 1998.
[25] R. Eppenga, M.F.H. Schuurmans, Phys. Rev. B 37 (1988) 10923.

JOURNAL OF APPLIED PHYSICS 98, 023716 (2005)

Time-resolved spin filtering in semiconductor symmetric resonant barrier structures

Leo Yu[a] and O. Voskoboynikov
National Chiao Tung University, 1001 Ta Hsueh Road, Hsinchu 300, Taiwan, Republic of China

(Received 16 July 2004; accepted 14 June 2005; published online 29 July 2005)

Spin-dependent tunneling in semiconductor symmetric double barrier structures is studied theoretically. Our calculation is based on the effective one-band Hamiltonian and Dresselhaus spin-orbit coupling. We demonstrate that the ratio of the tunneling times of electrons with opposite spin orientations can vary over a few orders in magnitude. The large and tunable ratio of the tunneling times can serve as the basis in the development of all-semiconductor dynamic spin filters. © *2005 American Institute of Physics*. [DOI: 10.1063/1.1994945]

I. INTRODUCTION

Since the spin-dependent electronic device was proposed by Datta and Das,[1] the utilization of the spin-orbit coupling has been one of the key topics of semiconductor spintronics. However, a most elementary issue, an efficient means to obtain spin-polarized currents in semiconductor structures, has not been resolved yet. The conductivity mismatch between metals and semiconductors impedes the electron transport and makes the injection of spin-polarized electronic currents from strongly magnetized metals inefficient, as Schmidt *et al.*[2] pointed out. The reported experimental results on the polarization efficiency in metal-semiconductor junctions are less than 1%.[3] On the other hand, the spin-orbit interaction in semiconductors lifts the spin degeneracy of electrons' energy and results in spin-dependent transport through semiconductor junctions.

The spin-orbit interaction of electrons in III-V semiconductor materials is usually described by two contributions to the effective one-band spin-dependent Hamiltonian. One, often referred to as the Rashba term, is induced by the inversion asymmetry of the macroscopic potential,[4] which can be controlled by external electric-field or material growth techniques. The other, referred to as the Dresselhaus term,[5] is due to the inversion asymmetry of the zinc-blende lattice. The interplay between these two terms has been studied by de Andrada e Silva,[6] showing that for narrow-gap semiconductors, the contribution from the Rashba term to the spin-orbit interaction dominates over that from the Dresselhaus term. Hence the Dresselhaus term is often neglected. Calculations based on the Rashba spin-orbit interaction in III-V semiconductor heterostructures have been performed,[7–12] showing the all-semiconductor tunneling structures can be a feasible means to obtain electronic spin-polarized currents. However, it was suggested recently[11,13,14] that even through a single symmetric barrier, where the contribution from the Rashba term cancels out due to macroscopic symmetry,[7] electrons can tunnel highly spin-polarized because of the Dresselhaus term.

In this paper we elaborate on this idea and evaluate the spin-dependent tunneling (delay) time in a symmetric resonant tunneling structure. The tunneling time is an important quantity in a tunneling process that determines the dynamic working range of tunneling devices. In this work we take the "stationary phase approach" to define the tunneling time, as taken by Bohm[15] and Voskoboynikov *et al.*[16] Our following discussion will reveal that when the spin-orbit interaction effect comes into play, the ratio of the tunneling time between differently spin-polarized electrons can gain a few orders of magnitude. This provides the theoretical basis for time-resolved spin filtering. We also suggest that one can manipulate the tunneling time to a great variety by changing the barrier width. The relation between the delay time and the width is simple and can be used as a rule to select working frequencies.

This paper is organized as follows. In Sec. II we detail our calculation of the electron spin-dependent transmission amplitude, of polarization efficiency, and of tunneling time. In Sec. III, the results of calculations for InGaAs/InAlAs/InGaAs double barrier tunnel structure are presented. In Sec. IV we summarize the results.

II. POLARIZATION EFFICIENCY AND TUNNELING TIME

We consider the spin-dependent tunneling process through a symmetric double barrier structure grown along the $z\|[001]$ direction, as shown in Fig. 1(a). Taking the stationary phase approach the tunneling time is described to be the phase delay time, which is the energy derivative of the phase Θ of the transmission amplitude[16]

$$\tau_\sigma = \hbar \frac{\partial \Theta_\sigma}{\partial E_z}, \tag{1}$$

where $\Theta_\pm = \arg[t_\pm]$, E_z denotes the longitudinal component of the electron's energy (corresponding to a motion parallel to the heterostructure growth direction), and $\sigma = \pm 1$ refers to the spin polarization.

Our calculation is performed on the basis of the effective electronic one-band Hamiltonian, energy- and position-dependent electron effective mass approximation, and the Ben Daniel–Duke boundary conditions.[17] The layers of the structure are perpendicular to the z axis and the in-plane

[a]Electronic mail: leoyu.ee89@nctu.edu.tw

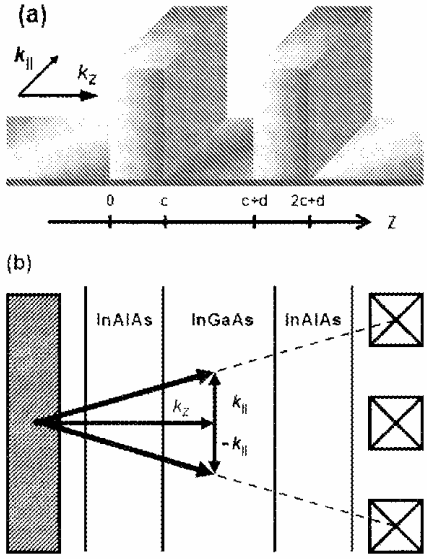

FIG. 1. (a) Sketch of electron tunneling with the wave vector $(\mathbf{k}, k_z)$, where $\mathbf{k}$ is the in-plane wave vector and $z\|[001]$ the direction of the structure growth. The variation of the band parameters forms a symmetric double barrier tunneling heterostructure. (b) A schematic illustration of a possible spin-filter implementation.

electron's wave vector is $\mathbf{k}$. With the above assumptions the electronic wave function in the jth region can be presented as

$$\Phi_\sigma(x,y,z) = \psi_{j\sigma}(z)\exp[i(k_x x + k_y y)], \tag{2}$$

where $k=\sqrt{k_x^2+k_y^2}$ and $\Psi_{j\sigma}(z)$ satisfies the z component of the Schrödinger equation

$$\hat{H}_{j\sigma}\psi_{j\sigma}(z) = E\Psi_{j\sigma}(z), \tag{3}$$

with the spin-dependent Hamiltonian in each region,[13]

$$\hat{H}_{j\sigma} = \hat{H}_{j0} + \hat{H}_{j\mathrm{SO}}. \tag{4}$$

In Eq. (4) H_{j0} is the Hamiltonian of the system without spin-orbit interaction,

$$\hat{H}_{j0} = -\frac{\hbar^2}{2m_j(E)}\left(\frac{d^2}{dz^2} - k^2\right) + E_{jc},$$

and

$$\frac{1}{m_j(E)} = \frac{2P^2}{3\hbar^2}\left[\frac{2}{E - E_{jc} + E_{jg}} + \frac{1}{E - E_{jc} + E_{jg} + \Delta_j}\right] \tag{5}$$

presents the energy- and position-dependent reciprocal effective mass. E_{jc}, E_{jg}, and Δ_j stand for the position-dependent conduction-band edge, band gap, and the spin-orbit splitting in the valence band. P is the momentum matrix element.[17] In Eq. (4) $\hat{H}_{j\mathrm{SO}}$ is the spin-dependent part of the Hamiltonian which originates from the Dresselhaus term (in the symmetrical structure the Rashba spin-orbit coupling vanishes[7]). When the kinetic energy of electrons is substantially smaller than the barrier's height we can present this term as the following:[13]

$$\hat{H}_{j\mathrm{SO}} = \gamma_j(\hat{\sigma}_x k_x - \hat{\sigma}_y k_y)\frac{d^2}{dz^2}, \tag{6}$$

where $\hat{\sigma}_x$ and $\hat{\sigma}_y$ are the corresponding x and y components of the vector of the Pauli matrices $\hat{\sigma}=\{\hat{\sigma}_x,\hat{\sigma}_y,\hat{\sigma}_z\}$ and γ_j is a material constant of the jth region.

The boundary conditions for the solution $\Psi_{j\sigma}(z)$ at the interface between the j and $j+1$ regions have been introduced in Ref. 17,

$$\frac{1}{m_j(E)}\left[\frac{d}{dz}\Psi_{j\sigma}(z)\right]_{z=z_j} = \frac{1}{m_{j+1}(E)}\left[\frac{d}{dz}\Psi_{j+1\sigma}(z)\right]_{z=z_j},$$

$$\Psi_{j\sigma}(z_j) = \Psi_{j+1\sigma}(z_j). \tag{7}$$

To diagonalize the Hamiltonian one can put the in-plane wave vector $\mathbf{k}$ along the x direction ($k_y=0$) and take the electronic wave functions to be

$$\Psi_{j\pm}(z) = \psi_{j\pm}(z)\begin{pmatrix}1\\ \mp 1\end{pmatrix},$$

which are eigenfunctions of $\hat{\sigma}_x$.

The general solution of Eq. (3) in a given jth region has the form

$$\psi_{j\sigma}(z) = a_{j\sigma}\phi^+_{j\sigma}(z) + b_{j\sigma}\phi^-_{j\sigma}(z),$$

where $\phi^{\pm}_{j\sigma}(z)$ is a pair of linearly independent solutions of Eq. (3) within that region. In the regions $j=1,3,5$ the solutions are the following plane wave sets:

$$\phi^{\pm}_{j\sigma}(z) = \exp(\pm ik_j z),$$

where

$$k_j(E_z,k) = \frac{\Sigma_{j\sigma}}{\hbar}\sqrt{2m_j(E_z,k)(E_z + E_{1c} - E_{jc}) - \hbar^2\left[1 - \frac{m_j(E_z,k)}{m_1(E_z,k)}\right]k^2},$$

$$\Sigma_{j\sigma} = \sqrt{1 + \sigma\frac{2\gamma_j m_j(E_z,k)}{\hbar^2}k},$$

and E_z is the longitudinal component of the total energy in the first region,

$$E = E_{1c} + E_z + \frac{\hbar^2 k^2}{2m_1(E_z,k)}.$$

We use this expression, along with Eq. (5), to find the dependence of $m_j(E_z,k)$ on $E(E_z,k)(j=1-5)$. In the regions $j=2,4$ the solutions are chosen to be

$$\phi^{\pm}_{j\sigma}(z) = \exp(\pm q_j z),$$

where

$$q_j(E_z,k) = \frac{\Sigma_{j\sigma}}{\hbar}\sqrt{2m_j(E_z,k)(E_{jc}-E_{1c}-E_z)+\hbar^2\left|1-\frac{m_2(E_z,k)}{m_1(E_z,k)}\right|k^2}.$$

The coefficients $\{a_{j\sigma},b_{j\sigma}\}$ are to be determined from the boundary conditions in Eq. (7). The sets of coefficients in neighboring regions are related by the transfer matrix M:[18]

$$\begin{pmatrix} a_{j\sigma} \\ b_{j\sigma} \end{pmatrix} = M_\sigma^j \begin{pmatrix} a_{j+1\sigma} \\ b_{j+1\sigma} \end{pmatrix}.$$

According to the boundary conditions in Eq. (7) the matrix M_σ^j is written as[7]

$$M_\sigma^j = \frac{1}{\Delta_j}\begin{pmatrix} \Lambda_{j+}^- & \Lambda_{j+}^+ \\ -\Lambda_{j-}^- & -\Lambda_{j-}^- \end{pmatrix},$$

with

$$\Delta_j = \Delta_j^+ - \Delta_j^-, \quad \Delta_j^\pm = \left\{\frac{d}{dz}\ln[\psi_{j\sigma}^\pm(z)]\right\}_{z=z_j}$$

$$\Lambda_{j+}^\pm = \left(\frac{m_j}{m_{j+1}}\Delta_j^\pm - \Delta_j^+\right)\frac{\psi_{j+1\sigma}^\mp(z_j)}{\psi_{j\sigma}^+(z_j)},$$

$$\Lambda_{j-}^\pm = \left(\frac{m_j}{m_{j+1}}\Delta_j^\pm - \Delta_j^-\right)\frac{\psi_{j+1\sigma}^\mp(z_j)}{\psi_{j\sigma}^+(z_j)}.$$

The double barrier tunneling structure consists of four interfaces, so the total transfer matrix is written as

$$M_\sigma = \Pi_{j=1}^4 M_\sigma^j.$$

Electrons are injected from the region of $j=1$. The transmitted waves will appear in the region of $j=5$. With this assumption the transmission amplitude is given by

$$t_\sigma = \frac{1}{(M_\sigma)_{11}},$$

and the spin-dependent delay time is written as

$$\tau_\sigma(E_z,k) = -\hbar\frac{\partial \arg[(M_\sigma)_{11}]}{\partial E_z}.$$

The polarization efficiency of the structure was defined in Ref. 7 to be

$$P = \frac{|t_+|^2 - |t_-|^2}{|t_+|^2 + |t_-|^2}.$$

III. CALCULATION RESULTS

In Fig. 2 we demonstrate the numerical results of the polarization efficiency P of an electron's tunneling through a resonant symmetric structure made of $In_{0.53}Ga_{0.47}As/In_{0.52}Al_{0.48}As$ heterojunctions. All calculations are performed within a region on the (E_z,k) plane where the total energy of electrons is substantially smaller than the barrier's height [see Eq. (6)]. The numerical values of γ in different materials are obtained for InAs and GaAs from Ref. 13, for AlAs from Ref. 21, and for alloys with the Vegard's superposition law in Ref. 22. One can see that the polarization efficiency shows

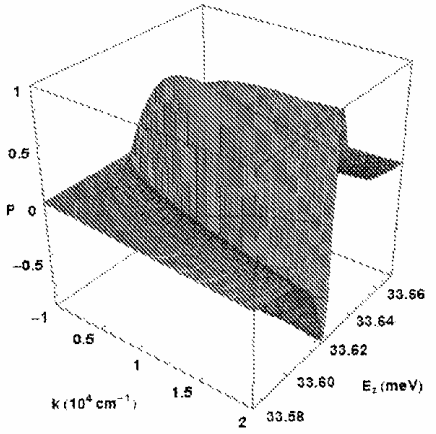

FIG. 2. Polarization efficiency P calculated for an $In_{0.53}Ga_{0.47}As/In_{0.52}Al_{0.48}As/In_{0.53}Ga_{0.47}As$ DBT structure (see Fig. 1). The structure parameters are obtained in Ref. 20: $E_{1s}=0.418$ eV, $E_{2s}=1.52$ eV, $\Delta_1=0.38$ eV, $\Delta_2=0.341$ eV, $m_1(0)=0.044m_0$, $m_2(0)=0.084m_0$ (m_0 is the free-electron mass), $\gamma_1=0.076\,9$ eV nm^3 (Ref. 13), $\gamma_2=0.073\,4$ eV nm^3 (Ref. 21), $c=6$ nm, and $d=12$ nm.

typical resonant behaviors as a function of the longitudinal energy and in-plane wave number. The peaks correspond to the spin-split lowest resonant levels on the (E_z,k) plane. The splitting of the resonant levels results in an abrupt change of the sign of the polarization efficiency.

The delay time of tunneling electrons with two opposite spin polarizations is presented in Fig. 3. The position of the peak corresponds to the resonant tunneling level, at which the tunneling electron is "trapped" in the quasibound states of the well. Although the positions of the peak for the two opposite spin polarizations do not seem to have the same functional dependence on (E_z,k), the distance between them in E_z is proportional to k, in accordance to the linear dependence on k of the Dresselhaus spin spliting of the levels in the well.

Since the positions of the peaks depend sharply on E_z and k, we present in a logarithmic scale the ratio of the delay time between oppositely spin-polarized electrons (see Fig. 4). This ratio increases with the length of k and can gain a few orders in magnitude.

The ratio of the delay times can be tuned by means of structural design. For this reason we present in Fig. 5 the dependence of the maximal delay time on the barrier thickness c and the well width d. The delay time increases with increasing c and d, but has different functional dependencies on each of them. From the calculation results presented in Fig. 5 for τ_+, one can approximate the dependencies as the following formula:

$$\tau_+ \propto d^2\exp(\alpha c),$$

where α is a constant; for τ_- of the same structure, one can recalculate it from the logarithmic ratio. For our symmetric InGaAs/InAlAs/InGaAs double barrier structure $\alpha \approx 0.074$ when $d=18$ nm. Applying this formula one can determine

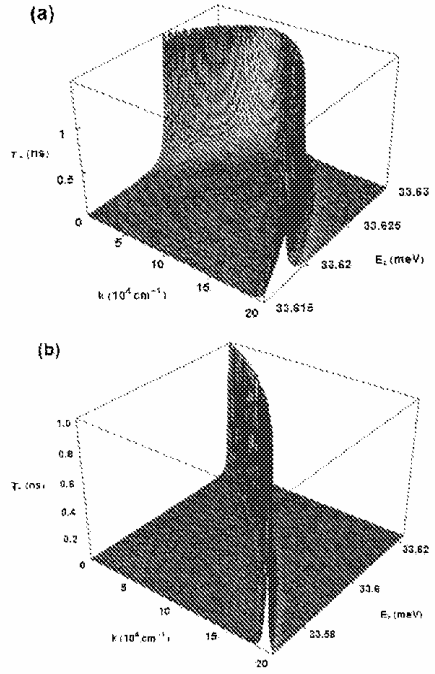

FIG. 3. The delay time for the structure in Fig. 2. (a) Delay time for electrons with spin "up." (b) Delay time for electrons with spin "down."

the actual region of frequencies where the structure is applicable to spin-dependent electronic devices.

The large and tunable ratio of spin-dependent delay times in symmetric structures provides a new method to perform spin filtering. Once we have clear spin-distinguishable times of the tunneling processes, the cutoff frequencies of electrons differently spin polarized will also split. By selecting an appropriate region of frequency, the current contribution from electrons with a lower cutoff frequency can be

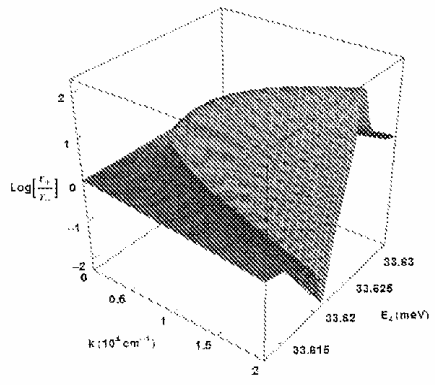

FIG. 4. Ratio between the delay time for different polarizations of the electron spin. The structure is the same as in Fig. 2.

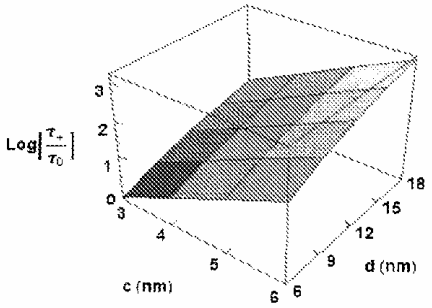

FIG. 5. The variation of the maximum delay time with respect to (a) the barrier thickness and (b) the well width. The constant $\tau_0 = 10^{-12}$ s is defined for normalization. The structure is the same as in Fig. 2.

greatly suppressed. In this sense we achieved time-resolved spin filtering. This dynamic regime is more efficient than the conventional static regime. Indeed, in the static regime the means to spin filtering is a large spin splitting of resonant levels in the well,[9] which requires a large transversal dc bias (or built-in electric field). In symmetrical structures instead one can perform the dynamic spin filtering even when only a weak time-dependent signal is applied. We mention by pass that the spin-relaxation processes can also be suppressed by the same means.

An important point that tends to be missed is the fact that the spin filtering based on the spin-orbit coupling requires a control of the electrons' in-plane momentum.[6,11,12] Figure 1(b) illustrates schematically the basic concept of a dynamic spin filter fabricated in a split multicollector configuration. The in-plane momentum control of electrons and the dynamic spin filtering are achieved by sending a series of high-frequency voltage pulses to different leads of the multicollector. Another method to control the electrons' in-plane momentum was demonstrated recently with side-gated resonant devices in a dc regime.[12]

IV. CONCLUSIONS

Based on the stationary phase concept and the effective one-band Hamiltonian with the Dresselhaus spin-orbit coupling, we present the numerical results of the tunneling time through a realistic InGaAs/InAlAs/InGaAs resonant symmetric structure. It is shown that the polarization efficiency of the structure has a well-defined resonance behavior, which leads to a considerable spin polarization of electrons tunneling through. In the lower-energy region, the ratio between the tunneling times of electrons with opposite spin orientations can vary over a few orders in magnitude. The results indicate that the Dresselhaus spin-orbit coupling separates the time-dependent response of differently spin-polarized tunneling electrons. Furthermore, the large and tunable ratio of the tunneling times provides a possible way to construct a dynamic spin filter. The characteristic time of such devices also has been estimated and presented, showing simple functional dependencies on the barrier thickness and the well width. The dependencies can be exploited to design spintronic devices working in the desired frequencies.

This work was supported by the National Science Council of R.O.C. under Contract No. NSC 93-2112-M-009-008.

[1]S. Datta and B. Das, Appl. Phys. Lett. **89**, 665 (1990).
[2]G. Schmidt, D. Ferrand, L. W. Molenkamp, A. T. Filip, and J. van Wees, Phys. Rev. B **62**, R4790 (2000).
[3]P. R. Hammar, B. R. Bennett, M. J. Yang, and M. Johnson, Phys. Rev. Lett. **83**, 203 (1999); S. Gardelis, C. G. Smith, C. H. W. Barnes, E. H. Linfield, and D. A. Ritchie, Phys. Rev. B **60**, 7764 (1999); *Semiconductor Spintronics and Quantum Computation*, edited by D. D. Awschalom, D. Loss, and N. Samarth (Springer, Berlin, 2002).
[4]Yu. A. Bychkov and E. I. Rashba, J. Phys. C **17**, 6039 (1984).
[5]G. Dresselhaus, Phys. Rev. **100**, 580 (1955).
[6]E. A. de Andrada e Silva, Phys. Rev. B **46**, 1921 (1992); E. A. de Andrada e Silva and G. C. La Rocca, *ibid.* **50**, 8523 (1994).
[7]A. Voskoboynikov, S. S. Liu, and C. P. Lee, Phys. Rev. B **59**, 12514 (1999).
[8]E. A. de Andrada e Silva and G. C. La Rocca, Phys. Rev. B **59**, 015583 (1999).
[9]A. Voskoboynikov, S. S. Liu, and C. P. Lee, J. Appl. Phys. **87**, 387 (2000).
[10]T. Koga, J. Nita, H. Takayanagi, and S. Datta, Phys. Rev. Lett. **88**, 126601 (2002).
[11]Z.-Y. Ting, D. X. Cartoixá, D. H. Chow, J. S. Moon, D. L. Smith, T. C. McGill, and J. N. Schulman, Proc. IEEE **91**, 741 (2003).
[12]J. S. Moon, D. H. Chow, J. N. Schulman, P. Deelman, J. J. Zinck, and D. Z.-Y. Ting, Appl. Phys. Lett. **85**, 678 (2004).
[13]V. I. Perel', S. A. Tarasenko, I. N. Yassievich, S. D. Ganichev, V. V. Bel'kov, and W. Prettl, Phys. Rev. B **67**, 201304 (2003).
[14]D. Z.-Y. Ting and X. Cartoixà, Phys. Rev. B **68**, 235320 (2003).
[15]D. Bohm, *Quantum Theory* (Prentice-Hall, New York, 1951); M. Buttiker and R. Landauer, Phys. Rev. Lett. **49**, 1739 (1982); D. Dragonman and M. Dragonman, IEEE J. Quantum Electron. **32**, 1932 (1996); G. Garcia-Calderon and A. Rubio, Phys. Rev. A **55**, 3361 (1997); J. U. Kim and H. H. Lee, J. Appl. Phys. **84**, 907 (1998).
[16]O. Voskoboynikov, S. S. Liu, and C. P. Lee, Solid State Commun. **155**, 477 (2000).
[17]G. Bastard, *Wave Mechanics Applied to Semiconductor Heterostructures* (Les Edition de Physique, Les Ulis, 1990).
[18]E. O. Kane, *Tunneling Phenomenon in Solids* (Plenum, New York, 1969).
[20]J. H. Davies, *The Physics of Low-dimensional Semiconductors: An Introduction* (Cambridge University Press, Cambridge, 1998).
[21]R. Eppenga and M. F. H. Schuurmans, Phys. Rev. B **37**, 10923 (1988).
[22]J. Singh, *Electronics and Optoelectronic Properties of Semiconductor Structures* (Cambridge University Press, Cambridge, 2003).

2.3 Main results and discussion

For the reason of spintonics development the electronic spin polarization (filtering) in solid-state systems has attracted considerable attention. Many possible structures were investigated to reach high level electronic spin filtering and injection. Most of them consist of magnetic material elements. But in principle one can use the all- semiconductor approach utilizing multi-layered nano-systems to generate and detect the electron spin polarization. The semiconductor approach has the advantage of being compatible with conventional semiconductor technology. From this point of view the most important property of semiconductors to be utilized in all semiconductor spintronic nano-devices is the spin-orbit (SO) interaction. The control of spin in semiconductors together with modern semiconductor technology can guarantee the future of the spintronics and result a valuable commercial interest.

In the bulk of III-V and II-VI semiconductor materials the SO interaction lifts the spin-degeneracy of the conduction states in the center of the Brillouin zone. This part of the SO interaction is called the bulk inversion asymmetry (BIA) type and it is presented by the effective Dresselhaus Hamiltonian. Macroscopic effective electric fields in semiconductor nano-structures result the structural inversion asymmetry (SIA) and a linear (on the electron wave-vector **k**) term (or the Rashba type) of the SO interaction. It has been found out recently by us that the Rashba spin-orbit coupling in conventional III-V semiconductor tunnel barrier structures can lead to the spin-dependent tunneling phenomenon. The spin-polarization ratio in tunneling structures is defined as $P(E_z,\mathbf{k})=\frac{T_+(E_z,\mathbf{k})-T_-(E_z,\mathbf{k})}{T_+(E_z,\mathbf{k})+T_-(E_z,\mathbf{k})}$, where $T_{\pm}(E_z,\mathbf{k})$ is spin-up(down) tunneling probability and E_z is the part of the electronic energy which corresponds to the perpendicular motion to the barrier (z-axis), and $\mathbf{k}=(k_x,k_y)$ is parallel to the barrier component of the electronic wave vector. In symmetric structures with the exceptional Rashba interaction included we need to apply an external perpendicular electric field F_z to generate the asymmetry of the tunneling probability. In the same time asymmetric structures the difference between T_+ and T_- exists with zero external electric field and there is a possibility to reverse the polarization by means of the change of the external electric field F_z. We further investigated spin-dependent tunneling probability for realistic symmetric tunneling structures with account both the Rashba and Dresselhaus couplings. Our calculation is performed for realistic semiconductor structures on the base of the effective electronic one band Hamiltonian, energy and position dependent electron effective mass approximation, and spin-dependent Ben Daniel-Duke boundary conditions. We demonstrated that the transmission tunneling probability for a realistic symmetric single barrier structure can gain a well recognizable spin dependence for not too large in-plane wave vector of tunneling electrons. In addition one can control the magnitude of the polarization ratio by external electric field. The described effect can be a base for more advanced spin-filtering techniques at zero magnetic field. Our calculation results show that interplay between BIA and SIA interactions makes the spin filtering processes more rich and controllable.

The tunneling time is a basic characteristic that determines the dynamic range of tunneling devices. Based on the stationary phase concept and the effective one-band Hamiltonian with the Dresselhaus spin-orbit coupling, we obtained numerical results on the tunneling time trough a realistic InGaAs/InAlAs/InGaAs resonant symmetric structure. It was shown that the polarization efficiency of the structure has a well defined resonance behavior that can lead to a considerable spin polarization of electrons tunneling trough the structure. In the low energy region, the ratio between the tunneling times of electrons with opposite spin orientation can reach a few orders in magnitude. The results indicate that the Dresselhaus spin-orbit coupling separates the time dependent response for electrons tunneling with different spin polarizations. Further the large and tunable ratio of the tunneling times provides a possible way to construct a dynamic spin filter. The characteristic time of such devices have also been estimated and presented as a simple functional dependence on the barrier and well width. The relation between the delay time and the width is simple and can be used as a design rule to select working frequencies of spintronic devices.

3. Spin-dependent scattering and the spin-dependent Hall effect

PERGAMON

Solid State Communications 125 (2003) 381–385

solid state communications

www.elsevier.com/locate/ssc

Spin-dependent electron single and double scattering from quantum dots and antidots

Edward Chen, O. Voskoboynikov*,[1], C.P. Lee

Department of Electronics Engineering, National Chiao Tung University, 1001, Ta Hsueh Road, Hsinchu 300, Taiwan, ROC

Received 24 October 2002; received in revised form 2 December 2002; accepted 6 December 2002 by H. Takayama

Abstract

We present a theoretical study of the spin-dependent electron scattering from spherical quantum dots (antidots) embedded into III–V semiconductors. To calculate the elastic scattering cross-section we use the effective one electron band Hamiltonian and spin-dependent boundary conditions generated by the spin–orbit interaction in the structures. It is demonstrated that the spin–orbit interaction can lead to a recognizable magnitude of polarization for single and double scattering at zero magnetic field.

PACS: 72.20.Dp; 72.25.Dc; 73.63.Kv

Keywords: A. Nanostructures; A. Semiconductors; D. Electronic transport; D. Spin–orbit effects

The asymmetric scattering of polarized electrons in gas and metallic systems has been extensively studied for decades (see Refs. [1–3] and references therein). The relaxation of electron and hole spin polarization due to spin-dependent scattering in semiconductor structures was also of great interest and has been studied both experimentally and theoretically [4–6]. Recently it was discovered that most of the scattering events conserve spin and the electron spin-relaxation time can become surprisingly long in III–V semiconductors (as 100 ns [6]). The spin-diffusion length is much longer than the electron mean free path, and in some III–V semiconductor nano-structures it may be of the order of the sample dimensions (100 μm [7]).

In semiconductors the most important interaction, which causes spin-dependent processes is the spin–orbit interaction [8,9]. The Rashba spin–orbit coupling [9] is an essential element of the spin field effect transistor proposed by Datta and Das [10]. A new branch of semiconductor electronics so called spintronics [11] became under an extensive development recently. For this reason, the spin-dependent kinetics of electrons in traditional III–V semiconductor heterostructures becomes a topic of a great.

This paper describes a model of the spin-dependent electron scattering from nano-scale semiconductor quantum dots (antidots). Recent advances in semiconductor nano-technology allow us to consider small spherical dots (antidots) of III–V semiconductors [12] as 'artificial defects' with controllable parameters. We calculate the polarization (the Sherman function [2,3]) after a single scattering and investigate how the polarization changes after the second scattering. In our calculation we use the effective one band Hamiltonian with the spin-dependent boundary conditions [13–15]. The rectangular hard-wall potential of the dots (antidots) is induced by the discontinuity of the conduction band edge of the system.

For three-dimensional semiconductor quantum dots (antidots) the approximate one electronic band effective

* Corresponding author. Tel.: +886-3-5712121x54174; fax: +886-3-5724361.

E-mail address: vam@cc.nctu.edu.tw (O. Voskoboynikov).

[1] Present address: Department of Electronics Engineering and Institute of Electronics, National Chiao Tung University, 1001 Ta Hsuch Rd. Hsinchu 300, Taiwan, ROC.

0038-1098/03/$ - see front matter © 2003 Elsevier Science Ltd. All rights reserved.
PII: S0038-1098(02)00850-5

Hamiltonian is given in the form [13]

$$\hat{H} = -\frac{\hbar^2}{2}\nabla_{\mathbf{r}}\frac{1}{m(E,\mathbf{r})}\nabla_{\mathbf{r}} + V(\mathbf{r}) + V_{so}(\mathbf{r}), \tag{1}$$

where $\nabla_{\mathbf{r}}$ stands for the spatial gradient, $m(E,\mathbf{r})$ is energy and position-dependent electron effective mass

$$\frac{1}{m(E,\mathbf{r})} = \frac{2P^2}{3\hbar^2} \times\left[\frac{2}{E+E_g(\mathbf{r})-V(\mathbf{r})} + \frac{1}{E+E_g(\mathbf{r})-V(\mathbf{r})+\Delta(\mathbf{r})}\right],$$

$V(\mathbf{r})$ is the hard-wall confinement potential of the dots or hard core repulsive potential of the antidots, $E_g(\mathbf{r})$ and $\Delta(\mathbf{r})$ stand for position-dependent band gap and the spin–orbit splitting in the valence band, P is the momentum matrix element. The spin–orbit interaction $V_{so}(\mathbf{r})$ for conducting band electrons is described by [9,14,15]

$$V_{so}(\mathbf{r}) = \mathrm{i}\nabla_{\mathbf{r}}\beta(E,\mathbf{r})\cdot[\hat{\boldsymbol{\sigma}}\times\nabla_{\mathbf{r}}], \tag{2}$$

where

$$\beta(E,\mathbf{r}) = \frac{P^2}{3} \times\left[\frac{1}{E+E_g(\mathbf{r})-V(\mathbf{r})} - \frac{1}{E+E_g(\mathbf{r})+\Delta(\mathbf{r})-V(\mathbf{r})}\right], \tag{3}$$

is the spin–orbit coupling parameter, and $\hat{\boldsymbol{\sigma}} = \{\sigma_x, \sigma_y, \sigma_z\}$ is the vector of the Pauli matrices.

For systems with a sharp discontinuity of the conduction band edge between the dot (antidot) (material 1) and the crystal matrix (material 2) the scattering potential can be presented as

$$V(\mathbf{r}) = \begin{cases} -V_0, & \mathbf{r}\in 1 \\ 0, & \mathbf{r}\in 2, \end{cases} \tag{4}$$

where the potential barrier is chosen as $V_0 \geq 0$ for dots and $V_0 \leq 0$ for antidots. From integration of the Shrödinger equation with Hamiltonian (1) along direction perpendicular to the interface ($\mathbf{r}_n$) we obtain the spin-dependent Ben Daniel–Duke boundary conditions for the electron wave function $\Psi(\mathbf{r})$

$$\Psi_1(\mathbf{r}_s) = \Psi_2(\mathbf{r}_s);$$
$$\left\{\frac{\hbar^2}{2m(E,\mathbf{r})}\nabla_{\mathbf{r}} - \mathrm{i}\beta(E,\mathbf{r})[\hat{\boldsymbol{\sigma}}\times\nabla_{\mathbf{r}}]\right\}_n \Psi_1(\mathbf{r}_s) = \left\{\frac{\hbar^2}{2m(E,\mathbf{r})}\nabla_{\mathbf{r}} - \mathrm{i}\beta(E,\mathbf{r})[\hat{\boldsymbol{\sigma}}\times\nabla_{\mathbf{r}}]\right\}_n \Psi_2(\mathbf{r}_s), \tag{5}$$

where $\mathbf{r}_s$ denotes the position of the system interface.

Considering dots (antidots) with spherical shapes we choose the solution of the scattering problem in spherical coordinates (r,θ,ϕ) as [1,16,17]

$$\Psi(\mathbf{r}) = (4\pi)^{1/2}\sum_{l,s=\pm 1} \mathrm{i}^l[l+(1+s)/2]^{1/2}R_l^s(r)\mathbf{Y}_l^s(\theta,\varphi), \tag{6}$$

where

$$\mathbf{Y}_l^s(\theta,\varphi) = s\sum_{s'=\pm 1} \mathbf{C}[l+s/2, 1/2; \times(1-s')/2, s'/2]\cdot Y_{l,(1-s')/2}(\theta,\varphi)\chi^{s'},$$

$\mathbf{C}[x,y;z,w]$ are the Clebsh–Gordan coefficients [1], $Y_{l,m}(\theta,\varphi)$ are the spherical harmonics, $s = \pm 1$ refers to the electron spin polarization, and χ^s is a spin function upon which the Pauli matrix vector operates:

$$\chi^{+1} = \begin{pmatrix}1\\0\end{pmatrix}, \qquad \chi^{-1} = \begin{pmatrix}0\\1\end{pmatrix}.$$

Substituting Eq. (6) into the Schrödinger equation, we obtain

$$\begin{aligned} &-\frac{\hbar^2}{2m_1(E)}\left[\frac{1}{r^2}\frac{\mathrm{d}}{\mathrm{d}r}r^2\frac{\mathrm{d}}{\mathrm{d}r} - \frac{l(l+1)}{r^2}\right]R_{1l}^s(r) \\ &= (E+V_0)R_{1l}^s(r), \quad r\geq r_0, \\ &-\frac{\hbar^2}{2m_2(E)}\left[\frac{1}{r^2}\frac{\mathrm{d}}{\mathrm{d}r}r^2\frac{\mathrm{d}}{\mathrm{d}r} - \frac{l(l+1)}{r^2}\right]R_{2l}^s(r) = ER_{2l}^s(r), \\ &r< r_0, \end{aligned} \tag{7}$$

where r_0 is the radius of the sphere. The spin-dependent boundary conditions (5) for the spherical quantum dot (antidot) can be written as

$$\begin{aligned} &R_{1l}^s(r_0) = R_{2l}^s(r_0), \\ &\frac{\hbar^2}{m_1(E)}\frac{\mathrm{d}}{\mathrm{d}r}R_{1l}^s(r)\Big|_{r0} - \frac{\hbar^2}{m_2(E)}\frac{\mathrm{d}}{\mathrm{d}r}R_{2l}^s(r_0)\Big|_{r0} + \frac{2[\beta_1(E)-\beta_2(E)]}{r_0} \\ &\times\left[j(j+1) - l(l+1) - \frac{3}{4}\right]R_{1l}^s(r_0) \\ &= 0, \end{aligned} \tag{8}$$

where $j = |l+s/2|$.

The method of partial waves is convenient in this specific case of spherical quantum dots (antidots) with short-range potentials (4), when we can solve the scattering problem without additional assumptions. The proper solution of Eq. (7) behaves like

$$\begin{aligned} R_{1l}^s(r) &= A_l^s g_l(\kappa r), \\ R_{2l}^s(r) &= B_l^s[j_l(kr) - \tan\delta_l^s \eta_l(kr)], \end{aligned} \tag{9}$$

where δ_l^s is the phase shift due to spin-dependent scattering, j_l and η_l are the spherical Bessel functions of the first and

second kind, respectively

$$k(E) = \frac{\sqrt{2m_2(E)E}}{\hbar},$$

and g_l is a solution in the dot (antidot) region. For the dot case:

$$g_l(\kappa r) = j_l(\kappa r),$$

where

$$\kappa(E) = \frac{\sqrt{2m_1(E)(E+V_0)}}{\hbar},$$

while for the antidot case:

$$g_l(\kappa r) = \sqrt{\frac{\pi}{2\kappa r}} I_{l+1/2}(\kappa r),$$

$$\kappa(\varepsilon) = \frac{\sqrt{2m_1(E)(|V_0|-E)}}{\hbar}.$$

($I_{l+1/2}(z)$ is the modified Bessel function of the first kind). The phase shift δ_l^s can be obtained from the values of the wave functions $R_l^s(r)$ at the dot boundary ($r = r_0$)

$$\tan\delta_l^s = \frac{kj_l'(kr_0) - \gamma_l^s j_l(kr_0)}{k\eta_l'(kr_0) - \gamma_l^s \eta_l(kr_0)}, \tag{10}$$

where

$$\gamma_l^s = \kappa\frac{m_2}{m_1}\frac{g_l'}{g_l} + \frac{2m_2(\beta_1-\beta_2)}{r_0\hbar^2}\left[j(j+1) - l(l+1) - \frac{3}{4}\right],$$

and primes denote the first derivatives with respect to the function argument.

The complex scattering amplitude [17] is defined as

$$\mathbf{F}^s = [f^s(\theta) + (\hat{\boldsymbol{\sigma}}\cdot n_1)g^s(\theta)]\chi^s, \tag{11}$$

where

$$f^s(\theta) = \frac{1}{k}\cdot\sum_{l=0}^{\infty}[(l+1)\exp(\mathrm{i}\delta_l^+)\sin\delta_l^+ + l\exp(\mathrm{i}\delta_l^-)\sin\delta_l^-]P_l(\cos\theta),$$

and

$$g^s(\theta) = \frac{\mathrm{i}}{k}\cdot\sum_{l=1}^{\infty}[\exp(\mathrm{i}\delta_l^+)\sin\delta_l^+ - \exp(\mathrm{i}\delta_l^-)\sin\delta_l^-]P_l^1(\cos\theta),$$

are the direct amplitude and the spin-flip amplitude, correspondingly, (is the scattering angle between initial $\mathbf{k}_i$ and final $\mathbf{k}_f$ wave vectors,

$$\mathbf{n}_1 = \frac{\mathbf{k}_i\times\mathbf{k}_f}{|k_i\times k_f|},$$

is a unit vector perpendicular to the scattering plane, $P_l(\cos\theta)$ and $P_l^1(\cos\theta)$ are the Legendre polynomial and Legendre associated function, respectively.The Mott scattering cross-section for spin-polarized electrons can be written in terms of the incident electron spin-polarization vector $\mathbf{P}_i$

$$\sigma(\theta) = I(\theta)[1 + S(\theta)\mathbf{P}_i\cdot\mathbf{n}_1], \tag{12}$$

where

$$I(\theta) = |f^s(\theta)|^2 + |g^s(\theta)|^2,$$

is the differential cross-section for an un-polarized incident beam and

$$S(\theta) = \frac{f^{s*}g^s + f^s g^{s*}}{|f^s(\theta)|^2 + |g^s(\theta)|^2}, \tag{13}$$

is the Sherman function [2,3]. The Sherman function characterizes the left–right asymmetry in the scattering cross-section for initially polarized electron beams and the average polarization after a single scattering $\mathbf{P}_f$ for an initially unpolirazed beam

$$\mathbf{P}_f = S(\theta)\mathbf{n}_1.$$

It follows from the equations above that the spin–orbit interaction influences the phase shifts with angular momentum $l > 0$. The effect is stronger for pairs of materials with a lager difference in the spin–orbit coupling parameters. Fig. 1

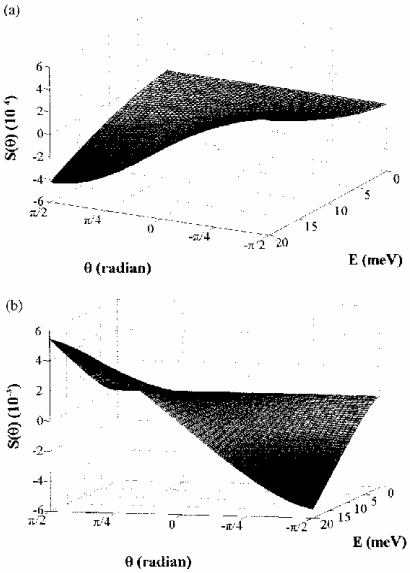

Fig. 1. The Sherman function for (a) spherical InAs/GaAs quantum dot with $r_0 = 1.3$ nm and (b) spherical GaAs/InAs antidot with $r_0 = 6$ nm. $E_{g\mathrm{InAs}} = 0.42$ eV, $E_{g\mathrm{GaAs}} = 1.52$ eV, $|V_0| = 0.77$ eV, $\Delta_{\mathrm{InAs}} = 0.38$ eV, $\Delta_{\mathrm{GaAs}} = 0.34$ eV, $m_{\mathrm{InAs}}(0) = 0.023m_0$, $m_{\mathrm{GaAs}}(0) = 0.067m_0$ (m_0—the free electron mass) [13].

presents the Sherman function versus the scattering angle and the energy of the incoming electrons calculated for a nano-scale quantum dot (InAs/GaAs) and antidot (GaAs/InAs). In the case of quantum dots (Fig. 1(a)) we avoided an additional complexity by neglecting the interaction of the scattered electrons with charges bound in the dots and the resonance effects. This restricts us to use dot sizes, which do not allow any bound states in the dots. The electron energy is adjusted to the electron band edge of GaAs. In the dot region the denominators of the spin–orbit coupling parameter (see Eq. (3)) are relatively large ($V_0 = 0.77$ eV, $E_{1g} = E_{gInAs} = 0.42$ eV, $\Delta_1 = \Delta_{InAs} = 0.38$ eV) that makes β_1, the total difference $\beta_1 - \beta_2$ and the effect rather small. For the antidot case, the situation is quite different. In antidot region the dominators are relatively small, so the parameter $\beta_1 - \beta_2$ is large. The Sherman function amplitude becomes much lager than that for the quantum dot case (see Fig. 1(b)).

Polarization produced by scattering of an unpolarized electron beam affects subsequent scattering processes. The first scattering generates a polarization that in the second scattering results in the left–right asymmetry in the scattering cross-section. If the azimuthal asymmetry after the second scattering can be measured, the scattering induced polarization can be found [1,16,17]. We consider double scattering in the same x–y plane as it is presented in Fig. 2. The polarization $\mathbf{P}_2$ in the double scattering process is parallel to $\mathbf{n}_1$ and it is described by

$$P_2^l(\theta_1, \theta_2) = \frac{S_1(\theta_1) + S_2(\theta_2)}{1 + S_1(\theta_1)S_2(\theta_2)},$$

when the second scattering occurs to the left of an observer standing to $\mathbf{n}_1$ and

$$P_2^r(\theta_1, \theta_2) = \frac{S_1(\theta_1) - S_2(\theta_2)}{1 - S_1(\theta_1)S_2(\theta_2)},$$

when the second scattering occurs to the right of the observer.

In Fig. 3 we present the calculated result of the left polarization for the double scattering from GaAs/InAs antidotes. The results demonstrate a well recognizable polarization after the second scattering. In addition, Fig. 4 shows the energy dependence of the polarization of the double scattering process with a fixed direction of the first scattering.

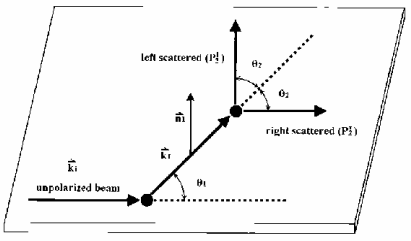

Fig. 2. Schematic diagram of single and double scattering.

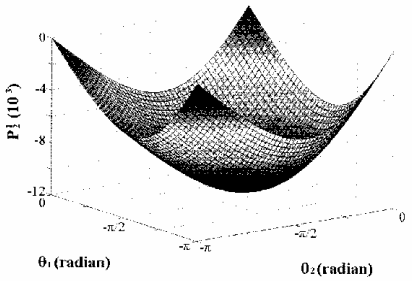

Fig. 3. Polarization of double scattering to the left ($P_2^l(\theta_1, \theta_2) = P_2^r(\theta_1, -\theta_2)$) induced by scattering from GaAs/InAs antidotes with $r_0 = 6$ nm and $E = 20$ meV.

Subsequent scatterings (more than double) generate more complicated angular dependencies of the polarization [1,2] and could be investigated theoretically one after another [2,17]. But in reality, the intensity of the polarized electrons is small. In addition the background scattering processes (phonons, impurities, defects, plural scatterings, etc.) should substantially randomize the subsequent polarization process [2]. From other side, this randomization in higher order scatterings provides some grounding in the kinetic theory of the anomalous Hall effect [18–21].

Following the method from [18–21], for degenerated electronic system and a random three dimensional array of the quantum dots (antidots) at zero magnetic field the anomalous Hall angle can be estimated as

$$|\theta_H| = \frac{\tau_0}{\tau_{11}}, \tag{14}$$

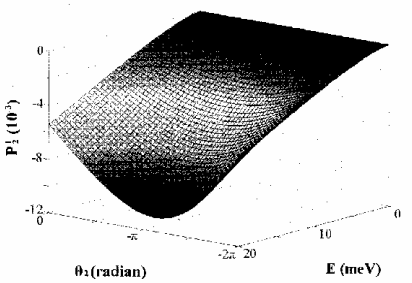

Fig. 4. Energy dependence of the left–right double scattering polarizations induced by scattering from GaAs/InAs antidotes with $r_0 = 6$ nm and $\theta_1 = -\pi/2$.

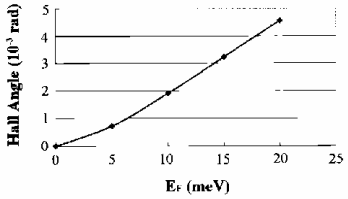

Fig. 5. The absolute value of the anomalous Hall angle for a random array of GaAs/InAs antidots with radius $r_0 = 6$ nm.

where

$$\frac{1}{\tau_0} = 2\pi N_d v_F \int_0^{\pi} d\theta\, I(\theta)(1 - \cos\theta)\sin\theta, \tag{15}$$

is the elastic scattering rate, and

$$\frac{1}{\tau_H} = 2\pi N_d v_F \int_0^{\pi} d\theta\, I(\theta)S(\theta)(1 - \cos\theta)\sin^3\theta, \tag{16}$$

is the spin-flip scattering rate. All functions are taken at the Fermi shell, N_d is the concentration of the dots (antidotes), v_F is the Fermi velocity, and it is assumed that the electron current is completely polarized. In Fig. 5 we present the result calculated for the anomalous Hall angle as a function on the Fermi energy for an array of GaAs/InAs antidotes. It should be noted, the anomalous Hall effect produced by quantum antidots has a measurable magnitude.

In summary, we discussed the influence of the spin–orbit interaction on the electron scattering from semiconductor quantum dots and antidots. The one electron band effective Hamiltonian and the spin-dependent boundary conditions for spherical quantum dots (antidots) allowed us to calculate a spin asymmetry in the electron scattering cross-section. We found a polarization produced by single and double scattering of unpolirazed electron beams due to the spin–orbit interaction. We would like to stress that, the polarization is caused by non-magnetic GaAs/InAs semiconductor structures without external magnetic fields. We should mention, that in the anomalous Hall effect the Hall angle is proportional to the Sherman function at the Fermi energy shell [18,19]. Our calculation results suggest a small but measurable magnitude of the Hall angle for antidots. The anomalous Hall effect produced by quantum antidots is expected to be reduced by the electron impurity scattering, but should still have a significant magnitude. This effect is potentially useful in integrated electron spin-polarization devices based on all-semiconductor heterostructures.

Acknowledgements

This work was supported by the National Science Council of Taiwan under contracts NSC-90-2215-E-009-022 and NSC-91-2219-M-009-003.

References

[1] N.F. Mott, H.S. Massey, The Theory of Atomic Collisions, Third ed., Oxford University Press, Oxford, 1987.
[2] J. Kessler, Polarized Electrons, Second ed., Springer, Berlin, 1985.
[3] T.J. Gay, F.B. Dunning, Rev. Sci. Instrum. 63 (1992) 1635.
[4] J. Fabian, S. Das Sarma, J. Vac. Sci. Technol. B 17 (1999) 1708.
[5] I. Žutić, J. Supercond. 15 (2002) 5.
[6] J.M. Kikkawa, D.D. Awschalom, Phys. Rev. Lett. 80 (1998) 4313.
[7] J. Kikkawa, D.D. Awschalom, Nature 397 (1999) 139.
[8] G. Dresselhaus, Phys. Rev. 100 (1955) 580.
[9] Yu.A. Bychkov, E.I. Rashba, J. Phys. C 17 (1984) 6039.
[10] S. Datta, B. Das, Appl. Phys. Lett. 56 (1990) 665.
[11] G. Prinz, Science 282 (1998) 1660.
[12] D. Bimberg, Semiconductors 33 (1999) 951.
[13] G. Bastard, Wave Mechanics Applied to Semiconductor Heterostructures, Les Edition de Physique, Les Ulis, 1990.
[14] E.A. de Andrada e Silva, G.C. La Rocca, F. Bassani, Phys. Rev. B 55 (1997) 16293.
[15] Th. Schäpers, G. Engels, J. Lange, Th. Klocke, M. Hollfelder, H. Lüth, J. Appl. Phys. 83 (1998) 4324.
[16] L.S. Rodberg, R.M. Thaler, Introduction to the Quantum Theory of Scattering, Academic Press, New York, 1967.
[17] C.J. Joachain, Quantum Collision Theory, North-Holland, Amsterdam, 1979.
[18] G. Bergmann, Phys. Rev. B 63 (2001) 193101.
[19] A. Crépieux, P. Bruno, Phys. Rev. B 64 (2001) 014416.
[20] V.N. Abakumov, I.Y. Yasievich, Zh. Eksp. Teor. Fiz. 61 (1972) 2571 Sov. Phys. JETP 34 (1972) 1375.
[21] V.N. Abakumov, V.V. Akulinichev, I.Y. Yasievich, Fiz. Thekh. Poluprovod. 9 (1975) 936 Sov. Phys. Semicond. 9 (1975) 612.

Spin-orbit interaction and electron elastic scattering from impurities in quantum wells

H. C. Huang, O. Voskoboynikov, and C. P. Lee
National Chiao Tung University, 1001 Ta Hsueh Road, Hsinchu, 300, Taiwan, Republic of China
(Received 4 November 2002; revised manuscript received 24 February 2003; published 30 May 2003)

We present a theoretical study of the spin-dependent scattering of electrons from screened impurities in III-V semiconductor quantum wells. Our calculation is based on the effective one-electronic-band Hamiltonian and the spin-orbit coupling with the Coulombic potential of the impurities. We demonstrate that the spin-orbit interaction can lead to recognizable magnitudes of spin asymmetry in the elastic-scattering cross section. Fairly large values of the Sherman function (about 0.01) are obtained for repulsive and attractive impurities in quantum wells of narrow gap semiconductors.

DOI: 10.1103/PhysRevB.67.195337 PACS number(s): 71.70.Ej, 72.10.−d, 73.21.Fg

I. INTRODUCTION

A large number of studies of the electron transport in two-dimensional (2-D) semiconductor systems has been carried out over the past 40 years (see, for instance, Refs. 1–8). This is especially important for electronic applications. Progress in modern semiconductor technologies has allowed us to experimentally and theoretically model the various scattering mechanisms in 2-D semiconductor structures within a wide range of material parameters.[4–8] It is commonly accepted now that the electron mobility of a semiconductor 2-D heterostructure is determined by impurity scattering at low temperatures and by the phonon scattering at high temperatures.

Recently there has been renewed interest in spin-dependent scattering and transport phenomena in semiconductor heterostructures because a branch of semiconductor electronics so called spintronics, has become a focus of interest (see Refs. 9–12, and references therein). The extra degree of freedom provided by the electron spin opens a new field for the development of semiconductor devices. In principle, one can use the semiconductor approach to generate, control, and detect electron-spin polarization.[11,13] This approach has the advantage of being compatible with conventional semiconductor technology.

In the absence of magnetic impurities, the main source of spin-dependent scattering processes at low temperatures is spin-orbit coupling to local defects. The effect of spin-orbit interaction on spin relaxation for semiconductor 2-D systems also has been studied for a long time.[14–17] Recently coherent spin transport has been demonstrated in homogeneous semiconductors and heterostructures.[19,18] Unfortunately, the theory of spin-dependent transport for semiconductor 2-D systems is still far from being complete. For this reason we recently investigated spin-dependent elastic-scattering processes in semiconductors in the presence of spin-orbit interaction.[20,21] In 2-D quantum wells,[20] this effect is expected to be stronger than that in the bulk[21] because of the localization of electronic wave functions in the conductive channel. It should be noted that the problem remains complicated even for the simplest models of 2-D electron motion because, in general, spin-orbit interaction should be described by a three-dimensional model.

Using the delta-doping technique, Coulomb attractive and repulsive impurities can be precisely placed in heterostructures. Using this fact one can model theoretically the scattering from the impurities located inside[2] or outside[22] the conductive channel. Most of the theoretical simulations of 2-D electron elastic-scattering processes from the impurities were conducted in detail in the first Born approximation.[2,4] However, it is well known that when perturbation theory is used, the dependence on spin in the elastic cross section appears only in the approximation that follows the first Born approximation.[23–26] For this reason, one should use other approaches in calculations of the spin-dependent scattering cross section. In particular, this is the partial-wave approach,[25,27] which was also used in some simulations of the spin-independent elastic-scattering cross section when the first Born approximation is not applicable.[28–30]

In this paper we calculate the spin-dependent elastic-scattering cross section for electrons scattered by impurities in 2-D heterostructures of III-V semiconductors. We use the effective one-electronic-band Hamiltonian[23] with Ben-Daniel-Duke boundary conditions for electronic envelope functions to calculate the spin-dependent cross section for electrons scattered from repulsive and attractive isolated impurities with spin-orbit coupling.[24–26] The impurities are located inside the quantum well. For narrow gap semiconductor quantum wells (systems with large spin-orbit coupling parameters) we found a large spin-related asymmetry in the cross section.

The paper is organized as follows: Section II begins with an introduction to the effective one-electronic-band 2-D Hamiltonian with impurities located inside semiconductor quantum wells. Section III gives details of the variable phase approach to spin-dependent elastic scattering in 2-D systems. The calculation results are presented in Sec. IV and conclusions are given in Sec. V.

II. BASIC EQUATIONS

We consider electrons in semiconductor heterostructures with charged impurities and use the approximate one-electronic-band effective Hamiltonian for the electron envelope wave functions

$$\hat{H}=\hat{H}_0+\hat{V}_{im}(\mathbf{r}). \tag{1}$$

In Eq. (1) $\hat{H}_0$ is the Hamiltonian of the system without impurities,[31–34]

$$\hat{H}_0 = -\frac{\hbar^2}{2}\nabla_{\mathbf{r}}\left[\frac{1}{m(E,\mathbf{r})}\right]\nabla_{\mathbf{r}} + V(\mathbf{r}),$$

where $\nabla_{\mathbf{r}}$ stands for the spatial gradient; $m(E,\mathbf{r})$ is the energy and position-dependent electron effective mass,

$$\frac{1}{m(E,\mathbf{r})} = \frac{2P^2}{3\hbar^2}\left[\frac{2}{E+E_g(\mathbf{r})-V(\mathbf{r})} + \frac{1}{E+E_g(\mathbf{r})+\Delta(\mathbf{r})-V(\mathbf{r})}\right],$$

where $V(\mathbf{r})$ is the confinement potential of the well; E is the electron energy; $E_g(\mathbf{r})$ and $\Delta(\mathbf{r})$ stand for the position-dependent band gap and the spin-orbit splitting in the valence band; P is the momentum matrix element; and $\hat{V}_{im}(\mathbf{r})$ is the scattering potential of the impurity.

The impurity scattering potential consists of two parts,

$$V_i(\mathbf{r}) = V_{ic}(\mathbf{r}) + V_{iso}(\mathbf{r}),$$

where $V_{ic}(\mathbf{r})$ is the Coulomb potential of the charged impurity and $V_{iso}(\mathbf{r})$ describes the spin-orbit interaction of electrons with the impurity

$$V_{iso}(\mathbf{r}) = -i\gamma(E,\mathbf{r})\nabla V_{ic}(\mathbf{r})\cdot[\hat{\boldsymbol{\sigma}}\times\nabla_{\mathbf{r}}], \tag{2}$$

where[32,34]

$$\gamma(E,\mathbf{r}) = \frac{P^2}{3}\left\{\frac{1}{[E+E_g(\mathbf{r})-V(\mathbf{r})]^2} - \frac{1}{[E+E_g(\mathbf{r})+\Delta(\mathbf{r})-V(\mathbf{r})]^2}\right\}. \tag{3}$$

The spin-orbit interaction in the form of Eq. (2) is the generalization of the well-known Rashba spin-orbit interaction,[33] which comes from system inversion asymmetry.[32,34] In semiconductor structures with the average uniform electric field $\mathbf{F}$ one can consider

$$\mathbf{F} = -\frac{1}{e}\nabla\tilde{V}_p(\mathbf{r}),$$

where e is the electron charge and $\tilde{V}_p(\mathbf{r})$ is the average space-charge electric potential. When the electron with the wave vector $\mathbf{k}\perp\mathbf{F}$ is moving in the field, one can readily obtain from Eq. (2) the well-known Rashba interaction

$$V_{so}(\mathbf{r}) = \alpha\mathbf{n}\cdot[\hat{\boldsymbol{\sigma}}\times\mathbf{k}],$$

where $\alpha = -e\gamma F$ and $\mathbf{n}$ is the unit vector parallel to the field.[33]

Here we consider III-V semiconductor symmetrical quantum wells of thickness L. In the structure we denote by z the direction perpendicular to the well interfaces, and $\rho=(x,y)$ is the position vector parallel to the interfaces ($z=0$ is the center of the well). For systems with sharp discontinuity in the conduction-band edge between the quantum well (material 1) and the barrier region (material 2) the potential can be presented as

$$V(\mathbf{r}) = \begin{cases} 0, & -\frac{L}{2} \leqslant z \leqslant \frac{L}{2}; \quad (\mathbf{r}\in 1), \\ V_0, & |z| > \frac{L}{2}; \quad (\mathbf{r}\in 2). \end{cases} \tag{4}$$

We assume that an isolated impurity is located at $z=d$ and the unscreened Coulomb potential of the impurity is given as

$$V_{ic}^0(\mathbf{r}) = \frac{Ze^2}{\varepsilon_s[\rho^2+(z-d)^2]^{1/2}}, \tag{5}$$

where ε_s is the relative permittivity of the system and Z is the charge of the impurity. For most III-V quantum wells we can neglect the image potential and use for simplicity $\varepsilon_s = (\varepsilon_1+\varepsilon_2)/2$ (ε_1 and ε_2 are the dielectric constants of materials 1 and 2, correspondingly).

Following Refs. 1, 2, and 31 we present the solution of the confinement problem with the Hamiltonian $\hat{H}_0$ as

$$\Psi_{n,s}(\boldsymbol{\rho},z) = \psi^s(\boldsymbol{\rho})\varphi_n(z),$$

where n labels the eigenenergies in the normal direction (E_n), and $s=\pm 1$ is the quantum number related to the spin polarization along the z direction.

As is shown in Ref. 32, due to the reflection symmetry of the well in the z direction (there are no built-in electric fields) the Rahsba spin splitting in the electron spectrum does not occur and one can use the conventional Ben-Daniel-Duke boundary conditions[31] for the wave function $\varphi_n(z)$,

$$\varphi_n(z), \quad \frac{1}{m(E,z)}\frac{d}{dz}\varphi_n(z)$$

continuous at

$$z = \pm\frac{L}{2}. \tag{6}$$

Considering for simplification only the first subband as being populated we describe only intrasubband elastic-scattering processes. First we obtain the ground state (the first subband with $n=1$). The wave function of this ground state has the well-known form

$$\varphi_1(z) = \begin{cases} A\cos\kappa z, & |z| \leqslant \frac{L}{2}; \\ B\exp(-\mu z), & |z| > \frac{L}{2}; \end{cases} \tag{7}$$

where

$$\kappa = \sqrt{2m_1(E)E_1}/\hbar,$$

$$\mu = \sqrt{2m_2(E)(V_0-E_1)}/\hbar,$$

and $E=E_\rho+E_1$ consists of the energies of the ρ and z directions of motion, correspondingly. From the Ben-Daniel-Duke boundary conditions (6) we obtain the spinless transcendental equation

$$\tan[\kappa(E_\rho,E_1)L/2]=\frac{m_1(E)\mu(E_\rho,E_1)}{m_2(E)\kappa(E_\rho,E_1)}. \tag{8}$$

Equation (8) gives us the eigenenergy in the z direction in an implicit form.

The wave function (7) (after proper normalization), we substitute into the three-dimensional Schrödinger equation with the Hamiltonian (1) and integrate out the z coordinate by taking the average,

$$\hat{H}_\rho=\int_{-\infty}^{+\infty}dz\varphi_1^*(z)\hat{H}\varphi_1(z).$$

After the averaging and introducing the screening of the impurity at low temperatures by means of Refs. 1 and 23 the quasi-2-D Schrödinger equation in the polar coordinates $\rho=(\rho,\phi)$ is given by

$$\left[\frac{1}{\rho}\frac{\partial}{\partial\rho}\left(\rho\frac{\partial}{\partial\rho}\right)-\frac{1}{\rho^2}\frac{\partial^2}{\partial\phi^2}-\tilde{V}(\rho)+is\tilde{W}(\rho)\frac{\partial}{\partial\phi}+k^2\right]\psi^s(\boldsymbol{\rho})=0, \tag{9}$$

where

$$\tilde{V}(\rho)=\frac{2Z}{a_B^*}\frac{\tilde{m}(E)}{m_1(0)}\int_0^\infty\frac{dq}{\varepsilon(q)}J_0(q\rho)\int_{-\infty}^{+\infty}dz|\varphi_1(z)|^2e^{-q|z-d|}$$

is the statically screened Coulomb potential in the quantum well plane,

$$\tilde{W}(\rho)=-\frac{2Z}{a_B^*\rho}\frac{\tilde{m}(E)}{m_1(0)}\int_0^\infty\frac{qdq}{\varepsilon(q)}J_1(q\rho)\times\left[\alpha_1(E)\int_{z\leqslant|L/2|}dz|\varphi_1(z)|^2e^{-q|z-d|}+\alpha_2(E)\int_{z\geqslant|L/2|}dz|\varphi_1(z)|^2e^{-q|z-d|}\right]$$

is the screened spin-orbit interaction, $a_B^*=\varepsilon_s\hbar^2/e^2m_1(0)$ is the effective Bohr radius in the well,

$$k^2=\frac{2\tilde{m}(E)E_\rho}{\hbar^2},$$

$$\frac{1}{\tilde{m}(E)}=\frac{1}{m_1(E)}\int_{z\leqslant|L/2|}dz|\varphi_1(z)|^2+\frac{1}{m_2(E)}\int_{z\geqslant|L/2|}dz|\varphi_1(z)|^2,$$

$J_n(x)$ is the Bessel function,

$$\varepsilon(q)=1+\frac{q_f}{q}$$

is the 2-D electronic dielectric function,

$$q_f=\frac{e^2m_1(E_F)}{2\pi\hbar^2\varepsilon_s}\left\{1+\frac{d}{dE}\ln[m_1(E)]\Big|_{E_F}\right\}$$

is the 2-D Thomas-Fermi screening constant in the degenerated electronic system, and E_F is the Fermi energy of the system.[35] The Fermi wave vector $k_F(E_F)$ must be defined by means of the solution of the following equation:

$$E_F=\frac{\hbar^2k_F^2}{2m_1(E_F)}.$$

III. TWO-DIMENSIONAL ELASTIC SCATTERING AND SHERMAN FUNCTION

Due to the radial symmetry of the potentials $\tilde{V}_c(\rho)$ and $\tilde{W}(\rho)$ in Eq. (9) the method of partial waves is convenient for our consideration. One can separate variables in the expression for the wave function as the following:[23–25]

$$\psi^s(\boldsymbol{\rho})=\sum_{l=-\infty}^{l=+\infty}R_l^s(\rho)e^{il\phi}\boldsymbol{\chi}^s,$$

where l is the orbital momentum number and χ^s is a spin function upon which the Pauli matrix vector operates,

$$\boldsymbol{\chi}^{+1}=\begin{pmatrix}1\\0\end{pmatrix},\quad \boldsymbol{\chi}^{-1}=\begin{pmatrix}0\\1\end{pmatrix}.$$

The Schrödinger equation for the radial wave function becomes of the following form:

$$\left[\frac{1}{\rho}\frac{d}{d\rho}\left(\rho\frac{d}{d\rho}\right)-\frac{l^2}{\rho^2}-\tilde{V}(\rho)-sl\tilde{W}(\rho)+k^2\right]R_l^s(\rho)=0.$$

At a large distance from the scattering center the asymtotic value of the radial function is given by

$$R_l^s(\rho)\to A_l^s[\cos\delta_l^sJ_l(k\rho)-\sin\delta_l^sN_l(k\rho)];\quad \rho\to\infty,$$

where δ_l^s is the spin-dependent scattering phase shift[24–27] and N_l is the Neumann function.

In the variable phase approach[27,36] the phase function $\delta_l^s(\rho)$ at the point ρ determines the phase shift produced by the part of the potential contained within the cycle of a radius ρ. The scattering phase shift for the total potential is equal to the asymptotic value

$$\delta_l^s=\lim_{\rho\to\infty}\delta_l^s(\rho).$$

The phase function $\delta_l^s(\rho)$ satisfies the following differential equation:[27,36]

$$\frac{d\delta_l^s(\rho)}{d\rho} = -\frac{\pi}{2}\rho[\tilde{V}(\rho) + sl\tilde{W}(\rho)][\cos\delta_l^s(\rho)J_l(k\rho) - \sin\delta_l^s(\rho)N_l(k\rho)]^2 \quad (10)$$

with the boundary condition

$$\delta_l^s(0) = 0. \quad (11)$$

The complex 2-D scattering amplitude can be expressed as[20,24,25]

$$\mathbf{F}^s(\theta) = [f(\theta) + \sigma_z g(\theta)]\chi^s, \quad (12)$$

where $f^s(\theta)$ and $g(\theta)$ describe scattering without and with electron-spin reorientation, and they are determined by the expressions

$$f(\theta) = \sum_{l=0}^{\infty} f_l \cos(l\theta), \quad (13)$$

$$g(\theta) = \sum_{l\geqslant 1}^{\infty} g_l \sin(l\theta), \quad (14)$$

where

$$f_l = \sqrt{\frac{1}{2\pi k}} \begin{cases} \exp(2i\delta_0) - 1; & l = 0; \\ \exp(i2\delta_l^+) + \exp(i2\delta_l^-) - 2; & l \geqslant 1; \end{cases}$$

$$g_l = i\sqrt{\frac{1}{2\pi k}}[\exp(i2\delta_l^+) - \exp(i2\delta_l^-)],$$

where θ is the scattering angle between initial ($\mathbf{k}_i$) and final ($\mathbf{k}_f$) wave vectors.

The Mott scattering[24] cross section for electrons spin polarized parallel to the z axis can be expressed in terms of the incident electron-beam spin polarization P_i along the z direction as the following:

$$\sigma(\theta) = I(\theta)[1 + S(\theta)P_i], \quad (15)$$

where $I(\theta)$ is the differential cross section for unpolarized incident electrons,

$$I(\theta) = |f(\theta)|^2 + |g(\theta)|^2, \quad (16)$$

and

$$S(\theta) = \frac{f^*(\theta)g(\theta) + f(\theta)g^*(\theta)}{|f(\theta)|^2 + |g(\theta)|^2} \quad (17)$$

is the Sherman function for 2-D electrons. The Sherman function is an important characteristic of the spin-dependent scattering (see Refs. 37 and 38, and references therein). It presents the left-right asymmetry in the scattering cross section for initially polarized electron beams and the average polarization of unpolarized electrons after the scattering. This characteristic is important in the evaluations of the anomalous Hall effect in different materials and structures. For degenerated electronic systems, for instance, the Hall angle is proportional to the Sherman function at the Fermi energy shell.[26,39–41]

IV. CALCULATION RESULTS

To present the realistic estimation of the effect of the spin-orbit coupling on the electron elastic cross section we choose two types of symmetrical quantum well structures: type I is $Al_{0.48}In_{0.52}As/In_{0.53}Ga_{0.47}As/Al_{0.48}In_{0.52}As$ (where $E_{g1} = 0.813$ eV, $E_{g2} = 1.508$ eV, $\Delta_1 = 0.361$ eV, $\Delta_2 = 0.332$ eV, $m_1(0) = 0.041m_0$, $m_2(0) = 0.075m_0$, $\varepsilon_1 = 14$, $\varepsilon_2 = 12.5$, $V_0 = 0.504$ eV,[41] $m_0 is$ the free-electron mass) and type II is CdTe/InSb/CdTe [where $E_{g1} = 0.24$ eV, $E_{g2} = 1.59$ eV, $\Delta_1 = 0.81$ eV, $\Delta_2 = 0.8$ eV, $m_1(0) = 0.015m_0$, $m_2(0) = 0.08m_0$, $\varepsilon_1 = 16.8$, $\varepsilon_2 = 10.2$, $V_0 = 0.55$ eV (Refs. 42 and 43)]. While type I presents quantum well structures with well-developed growth technology, type II demonstrates

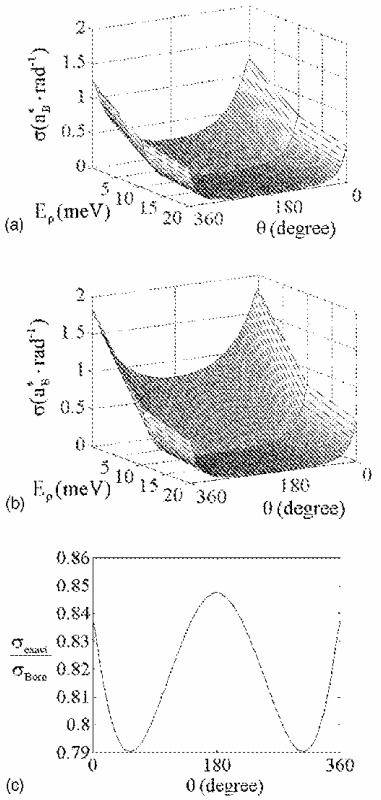

FIG. 1. The scattering cross section for the screened impurities in the type-I structure ($L = 20$ nm): (a) repulsive ($Z = +1$) impurity; (b) attractive ($Z = -1$) impurity; (c) the ratio between the complete numerical result (σ_{exact}) and the first Born approximation (σ_{Born}) for the repulsive impurity when $ka_B^* = 1.8$ ($E_\rho = 0.01$ eV).

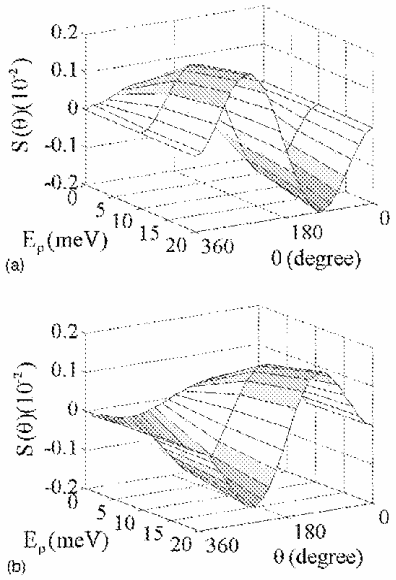

FIG. 2. The Sherman function for the type-I structure ($L=20$ nm): (a) repulsive impurity; (b) attractive impurity.

the largest spin-coupling effects. In all calculations we assure the validity of the one-subband scattering model,when the intersubband gap is larger than the energy of the ρ-direction motion: $E_\rho < E_2 - E_1$. This allows us to consider scattering of electrons with the following wave vectors: for type-I structures with $L \leqslant 30$ nm, $k \leqslant k_F^I = 2.5(a_B^*)^{-1}$ (the electron concentration $n_s = 3.5\times 10^{11}$ cm^{-2}); for type-II structures with $L \leqslant 30$ nm, $k \leqslant k_F^{II} = 6.6(a_B^*)^{-1}$ ($n_s = 3\times 10^{11}$ cm^{-2}). Notice that a_B^* is taken to be different according to the definitions for the different types of the systems.

The phase shifts were obtained by the numerical solution of Eq. (10) with the initial condition of Eq. (11) and then used in Eqs. (12)–(17) to calculate the elastic-scattering cross section. From our calculation experience the convergence criteria on the cross section (the maximum net error is less than 10^{-4}) can be reached by taking the necessary number $|l| \leqslant 70$ of the partial waves included Eqs. (13) and (14). Figure 1 shows energy and angle dependencies of the elastic-scattering cross section for 2-D electrons scattered from attractive ($Z=+1$) and repulsive ($Z=-1$) impurities located in the center of the type-I structure. The cross sections demonstrate the well-known logarithmic divergence at zero energy ($E_\rho \to 0$) for both types of impurities (repulsive and attractive).[28] In Fig. 1(c) we compare our results with the cross section obtained within the first Born approximation[27,28] when

$$f_l \approx -\sqrt{\frac{\pi}{2k}}\int_0^\infty J_l^2(k\rho)\tilde{V}(\rho)\rho d\rho \times \begin{cases} 1, & l=0; \\ 2, & l \geqslant 1; \end{cases} \qquad (18)$$

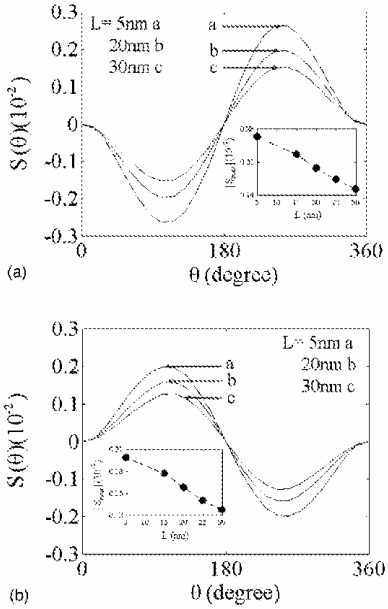

FIG. 3. The Sherman function for the type-I structures with different well widths ($E_\rho = 0.02$ eV): (a) repulsive impurity; (b) attractive impurity. Insets: the dependencies of the Sherman function amplitude on the well width.

$$g_l \approx il\sqrt{\frac{\pi}{2k}}\int_0^\infty J_l^2(k\rho)\tilde{W}(\rho)\rho d\rho \times \begin{cases} 1, & l=0; \\ 2, & l \geqslant 1. \end{cases} \qquad (19)$$

It is known[1,44] that the first Born approximation is valid for 2-D elastic scattering when

$$ka_B^* \gg 1.$$

It is worth noting, that the numerically calculated cross section for the 2-D screened Coulomb potential is different from that obtained in the first Born approximation near the edge of the approximation validity ($ka_B^* = 1.8$). In addition, it can be seen from Eqs. (18) and (19) that in the first Born approximation all spin-polarization effects in the elastic cross section vanish:[23,24,26]

$$S(\theta) \sim f^*(\theta)g(\theta) + f(\theta)g^*(\theta) = 0.$$

Thus, the Sherman function should be calculated only by going beyond the first Born approximation and taking into consideration the higher partial waves ($|l|>0$). The complete numerical solution allows us to do that.

Figure 2 shows the Sherman functions for the type-I structure, when the repulsive [Fig. 1(a)] and attractive [Fig. 1(b)] impurities are located in the center of the well with the width $L=20$ nm. We first note that, in the energy range considered, the effect is slightly larger for the repulsive scattering center. Since $S(\theta)$ is closely connected to the cross sec-

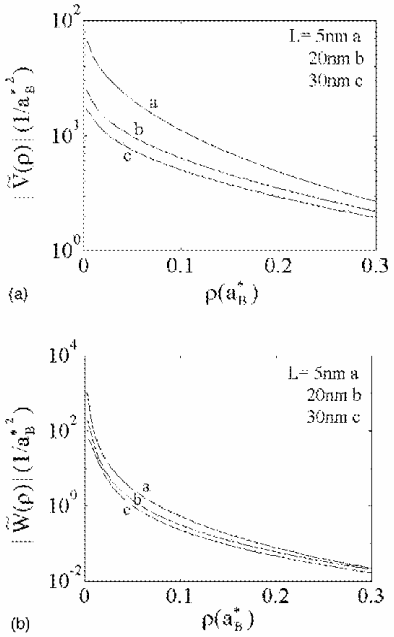

FIG. 4. The dependencies of the effective averaged potentials on the well width for the type-I structures: (a) spinless part $\tilde{V}(\rho)$, (b) spin-orbit coupling part $\tilde{W}(\rho)$.

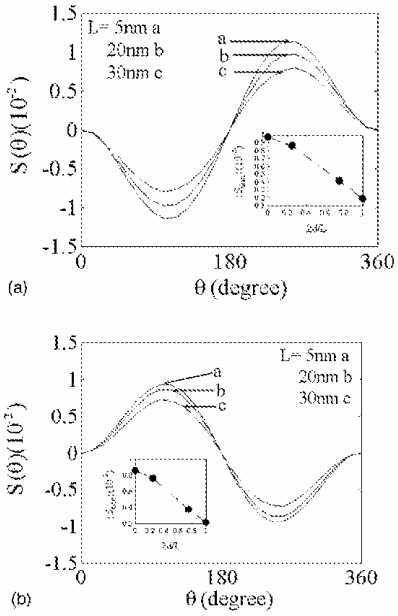

FIG. 5. The Sherman function for the type-II structures with different well widths (E_ρ=0.04 eV): (a) repulsive impurity; (b) attractive impurity. Insets: the dependencies of the Sherman function amplitude on the impurity location in the well.

tion curves, the high values of the Sherman function occur where the cross-section is small and vice versa. The change of the impurity sign leads to inversion in the three-dimensional plots. This is a direct and clear consequence of sign altering in the potentials $\tilde{V}(\rho)$ and $\tilde{W}(\rho)$ [see Eq. (10)]. It can be seen that with suitable electron energies and the large scattering angles one can reach polarizations of more than 0.1%.

In our simulation we found a decrease in the polarization effect when well width increases. The dependence of the Sherman function on the well width L for the type-I structure is presented in Figs. 3(a) and 3(b) (the impurity is located in the center of the well: $d=0$). This decrease is obviously connected to the form of the averaged effective potentials $\tilde{V}(\rho)$ and $\tilde{W}(\rho)$. The various potentials for different well widths are shown in Fig. 4. The curves represent the absolute value of the potentials [for the repulsive center $\tilde{V}(\rho)$ is positive and $\tilde{W}(\rho)$ is negative; for the attractive center $\tilde{V}(\rho)$ is negative and $\tilde{W}(\rho)$ is positive] and demonstrate the influence of the 2-D confinement and screening on the elastic scattering processes in quantum wells.[2,3,28] The figure shows that the spin-orbit coupling potential becomes stronger near the impurity site when the well width decreases. Electrons that are scattered at large angles (where the polarization effects are expected to be higher) pass through the relatively strong fields at fairly small distances from the impurity site. This causes the stronger polarization effects for the relatively narrow wells (as is shown in the insets of the Fig. 3). This result suggests the possibility of controlling Sherman function by means of the well size.

The spin-orbit interaction is known to be larger in small gap semiconductors. Based on this fact, we show in Fig. 5, as an example, the calculation results for the type-II structures. The asymmetry effect in the scattering cross section for those structures can reach about 1% for electrons with moderate energy, when the impurity is located in the center of the well. The insets show the dependencies of the amplitude of the Sherman function on the position of the impurity in the wells. Obviously, the magnitude of the Sherman function decreases when d increases. But the effect remains valuable even for the impurities located at the edge of the well ($d=L/2$).

In addition, we notice that the spin-dependent asymmetry for the elastic-scattering cross section for the impurities located in the wells (2-D systems) is significantly larger than calculated for 3-D spin-dependent elastic scattering from impurities in the bulk. To demonstrate the difference we present in Table I our results for the type-II structure and results obtained in Ref. 26 and 39, when all parameters of the systems are chosen the same (the systems differ only in the dimensionality). In the table, δ_0 is the phase shift for $l=0$ and δ_1^{spin} is the correction to the phase shift of the partial wave with $l=1$ when the spin-orbit coupling is included.

TABLE I. The ratio $\nu=\delta_1^{spin}/\delta_0$ for InSb structures ($L=5$ nm).

Impurity type	ν for 3-D system [a]	ν for 2-D system
$Z=-1$	3.7×10^{-5}	2.8×10^{-2}
$Z=+1$	2.3×10^{-6}	2.7×10^{-2}

[a]Reference 26.

This result suggests that the spin-orbit coupling with the charged impurities in 2-D systems can provide sufficiently larger spin-dependent effects than those in the bulk.

V. CONCLUSIONS

We have presented a theoretical study of the elastic spin-dependent scattering of 2-D electrons from the screened Coulomb centers located in quantum wells. The one-electronic-band effective Hamiltonian and spin-orbit coupling potential of the impurities allow us to calculate the left-right asymmetry in the electron elastic-scattering cross section. We have found a large spin-dependent asymmetry in the cross section for electrons scattered from impurities in AlInAs/InGaAsAs/AlInAs and CdTe/InSb/CdTe symmetrical quantum wells.

For the CdTe/InSb/CdTe quantum well we found that the spin-orbit coupling in the two-dimensional systems leads to larger spin-dependent asymmetry in the scattering cross section than that in the bulk. The calculated amplitude of the Sherman function for this structure is more than 0.01. This could be detected in the measurements of the Hall effect at low temperatures[26,39,40,45] and this is potentially useful in integrated electron-spin polarization devices based on semiconductor heterostructures. It also can be used as a tool to determine spin-coupling parameters in III-V narrow gap semiconductor heterostructures.

Finally, we would like to point out that the described effect is a clear analog of the well-known effect of spin-dependent scattering in magnetic materials (see Ref. 37), but it can also be realized in nonmagnetic semiconductor structures. Our model can be used as the starting point for more detailed calculations. Experimental investigations need to be conducted to verify our theory predictions.

ACKNOWLEDGMENTS

This work was supported by the National Science Council of the Republic of China under Contract Nos. NSC-90-2215-E-009-022 and NSC-91-2119-M-009-003.

[1]F. Stern and W. E. Howard, Phys. Rev. **163**, 816 (1967).
[2]T. Ando, A. B. Fowler, and F. Stern, Rev. Mod. Phys. **54**, 437 (1982).
[3]C. Weisbuch and B. Vinter, *Quantum Semiconductor Structures, Fundamental and Applications* (Academic, New York, 1991).
[4]W. Walukiewicz, H. E. Ruda, J. Lagowski, and H. C. Gatos, Phys. Rev. B **30**, 4571 (1984).
[5]L. Pfeiffer, K. W. West, H. L. Stormer, and K. W. Baldwin, Appl. Phys. Lett. **33**, 665 (1978).
[6]M. Kudo, T. Mishima, T. Tanitomo, and M. Washima, Jpn. J. Appl. Phys., Part 1 **33**, 971 (1994).
[7]M. L. Ke, D. Westwood, R. H. Williams, and M. J. Godfrey, Phys. Rev. B **51**, 5038 (1995).
[8]J. Dickman, Appl. Phys. Lett. **60**, 88 (1992).
[9]G. A. Prinz, Science **282**, 1660 (1998).
[10]J. Fabian and S. Das Sarma, J. Vac. Sci. Technol. B **17**, 1708 (1999).
[11]H. Ohno, J. Vac. Sci. Technol. B **18**, 2039 (2000).
[12]P. R. Hammar and M. Johnson, Phys. Rev. B **61**, 7207 (2000).
[13]C. M. Hu, J. Nitta, A. Jensen, J. B. Hansen, H. Takayanagi, T. Matsuyama, D. Heitman, and U. Merkt, J. Appl. Phys. **97**, 7251 (2002).
[14]M. I. D'yakonov and V. Yu. Kachorovskii, Fiz. Tekh. Poluprovodn. **20**, 178 (1986) [Sov. Phys. Semicond. **20**, 100 (1986)].
[15]Y. A. Bychkov and E. I. Rashba, Pis'ma Zh. Éksp. Teor. Fiz. **39**, 66 (1984) [JETP Lett. **39**, 78 (1984)].
[16]V. M. Edelstein, Physica B **284–288**, 1217 (2000).
[17]T. P. Pareek and P. Bruno, Pramana, J. Phys. **57**, 1 (2002).
[18]J. M. Kikkawa and D. D. Awschalom, Phys. Rev. Lett. **80**, 4313 (1998).
[19]I. Malajovich, J. M. Kikkawa, D. D. Awschalom, J. J. Berry, and N. Samarth, Phys. Rev. Lett. **84**, 1015 (2000).
[20]O. Voskoboynikov, H. C. Huang, C. P. Lee, and O. Tretyak, Physica E (Amsterdam) **12**, 252 (2002).
[21]Edward Chen, O. Voskoboynikov, and C. P. Lee, Solid State Commun. **125**, 381 (2003).
[22]W. T. Masselink, Phys. Rev. Lett. **66**, 1513 (1991).
[23]A. S. Davydov, *Quantum Mechanics* (Pergamon, London, 1965).
[24]N. F. Mott and H. S. Massey, *The Theory of Atomic Collisions*, 3rd ed. (Oxford University, London, 1987).
[25]C. J. Joachain, *Quantum Collision Theory* (North-Holland, Amsterdam, 1979).
[26]V. N. Abakumov and I. N. Yassievich, Zh. Éksp. Teor. Fiz. **61**, 2571 (1972) [Sov. Phys. JETP **34**, 1375 (1972)].
[27]F. Cologero, *Variable Phase Approach to Potential Scattering* (Academic, New York, 1967).
[28]P. G. Averbuch, J. Phys. A **19**, 2325 (1986).
[29]I. A. Larkin, Fiz. Tekh. Poluprovodn. **22**, 2008 (1988) [Sov. Phys. Semicond. **22**, 1271 (1988).
[30]M. E. Portnoi and I. Galbreith, Solid State Commun. **103**, 325 (1997).
[31]G. Bastard, *Wave Mechanics Applied to Semiconductor Heterostructures* (Les Editions de Physique, Les Ulis, 1990).
[32]E. A. de Andrada e Silva, G. C. La Rocca, and F. Bassani, Phys. Rev. B **55**, 16 293 (1997).
[33]Yu. A. Bychkov and E. I. Rashba, J. Phys. C **17**, 6039 (1984).
[34]Th. Schäpers, G. Engels, J. Lange, Th. Klocke, M. Hollfelder, and H. Lüth, J. Appl. Phys. **83**, 4324 (1998).
[35]D. K. Ferry and S. M. Goodnick, *Transport in Nanostructures*

(Cambrige University, Cambridge, England, 1997).
[36] A.G. Sitenko, *Scattering Theory* (Springer-Verlag, Berlin, 1990).
[37] J. Kessler, *Polarized Electrons* (Springer-Verlag, Berlin, 1985).
[38] T. J. Gay and F. B. Dunning, Rev. Sci. Instrum. **63**, 1635 (1992).
[39] J. N. Chazalviel, Phys. Rev. B **11**, 3918 (1975).
[40] G. Bergmann, Phys. Rev. B **63**, 193101 (2001).
[41] S. L. Chuang, *Physics of Optoelectronic Devices* (Wiley-Interscience, New York, 1995).
[42] E. T. Yu, J. O. McCaldin, and T. C. McGill, Solid State Phys. **46**, 2 (1992).
[43] *Handbook Series on Semiconductor Parameters*, edited by M. Levinshtein, S. Rumyantsev, and M. Shur (World Scientific, Singapore, 1999).
[44] G. Barton, Am. J. Phys. **51**, 420 (1983).
[45] A. Crépieux and P. Bruno, Phys. Rev. B **64**, 014416 (2001).

JOURNAL OF APPLIED PHYSICS VOLUME 95, NUMBER 4 15 FEBRUARY 2004

Spin-dependent Hall effect in semiconductor quantum wells

H. C. Huang, O. Voskoboynikov,[a] and C. P. Lee
National Chiao Tung University, 1001 Ta Hsueh Rd., Hsinchu, 300, Taiwan, Republic of China

(Received 21 July 2003; accepted 21 November 2003)

We present a theoretical study of the spin-dependent scattering of electrons from screened attractive and repulsive impurities in III-V semiconductor quantum wells. The effective one-band Hamiltonian and the Rashba spin–orbit interaction are used. We demonstrated that the asymmetry of the spin-dependent skew-scattering and side-jump effect can lead to a quite large spin-dependent (anomalous) Hall effect at zero magnetic field in all-semiconductor quantum well structures. Our theory predicts a measurable spin-dependent Hall angle that reaches about 2.5×10^{-3} rad for a CdTe/InSb/CdTe quantum well with impurities doped in the center of the well. © *2004 American Institute of Physics.* [DOI: 10.1063/1.1641147]

I. INTRODUCTION

The extra degree of freedom provided by the electron spin may open up further enhancements for semiconductor devices. The spin-transistor proposed by Datta and Das[1] is an example of a spin-controlled device based on semiconductor two-dimensional (2-D) channels. For this reason, theoretical studies of spin-dependent electron processes in 2-D semiconductor structures have attracted a lot of interest since a particular branch of semiconductor electronics (so-called spintronics) has become a focus of study.[2–4]

Recently, detection of the electron polarization in paramagnetic metals[5,6] and semiconductors[7] through the spin-dependent Hall effect (SDHE) has been proposed. This is quite similar to the exploitation of the anomalous Hall effect (AHE), which can be observed in magnetic metals or semiconductors without external magnetic field (see, for instance Ref. 8, and references therein). The key point of the explanation of those effects is the presence of the spin–orbit interaction (SOI). Considerable work on the AHE has been done in the last 50 years since the pioneering work of Karplus and Luttinger.[9] It is generally recognized that two mechanisms contribute to the AHE. Those are the side-jump effect (SJ) proposed by Karplus and Luttinger[9] and Berger,[10] and the skew-scattering (SS) proposed by Smit.[11] It is commonly believed that the first mechanism can be more significant in metal alloys or semiconductors with relatively large resistivity, while the second one prevails in systems with low resistivity.

In the absence of magnetic impurities and at low temperatures, the main source of the spin-dependent scattering processes is the SO coupling to local defects. The effect of the SOI on the electron transport and relaxation in 2-D semiconductor systems has been studied for a long time.[12–15] We recently investigated the spin-dependent scattering processes in the bulk of nonmagnetic semiconductors in the presence of the SOI.[16] In semiconductor quantum wells (QWs) the effect of the SOI on the processes of scattering becomes even more stronger that in the bulk. This is a result of the localization of electrons' wave functions in the conduction channel.[17,18]

In this article, we present a model of the spin-dependent electron scattering from impurities located in the center QWs of nonmagnetic III-V semiconductors. We calculate contributions from the SS and SJ mechanisms to the SDHE. Our calculation is based on the effective-one-band Hamiltonian[19,20] and Rashba-type model of the SOI.[12,21,22] For QWs of narrow-gap semiconductors (systems with large SO coupling parameters) and with impurities located in the center of the wells, we obtained relatively large spin-dependent Hall angles (SOHAs).

The article is organized as follows. Section II describes the method we use to calculate the spin-dependent (Mott) cross section for 2-D electrons scattered from impurities in semiconductor QWs. Section III presents the method of calculation of the off-diagonal element of the conductivity tensor in QWs with account of the Mott scattering. The calculation results are presented in Sec. IV and conclusions are given in Sec. V.

II. BASIC EQUATIONS AND DESCRIPTION OF THE SPIN-DEPENDENT SCATTERING

We consider III-V semiconductor QWs with charged impurities and use the approximate one-electron-band effective Hamiltonian in the following form:[19,20]

$$\hat{H}=\hat{H}_0+\hat{V}_{\rm im}(\mathbf{r}), \tag{1}$$

where H_0 is the Hamiltonian of the system without impurities:

$$\hat{H}_0=-\frac{\hbar^2}{2}\nabla_{\mathbf{r}}\left[\frac{1}{m(E,\mathbf{r})}\right]\nabla_{\mathbf{r}}+V(\mathbf{r}).$$

$\hat{V}_{\rm im}(\mathbf{r})$ is the impurity potential, $\nabla_{\mathbf{r}}$ stands for the spatial gradient, $m(E,\mathbf{r})$ is the energy, and position-dependent electron effective mass is

[a]Electronic mail: vam@cc.nctu.edu.tw

$$\frac{1}{m(E,\mathbf{r})}=\frac{2P^2}{3\hbar^2}\left[\frac{2}{E+E_g(\mathbf{r})-V(\mathbf{r})}+\frac{1}{E+E_g(\mathbf{r})+\Delta(\mathbf{r})-V(\mathbf{r})}\right],$$

where E is the electron energy, $V(\mathbf{r})$ is the confinement potential of the well, $E_g(\mathbf{r})$ and $\Delta(\mathbf{r})$ stand for the position-dependent band gap and the SO splitting in the valence band, respectively, and P is the momentum matrix element.

The impurity potential consists of two parts,

$$\hat{V}_{\mathrm{im}}(\mathbf{r})=V_c(\mathbf{r})+V_{\mathrm{so}}(\mathbf{r}),$$

where $V_c(\mathbf{r})$ is the Coulomb potential of the charged impurity and $V_{\mathrm{so}}(\mathbf{r})$ describes the SO coupling with the impurity

$$V_{\mathrm{so}}(\mathbf{r})=i\alpha(E,\mathbf{r})\nabla V_c(\mathbf{r})\cdot[\hat{\boldsymbol{\sigma}}\times\nabla_{\mathbf{r}}],$$

where[12,18,21,22]

$$\alpha(E,\mathbf{r})=\frac{P^2}{3}\left[\frac{1}{[E+E_g(\mathbf{r})-V(\mathbf{r})]^2}-\frac{1}{[E+E_g(\mathbf{r})+\Delta(\mathbf{r})-V(\mathbf{r})]^2}\right]. \quad (2)$$

We describe symmetrical QWs of thickness L and denote by z the direction perpendicular to the well interfaces. For systems with sharp discontinuity in the conduction band edge between the QW (material 1) and the barrier region (material 2), the confinement potential can be presented as

$$V(\mathbf{r})=\begin{cases}0, & -L/2\leqslant z\leqslant L/2;(\mathbf{r}\in 1)\\ V_0, & |z|>L/2;(\mathbf{r}\in 2)\end{cases}. \quad (3)$$

We assume that an isolated impurity is located in the center of the wells ($z=0$), and the unscreened Coulomb potential of the impurity is given as

$$V_c^0(\mathbf{r})=-\frac{Ze^2}{4\pi\epsilon_s[\rho^2+z^2]^{1/2}}, \quad (4)$$

where $\boldsymbol{\rho}=(x,y)$ is the position vector parallel to the interfaces, $\epsilon_s=(\epsilon_1+\epsilon_2)/2$ is the average permittivity of the system, Z is the charge of the impurity, and e is the electron charge. For most III-V semiconductor QWs, we can neglect the image potential, and we assume that for simplicity.

The Rashba term in $\hat{H}_0$ does not occur due to the reflection symmetry of the quantum well.[21,22] Considering only the electrons' elastic scattering within the first subband of the well, we present the solution of the confinement problem with the Hamiltonian $\hat{H}_0$ as[19,23]

$$\Psi(\boldsymbol{\rho},z)=\psi^s(\boldsymbol{\rho})\varphi_1(z), \quad (5)$$

where $\varphi_1(z)$ is the normalized electron wave function in z direction, and $s=\pm 1$ is the quantum number related to the spin states. The eigen-energy E_{nz} in z direction can be obtained easily from the well-known Ben–Daniel–Duke boundary conditions.[20,21]

By taking the average

$$\tilde{V}(\rho)=\int_{-\infty}^{+\infty}dz\,\varphi_1^*(z)V_{\mathrm{im}}(r)\varphi_1(z),$$

and following the approach described in Refs. 19, 23 and 24, we obtain statistically screened and averaged quasi-2-D scattering potential in the following form:

$$\tilde{V}_c(\rho)=-\frac{\hbar^2Ze^2}{a_B^*m_1(0)}\int_0^\infty\frac{dq}{\epsilon(q)}J_0(q\rho)\times\int_{-\infty}^{+\infty}dz|\varphi_1(z)|^2e^{-q|z|},$$

$$\tilde{V}_{\mathrm{so}}(\rho)=i\frac{\hbar^2Ze^2}{a_B^*m_1(0)}\int_0^\infty\frac{qdq}{\epsilon(q)}J_1(q\rho)\cdot\left[\alpha_1(E)\int_{z\leqslant|L/2|}dz|\varphi_1(z)|^2e^{-q|z|}+\alpha_2(E)\int_{z\geqslant|L/2|}dz|\varphi_1(z)|^2e^{-q|z|}\right]\times\frac{s}{\rho}\frac{\partial}{\partial\phi},$$

where $a_B^*=\epsilon_s\hbar^2/e^2m_1(0)$ is the effective Bohr radius in the well, $J_n(x)$ is the Bessel function,

$$\epsilon(q)=1+\frac{q_f}{q}$$

is the 2-D dielectric function,

$$q_f=\frac{1}{a_B^*}\frac{m_1(E_f)}{m_1(0)}\left\{1+\frac{d}{dE}\ln[m_1(E)]\big|_{E_{\mathrm{F}}}\right\}$$

is the 2-D Thomas–Fermi screening constant, E_{F} is the Fermi energy of the system,[24] and

$$E=E_\rho+E_{1z}.$$

Due to the radial symmetry of the potentials $\tilde{V}_c(\rho)$ and $\tilde{V}_{\mathrm{so}}(\rho)$, we can present the wave function $\psi^s(\boldsymbol{\rho})$ as the following:

$$\psi^s(\boldsymbol{\rho})=\sum_{l=-\infty}^{l=+\infty}R_l^s(\rho)e^{il\phi}\boldsymbol{\chi}^s.$$

where l is the orbital momentum number and χ^s is the spin function upon which the Pauli matrix vector operates.

The quasi-2-D Schrödinger equation for the radial wave function is given by

$$\left\{\frac{\hbar^2}{2\tilde{m}(E)}\left[\frac{1}{\rho}\frac{d}{d\rho}\left(\rho\frac{d}{d\rho}\right)-\frac{l^2}{\rho^2}+k^2\right]-\tilde{V}_c(\rho)+l\tilde{V}_{\mathrm{so}}(\rho)\right\}R_l^s(\rho)=0, \quad (6)$$

where

$$k=\frac{1}{\hbar}\sqrt{2\tilde{m}(E)E_\rho}$$

is the wave vector of the 2-D electrons, and

$$\frac{1}{\tilde{m}(E)}=\frac{1}{m_1(E)}\int_{z\leqslant|L/2|}dz|\varphi_1(z)|^2+\frac{1}{m_2(E)}\int_{z\geqslant|L/2|}dz|\varphi_1(z)|^2.$$

At a large distance from the scattering center, the asymptotic of the radial function is given by

$$R_l^s(\rho)\to A_l^s[\cos\delta_l^s J_l(k\rho)-\sin\delta_l^s N_l(k\rho)];\quad \rho\to\infty,$$

where δ_l^s is the scattering phase shift[25,26] and N_l is the Neumann function. To solve the scattering problem we use the variable phase approach,[26,27] which assumes that the phase function $\delta_l^s(\rho)$ at the point ρ determines the phase shift produced by the part of the potential contained within the cycle of a radius ρ. The scattering phase shift for the total potential is equal to the asymptotic value

$$\delta_l^s=\lim_{\rho\to\infty}\delta_l^s(\rho).$$

The phase function $\delta_l^s(\rho)$ satisfies the following differential equation:

$$\frac{d\delta_l^s(\rho)}{d\rho}=-\frac{2\pi\tilde{m}(E)}{\hbar^2}\rho[\tilde{V}_c(\rho)-l\tilde{V}_{so}(\rho)]\times[\cos\delta_l^s(\rho)J_l(k\rho)-\sin\delta_l^s(\rho)N_l(k\rho)]^2, \quad (7)$$

with the boundary condition

$$\delta_l^s(0)=0. \quad (8)$$

The complex 2-D scattering amplitude we present as[25,28]

$$\mathbf{F}^s(E,\theta)=[f(E,\theta)+\sigma_z g(E,\theta)]\boldsymbol{\chi}^s, \quad (9)$$

where $f^s(\theta)$ and $g(\theta)$ describe scattering without and with electron spin reorientation, respectively, and they are determined by the following:[28]

$$f(E,\theta)=\sum_{l=0}^{\infty}f_l\cos(l\theta), \quad (10)$$

$$g(E,\theta)=\sum_{l\geqslant 1}^{\infty}g_l\sin(l\theta), \quad (11)$$

where

$$f_l=\sqrt{\frac{1}{2\pi k}}\begin{cases}\exp(2i\delta_0)-1, & l=0\\ \exp(i2\delta_l^+)+\exp(i2\delta_l^-)-2, & l\geqslant 1\end{cases},$$

$$g_l=i\sqrt{\frac{1}{2\pi k}}[\exp(i2\delta_l^+)-\exp(i2\delta_l^-)],$$

θ is the scattering angle between initial ($\mathbf{k}_i$) and final ($\mathbf{k}_f$) wave vectors. When electrons are spin polarized parallel to the z axis, the Mott scattering cross section[29] can be expressed in terms of the incident electron spin-polarization P as the following:

$$\sigma(E,\theta)=I(E,\theta)+G(E,\theta)P, \quad (12)$$

where $I(\theta)$ is the differential cross section for the unpolarized incident electrons (the symmetric scattering part)

$$I(E,\theta)=|f(E,\theta)|^2+|g(E,\theta)|^2,$$

and

$$G(E,\theta)=f^*(E,\theta)g(E,\theta)+f(E,\theta)g^*(E,\theta), \quad (13)$$

is the spin-flip part of the scattering cross section (the asymmetric scattering part).

III. SPIN-DEPENDENT HALL EFFECT IN 2-D CHANNELS

In the Pauli approach to the explanation of the origin of the AHE,[8] the total electron velocity is presented as

$$\mathbf{v}_{\mathbf{k}}^s=\frac{1}{\hbar}\nabla_{\mathbf{k}}E_\rho(\mathbf{k})+\mathbf{w}_{\mathbf{k}}^s \quad (14)$$

where $E_\rho(\mathbf{k})$ is the dispersion relation of 2-D electrons in the well, and $\mathbf{w}_{\mathbf{k}}^s$ is the anomalous velocity, which can be written in the following form:[8,21,22]

$$\mathbf{w}_{\mathbf{k}}^s=\alpha\frac{[\mathbf{s}\times\mathbf{k}]}{\tau_{\text{im}}}, \quad (15)$$

where τ_{im} is the electron momentum relaxation time resulted from impurity scattering, and $\mathbf{s}$ is the unit vector parallel to the spin polarization.

The total electron current can be obtained by averaging the total velocity over the electron distribution function $f_s(\mathbf{k})$. In the linear approximation with respect to the external electric field $\mathbf{F}$,[30–32] this leads to

$$\mathbf{J}=-|e|\sum_{k,s}\mathbf{v}_{\mathbf{k}}^s f_s(\mathbf{k})=\mathbf{J}^0+\mathbf{J}^s=\sigma_c\mathbf{F}+\sigma_c^s\frac{[\mathbf{s}\times\mathbf{F}]}{s}, \quad (16)$$

where σ_c is the diagonal element of the conductivity tensor and σ_c^s is the spin-dependent Hall conductivity (off-diagonal element of the conductivity tensor). If the concentration of scatterers is low, one can assume these impurities scatter the electrons independently. In this approximation, the Boltzmann transport equation for the electron distribution function $f_s(\mathbf{k})$ is given by

$$-\frac{|e|}{\hbar}\mathbf{F}\nabla_{\mathbf{k}}f_s(\mathbf{k})=\sum_{\tilde{\mathbf{k}},s}W_0(\mathbf{k},\tilde{\mathbf{k}})+W_s(\mathbf{k},\tilde{\mathbf{k}})\times[f_s(\mathbf{k})-f_s(\tilde{\mathbf{k}})], \quad (17)$$

where

$$W_0(\mathbf{k},\tilde{\mathbf{k}})=\frac{8\pi\hbar^3}{A\tilde{m}^2(E)}kI(\mathbf{k},\tilde{\mathbf{k}})N_{\text{im}}\delta[E_\rho(\mathbf{k})-E_\rho(\tilde{\mathbf{k}})], \quad (18)$$

$$W_s(\mathbf{k},\tilde{\mathbf{k}})=\frac{8\pi\hbar^3}{A\tilde{m}^2(E)}kPG(\mathbf{k},\tilde{\mathbf{k}})N_{\text{im}}\delta[E_\rho(\mathbf{k})-E_\rho(\tilde{\mathbf{k}})], \quad (19)$$

$$I(\mathbf{k},\tilde{\mathbf{k}})=I[E_\rho(\mathbf{k}),\theta],\quad G(\mathbf{k},\tilde{\mathbf{k}})=G[E_\rho(\mathbf{k}),\theta], \quad (20)$$

$$P=\frac{1}{n}\sum_{s=\pm1}sn_s,\quad n=n_{+1}+n_{-1}, \quad (21)$$

where $W_0(\mathbf{k},\tilde{\mathbf{k}})$ and $W_s(\mathbf{k},\tilde{\mathbf{k}})$ are the scattering transition probabilities per unit time due to symmetric and asymmetric

scattering, respectively, $N_{\rm im}$ is the impurity concentration, P is the polarization of the 2-D electronic gas, n_s is the concentration of the s-polarized electrons in the 2-D channel, and A is the system area. In the linear approximation, the electron distribution function can be written in the form

$$f_s(\mathbf{k}) \approx f_0(E) + P_0(E)(\mathbf{k}\cdot\mathbf{F}) + P_s(E)(\mathbf{k}\cdot[\mathbf{s}\times\mathbf{F}]). \quad (22)$$

Substituting $f_s(\mathbf{k})$ into the Boltzmann equation, we obtain the coefficients $P_0(E)$ and $P_s(E)$, and then the components of the conductivity tensor.

Finally, the off-diagonal element of the conductivity tensor obtained from Eq. (16) consists of two parts,

$$\sigma_c^s = \sigma_{\rm SS}^s + \sigma_{\rm SJ}^s \quad (23)$$

where $\sigma_{\rm SS}^s$ is the contribution from the skew-scattering (which comes from the spin-dependent part of the elastic scattering) and $\sigma_{\rm SJ}^s$ is the side-jump contribution (which comes with the anomalous velocity). For the case of the degenerated electronic system (low-temperature limit), those two contributions can be presented as the following:

$$\sigma_{\rm SS}^s = \frac{\hbar e^2 N_{\rm im}}{2\pi} \sum_{s=\pm 1} s\left(\frac{\tau_{\rm im}^s}{\tilde{m}_s}\right)^2 \tilde{G}_s (k_{\rm F}^s)^3, \quad (24)$$

$$\sigma_{\rm SJ}^s = -\frac{e^2}{4\pi\hbar} \sum_{s=\pm 1} s\alpha_s (k_{\rm F}^s)^2. \quad (25)$$

In Eqs. (24) and (25),

$$\tilde{G}_s = \int_0^{2\pi} G(E_{\rm F}^s, \theta)[1-\cos(\theta)]\sin(\theta)d\theta, \quad (26)$$

$$\frac{1}{\tau_{\rm im}^s} = \frac{2\hbar N_{\rm im}}{\tilde{m}_s} k_{\rm F}^s \tilde{I}_s, \quad (27)$$

$$\tilde{I}_s = \int_0^{2\pi} I(E_{\rm F}^s, \theta)[1-\cos(\theta)]d\theta, \quad (28)$$

$\tilde{m}_s = \tilde{m}(E_{\rm F}^s)$, $\alpha_s = \alpha(E_{\rm F}^s)$, and the Fermi energy $E_{\rm F}^s$ for the s-group of the polarized electrons is the solution of the following equation:

$$E_{\rm F}^s = \frac{\hbar^2}{2\tilde{m}_s}(k_{\rm F}^s)^2 + E_{1z}, \quad (29)$$

with the electron Fermi wave vector defined as the following:

$$k_{\rm F}^s = [2\pi n(1+sP)]^{1/2}. \quad (30)$$

The tangent of the spin-dependent Hall angle (SDHA) is the sum of two tangents, and can be presented as

$$\tan(\theta_{\rm H}) = \tan(\theta_{\rm H}^{\rm SS}) + \tan(\theta_{\rm H}^{\rm SJ}), \quad (31)$$

where

$$\tan(\theta_{\rm H}^{\rm SS}) = \frac{\sigma_{\rm SS}^s}{\sigma}, \quad \tan(\theta_{\rm H}^{\rm SJ}) = \frac{\sigma_{\rm SJ}^s}{\sigma}, \quad (32)$$

and

$$\sigma_c = \frac{e^2 k_{\rm F}^{s2}}{4\pi\tilde{m}} \tau_{\rm im}^s|_{P=0}. \quad (33)$$

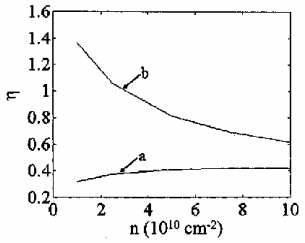

FIG. 1. The ratio $\eta = |\theta_{\rm H}^{\rm SJ}/\theta_{\rm H}^{\rm SS}|$ ($\theta_{\rm H}^{\rm SJ}$ and $\theta_{\rm H}^{\rm SS}$ are contributions into the total SDHA from the side-jump and skew-scattering parts, correspondingly) as the function on the electron concentration for two types of impurities located in the center of the IGA QW [$n = N_{\rm im}$, $L = 20$ nm; a is a repulsive impurity ($Z=-1$), b is an attractive impurity ($Z=+1$)].

IV. CALCULATION RESULTS

To demonstrate the actual value of the SDHE in semiconductor QWs, we first present results of our simulations for $Al_{0.48}In_{0.52}As/In_{0.53}Ga_{0.47}As/Al_{0.48}In_{0.52}As$ (IGA) symmetrical QWs, which possessed the well-developed growth technology. The parameters taken in this calculation are the following: $E_{g1} = 0.813$ eV, $E_{g2} = 1.508$ eV, $\Delta_1 = 0.361$ eV, $\Delta_2 = 0.332$ eV, $m_1(0) = 0.041m_0$, $m_2(0) = 0.075m_0$, $\epsilon_1 = 14$, $\epsilon_2 = 12.5$, and $V_0 = 0.504$ eV[33] (m_0 is the free electron mass). Secondly, we present our calculation results for CdTe/InSb/CdTe (IS) QWs [where $E_{g1} = 0.24$ eV, $E_{g2} = 1.59$ eV, $\Delta_1 = 0.81$ eV, $\Delta_2 = 0.8$ eV, $m_1(0) = 0.015m_0$, $m_2(0) = 0.08m_0$, $\epsilon_1 = 16.8$, $\epsilon_2 = 10.2$, and $V_0 = 0.55$ eV[34,35]]; these demonstrate about the largest spin-coupling effects. In all calculations, we assure the validity of the one-subband scattering model, when the intersubband gap is larger than the energy of the ρ-direction motion: $E_\rho < E_{2z} - E_{1z}$. This allows us to consider scattering of electrons with the following wave vectors: for the IGA structures with $L \lesssim 30\,{\rm nm} - k \lesssim k_{\rm F}^{\rm I} = 2.5(a_B^*)^{-1}$ (the electron concentration $n = 3.5 \times 10^{11}\,{\rm cm}^{-2}$); for the IS structures with $L \lesssim 30\,{\rm nm} - k \lesssim k_{\rm F}^{\rm II} = 6.6(a_B^*)^{-1}$ ($n = 3 \times 10^{11}\,{\rm cm}^{-2}$). Notice, that a_B^* is taken different by definition for the different types of the systems. We also assume in all our calculations the polarization of the 2-D electron gas to be 50%.

Two contributions to the total SDHA ($\theta_{\rm H}^{\rm SS}$ and $\theta_{\rm H}^{\rm SJ}$) come with different signs and different dependencies on the QW width, the electron and impurity concentrations. $\theta_{\rm H}^{\rm SJ}$ does not depend on the charge and concentration of the impurities, and obviously increases when the electron concentration increases. At the same time, $\theta_{\rm H}^{\rm SS}$ depends on the charge of scatterers (see Ref. 18) and on their concentration (it decreases when $N_{\rm im}$ increases). This generates a complicated interplay between $\theta_{\rm H}^{\rm SS}$ and $\theta_{\rm H}^{\rm SJ}$ contributions to the total SDHA $\theta_{\rm H}$. In Fig. 1, we present the ratio $\eta = |\theta_{\rm H}^{\rm SJ}/\theta_{\rm H}^{\rm SS}|$ as a function on the electron concentration for two types of scatterers located in the center of the IGA well with $L = 20$ nm. The concentration of scatterers and concentration of the electrons are taken to be equal: $n = N_{\rm im}$. It follows from the figure that for the repulsive potential ($Z=-1$) the skew-scattering mechanism is always predominant. For the case of the attractive impurities ($Z=+1$), each of them can be pre-

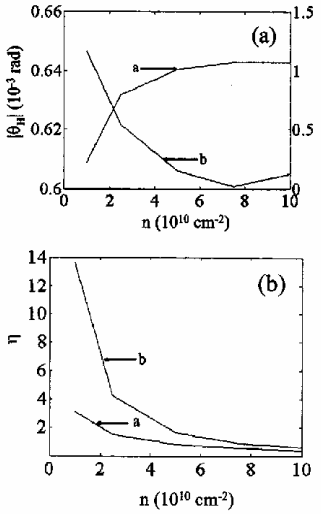

FIG. 2. (a) The absolute value of the SDHA in the IGA QW and (b) the ratio η as the function of the electron concentration ($N_{im}=10^{11}\,cm^{-3}$, $L=20$ nm; a: $Z=-1$, b: $Z=+1$).

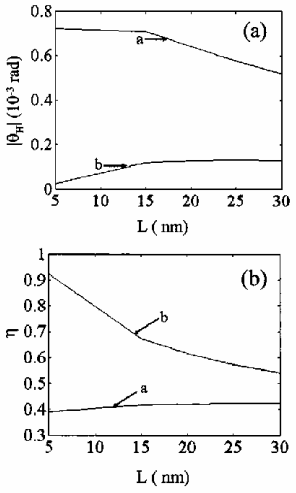

FIG. 3. (a) The absolute value of the SDHA in the IGA QW and (b) the ratio η as the function of the well width ($n=N_{im}=10^{11}\,cm^{-3}$; a: $Z=-1$, b: $Z=+1$).

dominant for certain concentrations; for the concentrations near $n=N_{im}\approx 3\times 10^{10}\,cm^{-2}$, those two mechanisms can cancel each other.

The actual magnitude of the total SDHA as the function of the electronic concentration for the IGA well is presented in Fig. 2(a). In this figure we fixed the impurity concentration to be $N_{im}=10^{11}\,cm^{-2}$. Despite the different behavior of the angle for systems with attractive and repulsive impurities, both demonstrate quite measurable magnitudes. Figure 2(b) clearly shows that the skew-scattering mechanism dominates for systems both with attractive and repulsive impurities up to the very high concentrations of the 2-D electrons.

In addition, one can manipulate the effect in 2-D systems with a variation of the well width. The impact of the well width on the skew-scattering mechanism is discussed in detail in Ref. 18. The main result is the following: the effect always decreases when the well width increases. The dependencies of the total (SDHA) on the well width for the IGA wells are demonstrated in Fig. 3. The figure shows that the side-jump contribution can make the effect stable for the well width variations in the case of the attractive impurities.

The SOI is known to be larger in narrow-gap semiconductors. For this reason, we show in Fig. 4, as an example, the calculation results for the IS wells. We consider here only the QWs with repulsive impurities, in which we can expect (as it follows from the IGA wells) the most interesting result. In this case the total SDHA reaches about 2.5×10^{-3} rad for the relatively narrow wells, and it increases when the electron concentration increases.

These results show how one can manipulate the formation of the effect mechanisms and magnitude as well by means of changes in the system parameters (n,N_{im},L). This possibility makes properties of the SDHE in 2-D semiconductor systems essentially different from those in the bulk. In three-dimensional systems, we only can manipulate N_{im}. In addition, we notice that the SDHA in the QWs is significantly larger (in few orders) than it was for the bulk (see Refs. 30, 31, and 36). In addition, the effect is easily tunable in QWs.

V. CONCLUSIONS

We described theoretically the SDHE in semiconductor QWs when the 2-D electrons are scattered and form the screened Coulomb centers located in the center of the wells. The one-electronic-band effective Hamiltonian and SO coupling potential of the impurities allow us to solve the 2-D spin-dependent Boltzmann equation and to calculate the SDHA at zero magnetic field. We have found large SDHAs for AlInAs/InGaAsAs/AlInAs and CdTe/InSb/CdTe symmetrical QWs. For instance, in the CdTe/InSb/CdTe narrow QWs the SDHE can reach 2.5×10^{-3} rad. This could be detected in the measurements of the Hall effect at low temperatures, and this is potentially useful in integrated electron

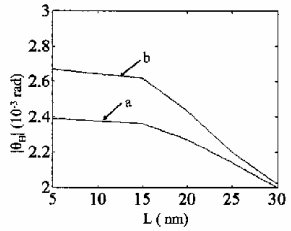

FIG. 4. The absolute value of the SDHA in the IS QW with repulsive impurities as the function of the well width ($N_{im}=10^{11}\,cm^{-3}$, a: $n=5\times 10^{10}\,cm^{-3}$, b: $n=10^{11}\,cm^{-3}$).

spin-polarization devices based on semiconductor heterostructures. It also can be used as a tool of determination of spin-coupling parameters in III-V narrow-gap semiconductor heterostructures. We suggest that experimental investigations should be conducted to verify our theory predictions.

ACKNOWLEDGMENTS

This work was supported by the National Science Council of R.O.C. under contract NSC-92-2112-M-009-015..

[1] S. Datta and B. Das, Appl. Phys. Lett. **56**, 665 (1990).
[2] G. A. Prinz, Science **282**, 1660 (1998).
[3] J. Fabian and S. Das Sarma, J. Vac. Sci. Technol. B **17**, 1708 (1999).
[4] M. E. Flatté, J. M. Hyers, and W. H. Lau, *Spin Dynamics in Semiconductors*, in *Semiconductor Spintronics and Quantum Computation*, edited by D. D. Awschalom, D. Loss, and N. Samarth (Springer, Berlin, 2002), pp. 107–145.
[5] J. E. Hirsch, Phys. Rev. Lett. **83**, 1834 (1999).
[6] G. Gergmann, Phys. Rev. B **63**, 193101 (2001).
[7] S. Zhang, Phys. Rev. Lett. **85**, 393 (2000); J. Appl. Phys. **89**, 7564 (2001).
[8] A. Crépieux and P. Bruno, Phys. Rev. B **64**, 0114416 (2001).
[9] R. Karplus and J. M. Luttinger, Phys. Rev. **95**, 1154 (1954).
[10] L. Berger, Phys. Rev. B **2**, 4559 (1970).
[11] J. Smit, Physica (Amsterdam) **21**, 877 (1955); **24**, 39 (1958).
[12] Y. A. Bychkov and E. I. Rashba, Pis'ma Zh. Eksp. Teor. Fiz. **39**, 66 (1984) [JETP Lett. **39**, 78 (1984)].
[13] M. I. D'yakonov and V. Yu. Kachorovskii, Fiz. Tekh. Poluprovodn. **20**, 178 (1986) [Sov. Phys. Semicond. **20**, 100 (1986)].
[14] V. M. Edelstein, Physica B **284–288**, 1217 (2000).
[15] T. P. Pareek and P. Bruno, Pramana, J. Phys. **57**, 1 (2002).
[16] E. Chen, O. Voskoboynikov, and C. P. Lee, Solid State Commun. **125**, 381 (2003).
[17] R. S. Silsbee, Phys. Rev. B **63**, 155305 (2001).
[18] H. C. Huang, O. Voskobounikov, and C. P. Lee, Phys. Rev. B **67**, 195337 (2003).
[19] F. Stern and W. E. Howard, Phys. Rev. **163**, 816 (1967).
[20] G. Bastard, *Wave Mechanics Applied to Semiconductor Heterostructures* (Editions de Physique, Les Ulis, 1990).
[21] E. A. de Andrada e Silva, G. C. La Rocca, and F. Bassani, Phys. Rev. B **55**, 16 293 (1997).
[22] Th. Schäpers, G. Engels, J. Lange, Th. Klocke, M. Hollfelder, and H. Lüth, J. Appl. Phys. **83**, 4324 (1998).
[23] T. Ando, A. B. Fowler, and F. Stern, Rev. Mod. Phys. **54**, 437 (1982).
[24] D. K. Ferry and S. M. Goodnick, *Transport in Nanostructures* (Cambridge University Press, Cambridge, UK, 1997).
[25] C. J. Joachain, *Quantum Collision Theory* (North-Holland, Amsterdam, 1979).
[26] A. G. Sitenko, *Scattering Theory* (Springer, Berlin, 1990).
[27] F. Cologero, *Variable Phase Approach to Potential Scattering* (Academic, New York, 1967).
[28] O. Voskoboynikov, H. C. Huang, C. P. Lee, and O. Tretyak, Physica E (Amsterdam) **12**, 252 (2002).
[29] N. F. Mott and H. S. Massey, *The Theory of Atomic Collisions*, 3rd ed. (Oxford University Press, Oxford, UK, 1987).
[30] V. N. Abakumov and I. N. Yassievich, Zh. Eksp. Teor. Fiz. **61**, 2571 (1972) [Sov. Phys. JETP **34**, 1375 (1972)].
[31] V. N. Abakumov, V. V. Akulinichev, and I. N. Yassievich, Fiz. Thekh. Poluprovod. **9**, 936 (1975) [Sov. Phys. Semicond. **9**, 612 (1975)].
[32] P. M. Levy, Phys. Rev. B **38**, 6779 (1988).
[33] S. L. Chuang, *Physics of Optoelectronic Devices* (Wiley-Interscience, New York, 1995).
[34] E. T. Yu, J. O. McCaldin, and T. C. McGill, Solid State Phys. **46**, 2 (1992).
[35] *Handbook Series on Semiconductor Parameters*, edited by M. Levinshtein, S. Rumyantsev, and M. Shur (World Scientific, Singapore, 1999).
[36] J. N. Chazalviel and I. Solomon, Phys. Rev. Lett. **29**, 1676 (1972).

3.4 Main results and discussion

In semiconductors the most important interaction, which causes spin-dependent processes is the spin-orbit interaction. The Rashba spin-orbit coupling is an essential element of the proposed by Datta and Das the spin field effect transistor. A new branch of semiconductor electronics so called spintronics became under an extensive development recently. For this reason, the spin dependent kinetics of electrons in traditional III-V semiconductor heterostructures becomes a topic of a great interest from theoretical and practical points of view. Our study deals with a model of the spin-dependent electron scattering from nano-scale semiconductor quantum dots (antidots). Recent advances in semiconductor nano-technology allow us to consider small spherical dots (antidots) of III-V semiconductors as “artificial defects” with controllable parameters. We calculated the polarization (the Sherman function) after a single scattering and than investigate how the polarization changes after the second scattering. The one electron band effective Hamiltonian and the spin dependent boundary conditions for spherical quantum dots (antidots) allowed us to calculate a spin asymmetry in the electron scattering cross-section. We found a polarization produced by single and double scattering of unpolirazed electron beams because by the spin-orbit interaction. We would like to stress that, the polarization is caused by non-magnetic GaAs/InAs semiconductor structures without external magnetic fields. We should mention that in the Anomalous Hall effect the Hall angle is proportional to the Sherman function at the Fermi energy shell. Our calculation results for three-dimensional random arrays of small semiconductor quantum dots (antidotes) suggest a small but measurable magnitude of the angle for antidotes. The anomalous Hall effect produced by quantum antidots is expected to be reduced by the electron impurity scattering, but should still have a significant magnitude. This effect is potentially useful in integrated electron spin-polarization devices based on all-semiconductor heterostructures.

In two-dimensional quantum wells, the spin-dependence of the scattering processes is expected to be stronger than in the bulk because of the localization of electrons' wave-functions in the conduction channel and well known peculiarities in the two-dimensional electron elastic scattering cross section. It should be noted, that the problem remains complicated even for a simplest two-dimensional electron motion because in general the spin-orbit interaction should be described by a three-dimensional model.

Using the delta-doping technique, the Coulomb attractive and repulsive impurities can be precisely placed in heterostructures. It allows us to model theoretically the effect the spin-dependent scattering from the impurities located inside or outside the conductive channel. Most of the theoretical simulations of two-dimensional electron elastic scattering processes from the impurities were conducted in details in the first Born approximation. However, it is well known, when the perturbation theory is used, the dependence on spin in the elastic cross section appears only in the approximation that follows the first Born approximation. For this reason, we used in our calculations of the spin-dependent scattering cross-section the partial wave approach, which was also used in some simulations of the spin-independent elastic scattering cross-section when the first Born approximation is not applicable. In this study we calculated the spin-dependent elastic scattering cross-section for electrons scattered by impurities in two-dimensional heterostructures of III-V semiconductors. We used the effective one band Hamiltonian with the Ben-Daniel-Duke boundary conditions for electronic envelop-functions to calculate the spin-dependent elastic cross-section for electrons scattered from screened repulsive and attractive isolated impurities with the spin-orbit coupling. The impurities are located inside the quantum well. The one electron band effective Hamiltonian and Rashba model of the spin-orbit interaction allow us to calculate the left-right asymmetry in the electron scattering cross-section. We have found a large spin-dependent asymmetry in the elastic cross-section for electrons scattered from impurities in AlInAs/InGaAsAs/AlInAs and CdTe/InSb/CdTe symmetrical quantum wells.

The Sherman function amplitude for the CdTe/InSb/CdTe quantum well is predicted to be about 0.05. This could be detected with the anomalous Hall angle at zero magnetic field in the

Hall effect measurements. This effect is potentially useful in integrated electron spin-polarization devices based on semiconductor heterostructures. It also can be used as a tool of determination of spin coupling parameters in III-V narrow gap semiconductor heterostructures.

We calculated contributions from the skew-scattering (SS) and side-jump (SJ) mechanisms to the spin-dependent Hall effect (SDHE). Our calculation is based on the effective one band Hamiltonian and Rashba type model of the spin-orbit interaction. We have found large spin-dependent Hall angles (SDHA) for AlInAs/InGaAsAs/AlInAs and CdTe/InSb/CdTe symmetrical quantum wells. For instance, in the CdTe/InSb/CdTe narrow quantum wells SDHA can reach 2.5×10^{-3} rad. This could be detected in the measurements of the Hall effect at low temperatures and this is potentially useful in integrated electron spin-polarization devices based on semiconductor heterostructures. It also can be used as a tool of determination of spin coupling parameters in III-V narrow gap semiconductor heterostructures. We suggest that experimental investigations should be conducted to verify our theory predictions.

4. Magnetic properties of semiconductor quantum dots and rings

Magnetic properties of parabolic quantum dots in the presence of the spin–orbit interaction

O. Voskoboynikov[a)]
National Chiao Tung University, 1001 Ta Hsueh Road, Hsinchu 300, Taiwan, Republic of China

O. Bauga
Kiev Taras Shevchenko University, 64 Volodymirska st., 01033 Kiev, Ukraine

C. P. Lee
National Chiao Tung University, 1001 Ta Hsueh Road, Hsinchu 300, Taiwan, Republic of China

O. Tretyak
Kiev Taras Shevchenko University, 64 Volodymirska st., 01033 Kiev, Ukraine

(Received 29 April 2003; accepted 6 August 2003)

We present a theoretical study of the effect of the spin–orbit interaction on the electron magnetization and magnetic susceptibility of small semiconductor quantum dots. Those characteristics demonstrate quite interesting behavior at low temperature. The abrupt changes of the magnetization and susceptibility at low magnetic fields are attributed to the alternative crossing between the spin–split electron levels in the energy spectrum, essentially due to the spin–orbit interaction (an analog of the general Paschen–Back effect). Detailed calculation using parameters of InAs semiconductor quantum dot demonstrates an enhancement of paramagnetism of the dots. There is an additional possibility to control the effect by external electric fields or the dot design.
 [DOI: 10.1063/1.1614426]

I. INTRODUCTION

With recent advanced technologies it has become possible to study in detail the electron energy levels of different kinds of quantum dots and operate with a precise number of electrons or with stabilized chemical potential in the dots.[1,2] Orbital and spin magnetization of those systems has been under an extensive study during the recent decade.[3–12] The point of interest is that the magnetization provides with information about multiparticle dynamics of the dots in an external magnetic field. In addition, recent development of spintronics requires an extensive study of magnetic properties of nanosystems.[13–16] The spin states in the quantum dots are promising candidates for realizations of qubit in the quantum computing.[17] Therefore, the study of the magnetic properties of quantum dots despite of the fascinating physics can provide us with additional tools to control the electronic magnetism in nanoscale structures.

The electron spin controls design of the energy shells and magnetic properties of semiconductor quantum dots.[1,18–20] Among other spin dependent interactions, the spin–orbit interaction (the interaction between orbital angular and spin momenta[21,22]) plays an observable role in the energy spectrum formation for III–V semiconductor nanostructures. When the potential through which the carriers move is inversion asymmetric one, the spin–orbit interaction removes the spin degeneracy of the energy levels even without external magnetic fields. It sufficiently alters the electronic properties of semiconductor nano-structures.[23–28]

The purpose of this article is to study possible consequences of the spin–orbit interaction in magnetic properties of quantum dots at weak magnetic fields. We calculate the magnetization and susceptibility of a cylindrical quantum dot with the parabolic confinement potential for electrons when the spin–orbit interaction is included into consideration. The effective single-particle lateral parabolic potential describes quite well the observed properties of quantum dots (artificial atoms) with a small number of electrons.[29,30] Application of a magnetic field along the dot axes generates a complicated structure of the electron energy levels and the theoretical analysis of the parabolic quantum dots in magnetic fields achieves a rich physics. The energy level behavior and thermodynamical properties of parabolic quantum dots in magnetic fields were discussed extensively.[4,6,11,12] Recently the well pronounced spin splitting was found for the parabolic confinement potential model of semiconductor quantum dots with parameters of InSb and InAs.[28] The spin splitting at zero magnetic field leads to a crossing of the energy levels in weak external magnetic fields (similarly to the general Paschen–Back effect) and can provide unusual magnetic properties of the quantum dots.

In order to examine evidences of the impact of the spin–orbit interaction on the magnetization and susceptibility of quantum dots we focus on the Rashba term[22,25] in the spin–orbit interaction potential. A generalization with including of the Dresselhaus interaction[21] can be done straightforward in future studies.

II. MODEL OF THE QUANTUM DOT

In the presence of a uniform magnetic field B applied along the axis of the dot (z direction) the single-particle Hamiltonian in the lateral cylindrical coordinates $\{\rho,\phi\}$ is written as[28]

a)Author to whom correspondence should be addressed; electronic mail: vam@cc.nctu.edu.tw

$$H=-\frac{\hbar^2}{2m(E)}\left[\frac{\partial}{\rho\partial\rho}\rho\frac{\partial}{\partial\rho}+\frac{1}{\rho^2}\frac{\partial^2}{\partial\phi^2}\right]-\frac{i}{2}\hbar\omega_c(E,B)\frac{\partial}{\partial\phi}$$
$$+\tfrac{1}{8}m(E)\omega_c^2(E,B)\rho^2+V_c(\rho)+V_{so}^R(\rho,\phi)$$
$$+\tfrac{1}{2}\sigma_z\mu_B g(E)B, \quad (1)$$

where

$$V_c(\rho)=\tfrac{1}{2}m(E)\omega_0^2\rho^2, \quad (2)$$

is the effective parabolic lateral confinement potential, $\hbar\omega_0$ is the characteristic confinement energy, the electron effective mass is given by[25,31]

$$\frac{1}{m(E)}=\frac{1}{m(0)}\frac{E_g(E_g+\Delta)}{(3E_g+2\Delta)}\left[\frac{2}{E+E_g}+\frac{1}{E+E_g+\Delta}\right] \quad (3)$$

[E denotes the electron energy in the conduction band, $m(0)$ is the conduction-band-edge effective mass, E_g and Δ are the main band gap and the spin–orbit band splitting, respectively]

$$\omega_c(E,B)=\frac{eB}{m(E)}$$

is the electronic cyclotron frequency, where σ_z is the Pauli z matrix

$$g(E)=2\left[1-\frac{m_0}{m(E)}\frac{\Delta}{3(E_g+E)+2\Delta}\right] \quad (4)$$

is the effective Lande factor of the semiconductor,[32] $\mu_B=e\hbar/2m_0$ is the Bohr magneton, e is the electron charge, and m_0 is the free electron mass.

The Rashba spin–orbit interaction term in Eq. (1) is given by[25,27,33,34]

$$V_{so}^R(\rho,\phi)=\boldsymbol{\sigma}_z\alpha\frac{dV_c(\rho)}{d\rho}\left(\mathbf{k}_\phi+\frac{e}{2\hbar}B\rho\right), \quad (5)$$

where $\mathbf{k}_\phi=-i(1/\rho)\partial/\partial\phi$, and α is the spin–orbit coupling parameter within the Rashba approach.[25]

The eigenenergies of the Hamiltonian can be obtained by means of a self-consistent solution of the following equation:[28]

$$E_{n,l,\sigma}=\hbar\Omega_\sigma(E_{n,l,\sigma},B)(2n+|l|+1)+l\frac{\hbar\omega_c(E_{n,l,\sigma},B)}{2}$$
$$+s\left[\frac{\mu_B}{2}g(E_{n,l,\sigma})B+l\alpha m(E_{n,l,\sigma})\omega_0^2\right], \quad (6)$$

where

$$\Omega_\sigma^2(E,B)=\omega_0^2+\frac{\omega_c^2(E,B)}{4}+s\alpha\frac{m(E)\omega_0^2}{\hbar}\omega_c(E,B),$$

n, l, and $s=\pm1$ refer to the main quantum number, orbital quantum number, and the electron spin polarization along the z axis correspondingly. The electron energy levels Eq. (6) with different spins and the same angular momentum $|l|>0$ due to the spin–orbit interaction are split at $B=0$ and cross with increasing of the magnetic field [see inset in Fig. 1(b)].[28] Note that the levels with parallel spin and angular momentum (antiparallel spin and angular momentum) remain twofold degenerated. This is the well known Kramers degeneracy.

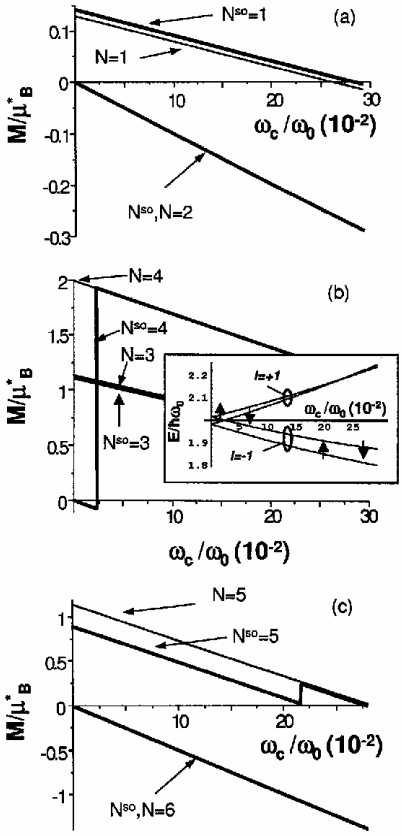

FIG. 1. Magnetization of InAs parabolic quantum dot with and without spin–orbit interaction: (a) for one and two electrons; (b) for three and four electrons (inset shows the dot energy levels for $|l|=1$ with the spin–orbit interaction included, arrows refer to the spin polarizations); (c) for five and six electrons. Index "so" marks calculations with spin-orbit interaction, $\mu_B^*=e\hbar/2m(0)$.

The first crossing point for the lowest spin-split levels ($|l|=1$) is determined by

$$\frac{\Phi}{\Phi_0}\approx\frac{\Delta E}{\hbar\omega_0}\ll1, \quad (7)$$

where Φ is the magnetic flux in the dot area, ΔE is the energy spin splitting at $B=0$, and Φ_0 is the magnetic flux quantum. The second crossing point occurs at[28]

$$\frac{\Phi}{\Phi_0}=\frac{2\Delta E}{(2\Delta E+g\hbar\omega_0)}. \quad (8)$$

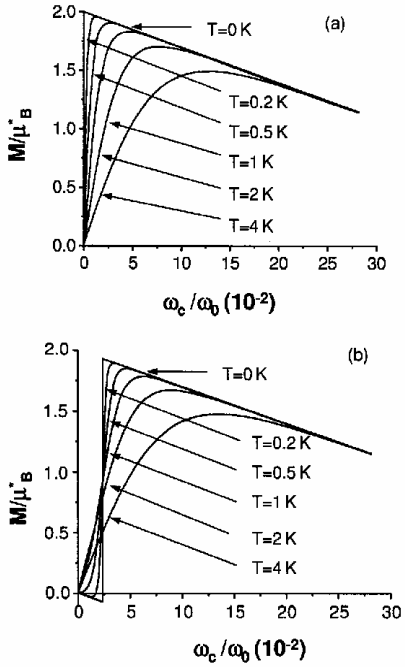

FIG. 2. Temperature dependence of InAs four electron quantum dot magnetization (a) without and (b) with spin–orbit interaction.

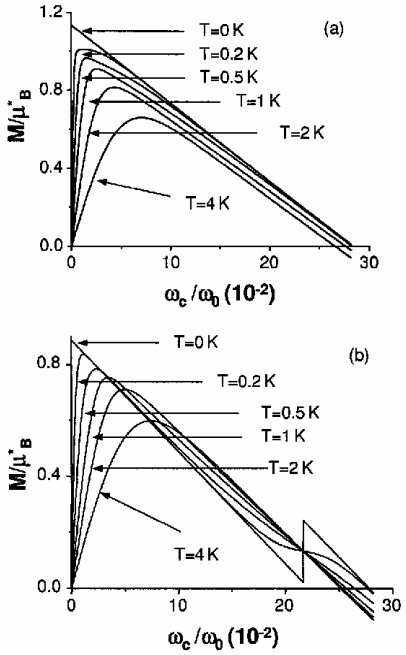

FIG. 3. Temperature dependence of InAs five electron quantum dot magnetization (a) without and (b) with spin–orbit interaction.

Being interested in the impact of the spin–orbit interaction on the magnetic properties of the dots we confine ourself on relatively weak magnetic fields as it is followed from Eqs. (7) and (8).

In our calculation we fix only the thermal average of the total electron number to a given value N. In the case of the fixed number of electrons one should use the canonical ensemble description.[6–8,35] The thermal average of the total magnetization M and magnetic susceptibility χ of the system connected to a reservoir and with a fixed chemical potential[35] are given by

$$M=\sum_{n,l,s}\left(-\frac{\partial E_{n,l,\sigma}}{\partial B}\right)f(E_{n,l,\sigma}-\xi), \tag{9}$$

and

$$\chi=\frac{\partial M}{\partial B}, \tag{10}$$

where $f(E)$ is the Fermi distribution function, and ξ is the chemical potential of the system determined by the following equation:

$$N=\sum_{n,l,s} f(E_{n,l,\sigma}-\xi). \tag{11}$$

III. CALCULATION RESULTS

The ultimate consequence of the spin–orbit interaction in the dot magnetization (the magnetic momentum of the dot) we describe first at zero temperature for quantum dots with few electrons. For small InAs quantum dots we choose $m(0)=0.04\,m_0$ (the tuned parameter from Ref. 36), $E_g=0.42$ eV, $\Delta=0.38$ eV, $\alpha=1.1$ nm^2, and $\hbar\omega_0=0.019$ eV.[28,31,37] The calculated magnetization of dots with 1–2, 3–4, and 5–6 electrons (when we consecutively fill up the energy levels of the dot to the shell with $n=0$, $|l|=1$) is shown in Fig. 1. For comparison, the magnetization for the same number of electrons but without the spin–orbit interaction is also presented in the figure. The magnetization calculated without the spin–orbit interaction demonstrates a clear shell filling behavior: for $N=2$, 6 [closed shells, see Figs. 1(a) and 1(c)] the magnetic momenta are canceled out at $B=0$; for $N=1$, 3, 4, 5 [partially occupied shells, see Figs. 1(a), 1(b), 1(c)] the magnetization takes a positive value at $B=0$. Our calculation results suggest that the spin–orbit interaction keeps the cancellation for the closed shells and slightly changes the magnetization for $N=1$, 3.[6]

The most interesting result we obtain for dots with four and five electrons. The spin–orbit splitting partially lifts up the degeneracy of $(0,\pm1,\pm1)$ levels and changes the electron structure making $E_{0,\pm1,\pm1}>E_{0,\mp1,\pm1}$.[28] This assures the magnetization to be zero at $B=0$ for dots with four electrons in contrast to the case without the spin–orbit interaction. When we increase magnetic field strength and reach condition (7) (at $B\approx0.14$ T) the crossing between levels $E_{0,1,-1}$ and $E_{0,-1,1}$ occurs [see inset in Fig. 1(b)]. For the quantum dot with four electrons the level crossing provides a sharp

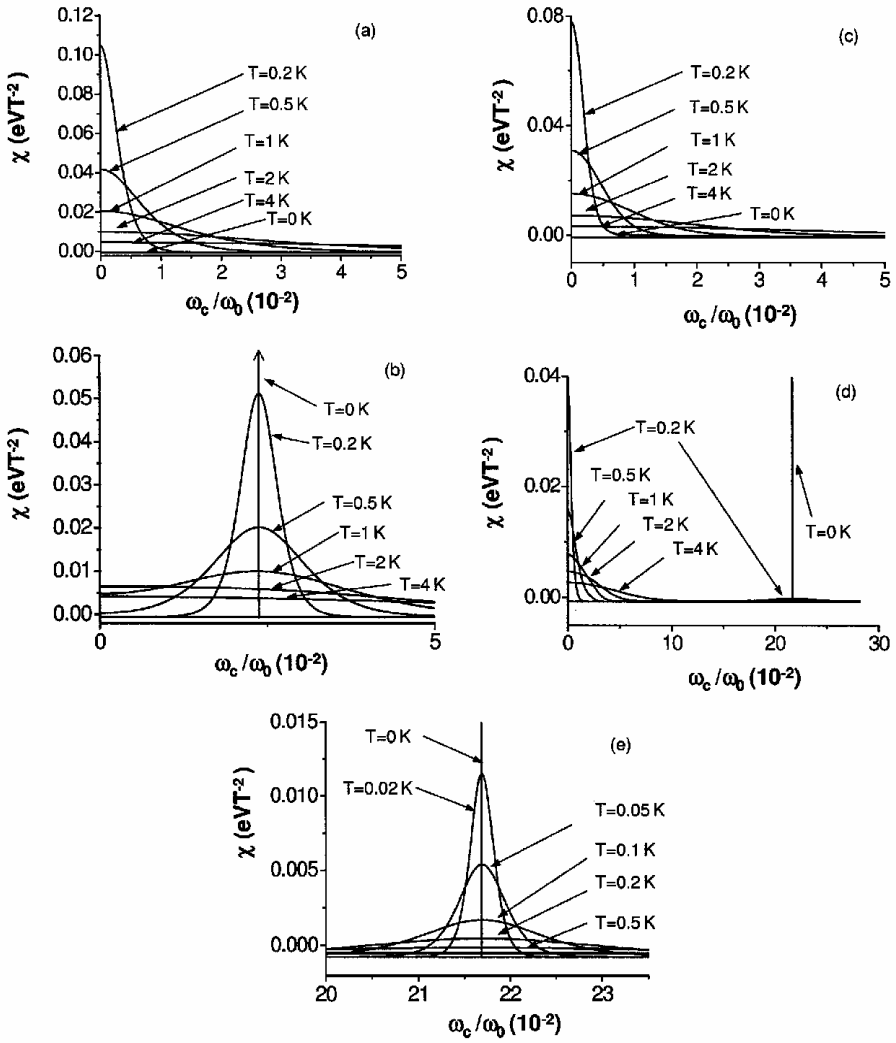

FIG. 4. Temperature dependence of the susceptibility of InAs parabolic quantum dot: (a) $N=4$; (b) $N^{so}=4$; (c) $N=5$; (d) $N^{so}=5$; and (e) $N^{so}=5$, at the region of the second peak.

jump in the magnetization. For the quantum dot with five electrons the jump reflects a crossing between $E_{0,1,-1}$ and $E_{0,1,1}$ levels for a higher magnetic field [condition (8)]: $B \approx 1.4$ T.

At a low but finite temperature $k_BT \ll \hbar\omega_0$ (k_B is the Boltzmann constant) the magnetization for dots with $N=1$, 2, 3, 6 follows the well known rule: totally occupied shells keep provide diamagnetic properties of the systems and partially filled shells demonstrate paramagnetic peaks. The peaks decrease exponentially [$\sim \exp(-k_BT/\hbar\omega_0)$] and the magnetization approaches the Landau diamagnetism limit when $k_BT \sim \hbar\omega_0$.[35]

The magnetization for the dot with four electrons at different temperatures is presented in Fig. 2. In this case $M \to 0$ for $B \to 0$ and $T \neq 0$. When the magnetic field increases the magnetization demonstrates the paramagnetic peak. The spin–orbit interaction shifts the position of the peak. For the dot with five electrons we obtain an additional paramagnetic peak at a higher magnetic field due to the crossing of the $E_{0,1,-1}$ and $E_{0,1,1}$ levels [it is shown in Fig. 3(b)].

The above described peculiarities in the magnetization of dots due to the spin–orbit interaction generate well understandable features of the magnetic susceptibility. In Fig. 4 we show χ as a function of B for dots with four and five elec-

trons at different temperatures. At nonzero temperatures without the spin-orbit interaction we obtain the paramagnetic peak near $B=0$ [see Figs. 4(a), 4(c)]. The spin–orbit interaction shifts the peak to the field defined by Eq. (7) for dots with four electrons [see Fig. 4(b)]. In the case of the dot with five electrons we observe at low temperature two peaks: near $B=0$ (the ordinary one) and at the field defined by Eq. (8) (generated by the spin–orbit interaction) [see Figs. 4(d), 4(e)]. Clearly, the differential susceptibility demonstrates unusual behavior, which is generated by the jumps of the magnetization and certainly occur only when the spin–orbit interaction is included.

One can control the spin coupling parameters in planar semiconductor systems by means of external or built-in electric fields.[22,25] By variations of the fields one can change magnitudes of the parameters. From the above it appears that the peaks of the magnetic susceptibility which are generated by the spin–orbit interaction should have the following interesting properties. It is possible to perform a switching between the configuration presented in Fig. 4(a) and the configuration of Fig. 4(b) for dots with four electrons by means of the external electric field or the design of quantum dots. The switching is also possible between the configurations of Fig. 4(c) and the configurations of Fig. 4(d) for dots with five electrons.

IV. CONCLUSIONS

Before we conclude, we would like to mention that in this article the Coulomb interaction between electrons is neglected for simplicity. The crossing in the energy levels can be generated also by including the electron–electron interaction into consideration. But in this case the crossing occurs between levels with different l and in stronger magnetic fields.[3–5,38,39] To fully understand the described effects a many electron problem should be solved.[2,30] However, the recent investigation[36] suggests that the effect of the electron–electron interaction in systems with strong confinement can enhance the spin–orbit interaction. On the other hand the jumps in the magnetization and following peaks in the susceptibility are clear consequences of the reordering and crossings in the dot energy system provided by the spin–orbit interaction. It is known from the physics of the atomic spectra, that the spin–orbit interaction always provides crossing (or anticrossing) configurations in dependencies of the energy levels on magnetic fields (the general Paschen–Back effect).[40] Therefore, the described effect has the clear physical meaning but the actual magnitude of it should be verified both experimentally and by means of more sophisticated calculations. We have to mention, that it is worth doing because (in contrast to natural atomic systems) quantum dots have an advantage that one can control magnetic properties of the dots by applying external electric fields and changing of the chemical potential.

In summary, we have studied interesting consequences of the spin–orbit interaction in small InAs parabolic quantum dots. The magnetization and magnetic susceptibility of dots with few electrons were calculated. The spin–orbit interaction was involved to control magnetic response of the dots at low temperature. An analog of the general Paschen–Back effect was found for dots with partially filled electronic shells. This property of III–V semiconductor material quantum dots could be useful for the future spintronics research.

ACKNOWLEDGMENTS

This work was supported in part by the National Science Council of Taiwan under Contract Nos. NSC-91-2215-E-009-059 and NSC-91-2119-M-009-003.

[1] D. Bimberg, Semiconductors **33**, 951 (1999).
[2] L. P. Kouwenhoven, D. G. Austing, and S. Tarucha, Rep. Prog. Phys. **64**, 701 (2001).
[3] P. A. Maksym and T. Chakraborty, Phys. Rev. B **45**, 1947 (1992).
[4] M. Wagner, U. Merkt, and A. V. Chaplik, Phys. Rev. B **45**, 1951 (1992).
[5] J. S. De Groote, J. E. M. Hornos, and A. V. Chaplik, Phys. Rev. B **46**, 12773 (1992).
[6] D. Yoshioka and H. Fukuyama, J. Theor. Soc. Jpn. **61**, 2368 (1992).
[7] B. L. Altshuler, Y. Gefen, Y. Imry, and G. Montambaux, Phys. Rev. B **47**, 10335 (1993).
[8] T. Swahn, E. N. Bogachek, Yu. M. Galperin, M. Jonson, and R. I. Shekhter, Phys. Rev. Lett. **73**, 162 (1994).
[9] K. Tanaka, Ann. Phys. (N.Y.) **268**, 31 (1998).
[10] W. C. Tan and J. C. Inkson, Phys. Rev. B **60**, 5626 (1999).
[11] I. Magnúsdotóttir and V. Gudmudsoon, Phys. Rev. B **61**, 10229 (2000).
[12] Y. P. Krasny, N. P. Kovalenko, U. Krey, and L. Jacak, J. Phys.: Condens. Matter **13**, 4341 (2001).
[13] G. A. Prinz, Science **282**, 1660 (1998).
[14] B. E. Kane, Nature (London) **393**, 133 (1998).
[15] D. D. Awschalom and J. M. Kikkawa, Phys. Today **52**, 33 (1999).
[16] S. Das Sarma, J. Fabian, X. Hu, and I. Žutic, Solid State Commun. **119**, 207 (2001).
[17] D. Loss and D. P. DiVincenzo, Phys. Rev. A **57**, 120 (1998).
[18] O. Steffens, M. Suhrke, and U. Rössler, Physica B **256–258**, 147 (1998).
[19] S. Tarucha *et al.*, Physica E (Amsterdam) **3**, 112 (1998).
[20] H. Tamura, Physica B **249–251**, 210 (1998).
[21] G. Dresselhaus, Phys. Rev. **100**, 580 (1955).
[22] Yu. A. Bychkov and E. I. Rashba, J. Phys. C **17**, 6039 (1984).
[23] D. Richards and B. Jusserand, Phys. Rev. B **59**, R2506 (1999).
[24] C. M. Hu, J. Nitta, T. Akazaki, J. Osaka, P. Pfeffer, and W. Zawadzki, Phys. Rev. B **60**, 7736 (1999).
[25] E. A. de Andrada e Silva, G. C. La Rocca, and F. Bassani, Phys. Rev. B **55**, 16293 (1997).
[26] A. Voskoboynikov, S. S. Liu, C. P. Lee, and O. Tretyak, J. Appl. Phys. **87**, 1 (2000).
[27] A. V. Moroz and C. H. W. Barnes, Phys. Rev. B **61**, R2464 (2000); **60**, 14272 (2000).
[28] O. Voskoboynikov, C. P. Lee, and O. Tretyak, Phys. Rev. B **63**, 165306 (2001).
[29] V. Fock, Z. Phys. **47**, 446 (1928).
[30] P. A. Maksym, H. Imamura, G. P. Mallon, and H. Aoki, J. Phys.: Condens. Matter **12**, R299 (2000).
[31] G. Bastard, *Wave Mechanics Applied to Semiconductor Heterostructures* (Les Edition de Physique, Les Ulis, France, 1990).
[32] L. M. Roth, B. Lax, and S. Zwerdling, Phys. Rev. **114**, 90 (1959).
[33] L. I. Magaril, D. A. Romanov, and A. V. Chaplik, Zh. Éksp. Teor. Fiz. **113**, 1411 (1998) [JETP **86**, 771 (1998)].
[34] L. I. Magaril and A. V. Chaplik, JETP Lett. **64**, 460 (1996); Zh. Éksp. Teor. Fiz. **115**, 1478 (1999) [JETP **88**, 815 (1999)].
[35] L. D. Landau and E. M. Lifshitz, *Statistical Physics*, Part 1 (Pergamon International Lib, 1975).
[36] G.-H. Chen and M. E. Raikh, Phys. Rev. B **60**, 4826 (1999).
[37] M. A. Cusack, P. R. Briddon, and M. Jaros, Phys. Rev. B **54**, 2300 (1996).
[38] O. Olenski, C. S. Kim, O. H. Chung, and C. S. Lee, Phys. Rev. B **55**, 9834 (1997).
[39] W. X. Qiang, J. Phys.: Condens. Matter **12**, 4207 (2000).
[40] I. I. Sobelman, *Atomic Spectra and Radiative Transitions* (Springer, Berlin, 1991).

4.2 Main results and discussion

We calculated the magnetization and susceptibility of a cylindrical quantum dot with the parabolic confinement potential for electrons when the spin-orbit interaction is included into consideration. Application of a magnetic field along the dot axes generates a complicated structure of the electron energy levels and the theoretical analysis of the parabolic quantum dots in magnetic fields achieves a rich physics. Recently the well pronounced spin-splitting was found by us for the parabolic confinement potential model of semiconductor quantum dots with parameters of InSb and InAs. The spin-splitting at zero magnetic field leads to a crossing of the energy levels in weak external magnetic fields (similarly to the general Paschen-Back effect) and can provide unusual magnetic properties of the quantum dots.

The magnetization for the same number of electrons with and without the spin-orbit interaction is also presented. The magnetization calculated without the spin-orbit interaction demonstrates a clear shell filling behavior: for N=2,6 (closed shells) the magnetic momentum are canceled out at B=0; for N=1,3,4,5 (partially occupied shells) the magnetization takes a positive value at B=0. Our calculation results suggest that the spin-orbit interaction keeps the cancellation for the closed shells and slightly changes the magnetization for N=1,3. The most interesting result we obtain for dots with four and five electrons. The spin-orbit splitting partially lifts up the degeneracy of levels and changes the electron structure. This assures the magnetization to be zero at B=0 for dots with four electrons in contrast to the case without the spin-orbit interaction. The crossing between levels for the quantum dot with four electrons produces a sharp jump in the magnetization and shifts the magnetic susceptibility peak. For the quantum dot with five electrons the jump reflects the crossing between another levels for a higher magnetic field and generates an additional (in comparison to the case with absent of the spin-orbit interaction) peak for the magnetic susceptibility. One can control the spin coupling parameters in planar semiconductor systems by means of external or build-in electric fields. By variations of the fields one can change magnitudes of the parameters. From the above it appears that the peaks of the magnetic susceptibility which are generated by the spin-orbit interaction should have the following interesting properties. It is possible to perform a switching between the configuration with and without spin-orbit interaction by means of the external electric field or the design of quantum dots.

The spin-orbit (SO) interaction in narrow-gap semiconductor quantum dots has been the object of extensive investigations recently. It links the spin and the charge dynamics and opens up the possibility of spin control by means of electric fields in non-magnetic structures. It was found that SO coupling can sufficiently change magnetic properties, far-infrared absorption, and spin relaxation rate in quantum dots. In this work we extended our previous calculations and employ the Local Spin Density Approximation to investigate ground state magnetic properties and addition energy spectra for few electron InSb parabolic quantum dots with strong SO coupling. We consider SO interaction in semiconductor cylindrical quantum dots with a quasi-two-dimensional parabolic confinement for electrons. The addition energy is defined like the following: $E_{add}(N) = E_{dot}(N + 1) - E_{dot}(N)$, where E_{dot} is total ground state energy of electronic system and N is the number of electrons in the dot. Magnetic field is applied along the dot axes generates a complicated structure of the electron energy levels. The addition energy spectrum shows for a small InSb parabolic quantum dot (effective radius ~ 15 nm) with and without including of SO interaction. The SO interaction in combination with weak magnetic fields can break the conventional sequence of “magic numbers” (N=2, 4, 6…) for the lowest stable electronic levels. The lover panel in the figure demonstrates the phenomenon – for the quantum dot with 3 electrons the addition energy is larger than that for 4 electrons. This property can be controlled by an external electric field.

We also investigated theoretically impact of SO interaction on magnetic properties of multi-electronic nano-rings. On the base of the approach described above we simulated the effect of the SO interaction on the electron magnetization and magnetic susceptibility of small rings. Those characteristics demonstrate quite interesting behavior at low temperature. The abrupt

changes of the magnetization and susceptibility at low magnetic fields are attributed to the crossing between the spin-split electron levels in the energy spectrum. Detailed calculation using parameters of InSb semiconductor quantum ring demonstrates an altering in magnetic properties of the ring: from diamagnetic to paramagnetic. We proposed an additional possibility to control the effect magnitude by external electric fields or design of the rings.

5. Nano-structured meta-materials built from non-magnetic InAs/GaAs nano-rings

PHYSICAL REVIEW B **71**, 245332 (2005)

Magneto-optical response of layers of semiconductor quantum dots and nanorings

O. Voskoboynikov
Department of Electronic Engineering and Institute of Electronics, National Chiao Tung University, 1001 Ta Hsueh Road, Hsinchu 300, Taiwan

C. M. J. Wijers
Faculty of Applied Science, University of Twente, P.O. Box 217, 7500 AE Enschede, The Netherlands

J. L. Liu
Department of Applied Mathematics, National Chiao Tung University, 1001 Ta Hsueh Road, Hsinchu 300, Taiwan

C. P. Lee
Department of Electronic Engineering and Institute of Electronics, National Chiao Tung University, 1001 Ta Hsueh Road, Hsinchu 300, Taiwan

(Received 17 February 2005; published 30 June 2005)

In this paper a comparative theoretical study was made of the magneto-optical response of square lattices of nanoobjects (dots and rings). Expressions for both the polarizability of the individual objects as their mutual electromagnetic interactions (for a lattice in vacuum) was derived. The quantum-mechanical part of the derivation is based upon the commonly used envelope function approximation. The description is suited to investigate the optical response of these layers in a narrow region near the interband transitions onset, particularly when the contribution of individual level pairs can be separately observed. A remarkable distinction between clearly quantum-mechanical and classical electromagnetic behavior was found in the shape and volume dependence of the polarizability of the dots and rings. This optical response of a single plane of quantum dots and nanorings was explored as a function of frequency, magnetic field, and angle of incidence. Although the reflectance of these layer systems is not very strong, the ellipsometric angles are large. For these isolated dot-ring systems they are of the order of magnitude of degrees. For the ring systems a full oscillation of the optical Bohm-Ahronov effect could be isolated. Layers of dots do not display any remarkable magnetic field dependence. Both type of systems, dots and rings, exhibit an outspoken angular-dependent dichroism of quantum-mechanical origin.

DOI: 10.1103/PhysRevB.71.245332 PACS number(s): 73.21.−b, 75.20.Ck, 75.75.+a

I. INTRODUCTION

It has been known for a long time that microstructured materials can manipulate electromagnetic radiation. Most of the research in that field focuses at present on photonic crystals, a concept introduced a long time ago.[1] It is known already that microstructured materials can act as photonic crystals. Recent advances in lithography, colloidal chemistry, and epitaxial growth have made it possible to manufacture artificial meta-materials from semiconductor nano-objects. Further application of these materials in technology demands the extension of the usable frequency range. These demands will push research efforts in this field to the limit. Scale reduction is the classical answer to meet these increased frequency demands and that holds particularly for the new nanostructured metamaterials. When these metamaterials can be made to manipulate electromagnetic fields in the optical range, this will be particularly beneficial for potential applications and devices, as well as for new basic science. The short list of possible implementations being at close range, consists of realization of optical quantum computing, metamaterials with negative refractive index[2,3] in the optical region, artificial magnetism in basically nonmagnetic materials[4] and further.

Semiconductor quantum dots and nanorings are nanosized objects resembling artificial atoms.[5,6] From these nanoobjects, the nanorings are the newest and they are topologically different from quantum dots since their geometry is nonsimply connected. This different and unique topology gives them unusual magnetic and magnetooptical properties.[6] The key characteristic of this topology, the center hole, enables trapping of magnetic flux quanta. This property of the nanorings leads to quantum oscillating behavior of the magnetic response of the nanoring for varying magnetic field **B**, the Aharonov-Bohm (AB) effect.[7] For a simultaneously applied optical beam this gives rise to the optical AB effects,[8,9] which can occur only in nanorings. Modification of material properties by means of a magnetic field is an inherent aspect of AB effects, including optical. This option is a prerequisite to make artificial materials, not resembling anything in nature, such as negative refractive index metamaterials.[2]

Up to now, most of the investigations done in the field of magneto-optical effects in nanorings has been about far-infrared (FIR) spectroscopy or magnetophotoluminescence (MP).[4,10–13] In these methods an additional stimulus has been used, apart from the electromagnetic beam, to determine the response of the rings. These stimuli can be the creation of an extrinsic carrier population (FIR) or an electromagnetic beam of higher frequency (MP). In this sense those methods

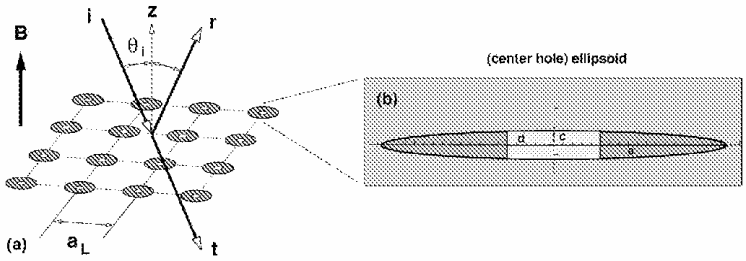

FIG. 1. Schematic diagram of magneto-optical phenomena in a layer of nanorings. a_L lattice constant square lattice. Modeling of dots/rings by means of ellipsoids and center hole ellipsoids. a, c long and short axis, d radius cylindrical center hole. i, r, t incoming, reflected, and transmitted beam, respectively. θ_i angle of incidence.

use preexcitation. The data obtained by these methods are very important, but actually only return averaged single nanoring information. For a quantitative characterization of the optical properties of nanoring-based metamaterials a highly developed optical spectroscopy, such as ellipsometry, and an advanced theoretical description are indispensable. Proper understanding and modeling of the collective electromagnetic response of nanoring layers requires a correct approach, taking into account their composite and discrete character.[14,16] In addition, comparison of the collective magneto-optical response of metamaterials made from semiconductor quantum dots and nanorings can provide important information about the basic physical distinctions between these two types of systems.

II. THEORY

In this paper the collective electromagnetic properties of layers of semiconductor quantum dots and nanorings in the optical range will be studied theoretically. It will be shown that the optical AB effect inherent to the ring structures can enrich the optical properties of nanostructured metamaterials. To reach this goal the theory of optical effects will be developed beyond the single (averaged) quantum dot and nanoring picture. It will turn out that, as a result, the magnitude of these effects is clearly within the range of a modern ellipsometric setup.

A. Polarizability: Quantum mechanics

The systems to be investigated here are two dimensional square lattices of InAs/GaAs quantum dots and nanorings, with lattice parameter a_L as shown in Fig. 1. The basic elements of those lattices are dots and "eye" shaped rings as obtained in recent experiments[17,18] (Fig. 2). For their static electromagnetic response properties these elements will be modeled by means of ellipsoids (for the dots) or center hole ellipsoids (for the rings). This comparative study will use the same outer diameter and aspect ratio for the ellipsoid modeling of both bodies.

Quantum dots and rings are generally classified as artificial atoms. Therefore their optical response should also be described in an atomiclike fashion, e.g., by means of polarizabilities. For atoms such description has been developed originally by Kramers and Heisenberg[19] and a multitude of derivations and modifications exist of this classical model. Optics in combination with quantum dot and ring structures relies either upon expressions for optical absorption[20] or for oscillator strengths,[21,22] being the squared modulus of the optical transition matrix element.[9] It is not straightforward, however, to transfer the Kramers-Heisenberg expressions to the case of a quantum ring or dot, described by means of envelope functions. To cope with the additional pitfalls we have (re)derived the Kramers-Heisenberg equations for this particular case.[23] The present commonly used description is only qualitative and the vector character of the electromagnetic response is not well described. Therefore we start this paper with a rehearsal of the main findings in Ref. 23.

To an arbitrary volume element V, containing material nanoobjects (dots/rings), an external electric field $\mathbf{E}_X(\mathbf{r},t)$ of frequency ω is applied. Electromagnetism requires this electric field to be real valued and it has to be described by

$$\mathbf{E}_X(\mathbf{r},t) = \mathbf{E}_X(\mathbf{r})\cos\omega t = \frac{1}{2}[e^{i\omega t} + e^{-i\omega t}]\mathbf{E}_X(\mathbf{r})$$

and it has been shown in Ref. 23 that for such field the corresponding dipole strength $\mathbf{d}$ induced in the volume V, can be described by

$$\langle \mathbf{d} \rangle_V(t) = \mathrm{Re}[\vec{\alpha}_G(\omega)\mathbf{E}_X(\mathbf{r})e^{-i\omega t}],$$

where α_G is the total monochromatic polarizability. The explicit expression for this monochromatic polarizability α_G is given by[23]

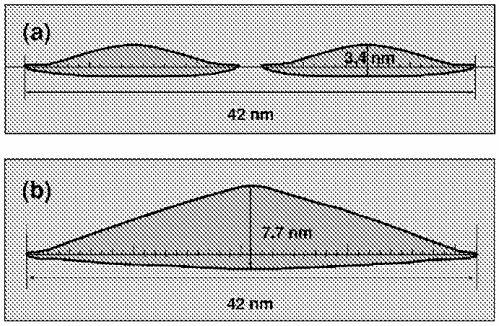

FIG. 2. Typical shape of nanoring and quantum dot structures. (a) Schematic InAs/GaAs "eye" shaped nanoring [after TEM picture (Ref. 17)]. (b) Schematic InAs/GaAs "eye" shaped quantum dot [after TEM picture (Ref. 18)].

$$\vec{\alpha}_G(\omega) = \frac{e^2}{\hbar}\sum_{lk} \langle k|\mathbf{r}|l\rangle_V \langle l|\mathbf{r}|k\rangle_V^T f_{lk}(\omega),$$

$$f_{lk}(\omega) = \left(\frac{2\,\omega_{lk}}{\omega}\right)\left[\frac{\omega[\omega_{lk}^2 - \omega^2 - \gamma_{lk}^2(\omega)] + i\,\gamma_{lk}(\omega)[\omega_{lk}^2 + \omega^2 + \gamma_{lk}^2(\omega)]}{[\omega_{lk}^2 - \omega^2 - \gamma_{lk}^2(\omega)]^2 + 4\omega_{lk}^2\gamma_{lk}^2(\omega)}\right], \quad (1)$$

where e is the electronic charge and $\langle k|\mathbf{r}|l\rangle$ is the transition matrix element. For each pair of levels l, k we have a transition frequency ω_{lk} and corresponding damping γ_{lk}.[23] We have used explicitly that the expression for $\gamma(\omega)$ has to be even in ω. For its specific shape as a function of ω has been chosen:

$$\gamma_{lk}(\omega) = \gamma_{lk}\left(\frac{2\omega_{lk}^2\omega^2}{\omega_{lk}^4 + \omega^4}\right).$$

This expression for $\gamma_{lk}(\omega)$ is just modeling, done such that it is not much different from the traditional ω-independent γ in the region of resonance, where $\omega \approx \omega_{lk}$, and resolves the singularity problems in the near static regime, where $\omega \approx 0$. Since it is in general not possible to obtain γ in a theoretically hard way, a simple algebraic format has been chosen to model it. Equation (1) can be considered to be the "Swiss army knife" of discrete optics. In a twofold sense it is going to be used in this paper. First we will use it to derive an expression for the polarizability of a nanoring in the envelope function approximation. Next we will use it to describe the bulk response of the same semiconductor material, the nanoobject is made from. Such relation is necessary to get an independent value for the matrix element controlling the nanoobject polarizability.

We will need for the two different systems, bulk and dot and ring, the following description for the quasiparticle states:

$$\Psi_{\mathrm{TB}}(\mathbf{r}) = e^{i\mathbf{k}\cdot\mathbf{r}}\phi(\mathbf{r}),\ \text{bulk},$$

$$\Psi_{\mathrm{env}}(\mathbf{r}) = F(\mathbf{r})\phi(\mathbf{r}),\ \text{nanoobject}, \quad (2)$$

where the bulk tight binding function $\phi(\mathbf{r})$ uses the conventional unit cell to define the periodic part of the Bloch states. For InAs the conventional cell consists of four elementary unit cells, each containing one In and one As atom. This cell is cubic and its size is given by the lattice constant a_c. The bulk wave function has to be normalized over the volume of the conventional unit cell $V_B = a_c^3$, and the envelope function over the volume V. This ends up in the conditions

$$\int_{V_B} d\mathbf{r}|\phi(\mathbf{r})|^2 = 1,$$

$$\int_V d\mathbf{r}|F(\mathbf{r})|^2|\phi(\mathbf{r})|^2 = 1. \quad (3)$$

We will need them for any quantitative determination of optical properties.

The first task is to determine the polarizability of a quantum dot or nanoring of volume V in the envelope function approximation. In this approximation the wave functions $\Psi_{uk}(\mathbf{r})$ of the nanoobject have to be written as

$$\Psi_{uk}(\mathbf{r}) = F_{uk}(\mathbf{r})\phi_u(\mathbf{r}),$$

where $F_{uk}(\mathbf{r})$ is the k^{th} envelope function of the nanoobject belonging to the u^{th} Bloch state $\phi_u(\mathbf{r})$ of InAs (or any other III-V compound from which the object is made). For u the value c will be used to describe the conduction and h to describe the valence band states, as before. The envelope function $F(\mathbf{r})$ is dimensionless. In what follows the envelope function matrix element $\langle F_{uk}|F_{ul}\rangle_V$ will be defined as

$$\langle F_{uk}|F_{ul}\rangle_V = \frac{1}{V_B}\int_V d\mathbf{r}\ F_{uk}^*(\mathbf{r})F_{ul}(\mathbf{r}) = \delta_{kl}.$$

The equality follows from combination of both equations in Eq. (3). Now the general expression for the polarizability of an arbitrary volume element (1) needs to be applied to a nanoobject in the envelope function approximation and we need an expression for the optical matrix element $\langle hk|\mathbf{r}|cl\rangle_V$. The Bloch states for the electron and hole states will be different and orthogonal. Then we have

$$\langle hk|\mathbf{r}|\mathrm{cl}\rangle_V = \sum_i^{N_C} F_{hk}^*(\mathbf{r}_i)F_{\mathrm{cl}}(\mathbf{r}_i)\left[\mathbf{r}_i\int_{V_i} d\mathbf{r}'\,\phi_h^*(\mathbf{r}')\phi_c(\mathbf{r}') + \int_{V_i} d\mathbf{r}'\,\phi_h^*(\mathbf{r}')\mathbf{r}'\,\phi_c(\mathbf{r}')\right] = \langle F_{hk}|F_{\mathrm{cl}}\rangle_V\mathbf{r}_{\mathrm{ch}},$$

$$\mathbf{r}_{\mathrm{ch}} = \int_{V_B} d\mathbf{r}'\,\phi_h^*(\mathbf{r}')\mathbf{r}'\,\phi_c(\mathbf{r}') = \langle c|\mathbf{r}|h\rangle_{V_B}, \quad (4)$$

where has been assumed that the entire nanoobject could be split into N_C copies V_i of the conventional unit cell. Inside these cells V_i the envelope function is supposed to be constant. Using the expression for the matrix element (4) we can write the polarizability (1) as

$$\vec{\alpha}_G = \frac{e^2}{\hbar}\sum_{hk,\mathrm{cl}} |\langle F_{hk}|F_{\mathrm{cl}}\rangle_V|^2[\mathbf{r}_{\mathrm{ch}}^*\mathbf{r}_{\mathrm{ch}}^T]f_{hk,\mathrm{cl}}(\omega).$$

Since the optical matrix elements $\langle c|\mathbf{r}|h\rangle_{V_B}$ depend only upon the Bloch states ϕ_u, they do not depend on the indices k, l of the envelope states determined by the geometry of the nanoobjects. Hence,

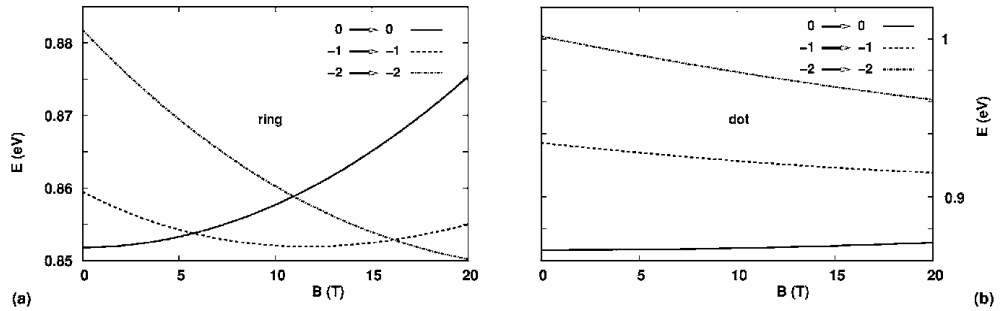

FIG. 3. Transition energy as a function of magnetic field $\mathbf{B}=(0,0,B)$ for $k=l=0,-1,-2$ optical transitions $(k\rightarrow l)$.

$$\vec{\alpha}_G = \frac{e^2}{\hbar}\sum_{h,c}\mathbf{r}_{\mathrm{ch}}^{*}\mathbf{r}_{\mathrm{ch}}^{T}\sum_{k,l}|\langle F_{hk}|F_{cl}\rangle_V|^2 f_{hk,cl}(\omega). \tag{5}$$

To each bulk state ϕ_u belong N_C envelope states. In the calculations to be done further in this paper only a very small number of these envelope states (typically six, three for the heavy hole and three for the electron states) being energetically closest to the energy gap, will be used. This implies that the summation over c involves only the electronic spin m_s. Such procedure is a good approximation for the imaginary part of the polarizability for energies near the band gap. For energies below this gap the polarizability is predominantly real and involves a summation over the tails of all pairs of states. The result of this summation, however, is almost constant as a function of frequency and can therefore be replaced by a constant value α_{GS}. In this approximation we obtain

$$\vec{\alpha}_G(\omega) = \vec{\alpha}_{GS} + \frac{e^2}{\hbar}\sum_{h,m_s}\mathbf{r}_{\mathrm{ch}}^{*}\mathbf{r}_{\mathrm{ch}}^{T}\sum_{k,l}^{3}|\langle F_{hk}|F_{cl}\rangle_V|^2 f_{hk,cl}(\omega). \tag{6}$$

The summation over bulk states is over the indices h, m_s. For the nanosized objects investigated here, only transitions from heavy hole to electronic Bloch states will be taken into account. The reason is that the dot-ring geometry causes the heavy and light hole states to be energetically different, even in the absence of a magnetic field $\mathbf{B}$.

The polarizability expression (6) embodies an intriguing hybrid of classical and quantum-mechanical thinking. The key ingredients of Eq. (6) are the static term α_{GS} and any dynamic single pair contribution in the summation over kl. The α_{GS} dominates the repsonse for frequencies ω being far below the energy gap E_G and is explicitly shape and volume dependent. For any pair kl being at resonance $(\hbar\omega \approx E_{kl})$ the polarizability is dominated by this single pair when the nanoobject and damping γ_{kl} are small enough (the basic assumption of this paper). Then the polarizability depends only weakly, if at all, on shape and volume (there is a volume and shape effect through the energies E_{ik}, but that effect has no influence on the strength of the polarizability as such). Any shape and volume dependence is only in the matrix element $\langle F_{hk}|F_{cl}\rangle_V$ and that is in general not much different from 1. This shape and volume insensitivity of the strength of the polarizability under well observable resonance conditions is a fully quantum-mechanical effect and finds its mirror in similar behavior known from conductance quantization[24]. The apparent and remarkable contrast in behavior of the two major components of the polarizability can be exploited to compare directly in one and the same system classical continuous and quantized electromagnetic response.

To determine theoretically the required polarizabilities, asks for calculation of the electron and hole energies and wave functions, adjacent to the energy gap (the edge of optical absorption), for our nanoobjects in the presence of a magnetic field $\mathbf{B}$ (see Fig. 3). It was found recently that experimentally relevant simulations of the behavior of the basic elements can only be obtained with three-dimensional models using the experimentally determined shape, strain and composition of the semiconductor nanoobjects.[9,11,4] In the calculation used here, we assume that the electronic structure of these nanoobjects is governed by the hard-wall confinement potential due to the discontinuity in effective mass parameters over the edges of these objects themselves. This model is commonly used to calculate electron energy states in quantum heterostructures[25] and allows us to solve the 3D Schrö dinger equation with a minor number of additional approximations. This is particularly useful in this study where we concentrate on the collective optical properties of systems of dots and rings.

Prior to writing the detailed description of the energetic structure of dots and rings we introduce the additional geometric index i:

$$i = (i),(e) \tag{7}$$

and where index u will be as defined before. If index i has value (i) it refers to the inner region of the dots and rings and with value (e) to the surrounding embedding matrix. The effective envelope function Hamiltonian is given in the form

$$\hat{H} = \mathbf{p}_c\frac{1}{2m_u(E,\mathbf{r})}\mathbf{p}_c + V_i(\mathbf{r}) + \mu_B\frac{g_u(E,\mathbf{r})}{2}\sigma\mathbf{B},$$

$$\mathbf{p}_c = -i\hbar\nabla_r + e\mathbf{A}(\mathbf{r}), \tag{8}$$

where $\mathbf{p}_c$ stands for the electronic canonical momentum operator, ∇_r is the spatial gradient, and $\mathbf{A}(\mathbf{r})$ is the vector potential $(\mathbf{B}=\nabla\times\mathbf{A})$. For electrons $m_c(E,\mathbf{r})$ and $g_c(E,\mathbf{r})$ are

the energy- and position-dependent effective mass and Landé factor, respectively,

$$\frac{1}{m_c(E,\mathbf{r})} = \frac{2P^2}{3\hbar^2}\left(\frac{2}{E+E_g(\mathbf{r})-V_c(\mathbf{r})} + \frac{1}{E+E_g(\mathbf{r})-V_c(\mathbf{r})+\Delta(\mathbf{r})}\right),$$

and

$$g_c(E,\mathbf{r}) = 2\left(1-\frac{m_0}{m_c(E,\mathbf{r})}\left[\frac{\Delta(\mathbf{r})}{3[E+E_g(\mathbf{r})-V_c(\mathbf{r})]+2\Delta(\mathbf{r})}\right]\right),$$

where $V_c(\mathbf{r})$ is the confinement potential, $E_g(\mathbf{r})$ and $\Delta(\mathbf{r})$ stand for position-dependent energy band gap and spin-orbit splitting in the valence band, P is the momentum matrix element (Kane parameter), and σ is the vector of the Pauli matrices. The free electron mass is m_0. For the heavy holes $m_{\mathrm{HH}}(E,\mathbf{r})$ and $g_{\mathrm{HH}}(E,\mathbf{r})$ are assumed to be not energy dependent. The hard-wall confinement potential V_u is given for both electrons and holes by

$$V_u^i(\mathbf{r}) = 0,$$

$$V_u^e(\mathbf{r}) = V_u^e. \tag{9}$$

We consider cylindrically symmetric nano-objects (dots and rings), the shape of which is generated by rotating the contours of Fig. 2 around the z axis.[4,9,11,26] When the magnetic field is directed along this z axis we can treat the problem in cylindrical coordinates (ρ,ϕ,z). The origin of the system is lying in the center of the object.

Because of the cylindrical symmetry of the system the full wave function can be represented as

$$\Psi(\mathbf{r}) = F_{uk}(\mathbf{r})\phi_u(\mathbf{r}),$$

$$F_{uk}(\mathbf{r}) = F_{uk}(\rho,z)e^{ik\phi}, \tag{10}$$

where $F_{uk}(\mathbf{r})$ is the envelope function and $\phi_u(\mathbf{r})$ is the periodic part of the Bloch state at Γ for the semiconductor it belongs to. Labels $k=0,\pm1,\pm2,\ldots$, are the orbital quantum numbers for the envelope function, of which only three will be used here for each bulk Bloch state. For the calculations of this paper we need especially detailed expressions for the heavy hole band states ϕ_{ljm_j} at Γ as required by the Kane model.[27] The quantum number l belongs to the orbital angular momentum, the quantum numbers j, m_j determine the total angular momentum. The hole states are

$$\phi_{1,3/2,3/2} = |h_{3/2}\rangle = \sqrt{\frac{1}{2}}[|p_x\rangle + i|p_y\rangle]\uparrow,$$

$$\phi_{1,3/2,1/2} = |h_{1/2}\rangle = -\sqrt{\frac{2}{3}}|p_z\rangle\uparrow + \sqrt{\frac{1}{6}}[|p_x\rangle + i|p_y\rangle]\downarrow,$$

$$\phi_{1,3/2,-1/2} = |h_{-1/2}\rangle = -\sqrt{\frac{1}{6}}[|p_x\rangle - i|p_y\rangle]\uparrow - \sqrt{\frac{2}{3}}|p_z\rangle\downarrow,$$

$$\phi_{1,3/2,-3/2} = |h_{-3/2}\rangle = \sqrt{\frac{1}{2}}[|p_x\rangle - i|p_y\rangle]\downarrow, \tag{11}$$

where the heavy hole states have $|m_j|=3/2$ and the light hole states have $|m_j|=1/2$.[27] The electron states in the conduction band are at Γ simple product functions

$$\phi_{0,1/2,1/2} = |c_\uparrow\rangle = |s\rangle\uparrow,$$

$$\phi_{0,1/2,-1/2} = |c_\downarrow\rangle = |s\rangle\downarrow. \tag{12}$$

The quantum number m_s determines the projection of the spin along the z axis with values $+\frac{1}{2}(\uparrow)$, $-\frac{1}{2}(\downarrow)$. The chosen geometry determines a 2D Schrödinger equation in the (ρ,z) coordinates

$$\left[-\frac{\hbar^2}{2m_u^i(E)}\left(\frac{\partial^2}{\partial z^2}+\frac{\partial^2}{\partial\rho^2}+\frac{1}{\rho}\frac{\partial}{\partial\rho}-\frac{k^2}{\rho^2}\right)+\frac{m_u^i(E)\Omega_u^{i\,2}(E)\rho^2}{8} + m_s\mu_B g_u^i(E)B+\frac{\hbar\Omega_u^i(E)}{2}k+V_{u0}^i\right]F_{uk}^i(\rho,z) = E_{uk}F_{uk}^i(\rho,z), \tag{13}$$

where we have introduced the cyclotron frequency $\Omega_u^i(E)$ as

$$\Omega_u^i(E) = \frac{eB}{m_u^i(E)}.$$

The Ben Daniel-Duke boundary conditions for the problem with the hard-wall potential[25] can be written as

$$F_{uk}^i[\rho,z(\rho)] = F_{uk}^e[\rho,z(\rho)], \tag{14}$$

$$\frac{1}{m_u^i(E)}\left[\frac{\partial F_{uk}^i[\rho,z(\rho)]}{\partial\rho}\right] = \frac{1}{m_u^e(E)}\left[\frac{\partial F_{uk}^e[\rho,z(\rho)]}{\partial\rho}\right][z=z(\rho)],$$

where $z=z(\rho)$ represents the generating contour for the dots or rings in the (ρ,z) plane. In the expression above we have omitted the explicit reference to electron and hole states for reasons of clarity.

B. Polarizability: Optical matrix element

In the expression (6) for the total polarizability α_G of the nanoobjects in the envelope function approximation a crucial bulk parameter is the optical matrix element $\mathbf{r}_{\mathrm{ch}}$. This matrix element connects the bulk valence and conduction band states at Γ as will be worked out here. Despite the advanced state of the field of optoelectronics[28–31] there is still uncertainty about the correct value of this optical matrix element. For this paper we will use the value given by Eliseev[31] since it is based upon experimental observations. As will be clear from the following we will have to assign to r_{ch} the value of 0.60 nm.

The optical response of a III-V semiconductor in the Kane description is governed by transitions between the full states $|h\rangle$ and $|c\rangle$ and not between the basic states $|p_{xyz}\rangle$ and $|s\rangle$. All transitions starting from the hole states $|h\rangle$ at the top of the (bulk) valence band and ending in the $|s\rangle\uparrow$ state yield three matrix elements

$$\mathbf{r}_{3/2\uparrow} = \langle e_\uparrow|\mathbf{r}|h_{3/2}\rangle = \sqrt{\frac{1}{2}}[\hat{\mathbf{x}} + i\hat{\mathbf{y}}]r_v,$$

$$\mathbf{r}_{1/2\uparrow} = \langle e_\uparrow|\mathbf{r}|h_{1/2}\rangle = -\sqrt{\frac{2}{3}}\hat{\mathbf{z}}\, r_v,$$

$$\mathbf{r}_{-1/2\uparrow} = \langle e_\uparrow|\mathbf{r}|h_{-1/2}\rangle = -\sqrt{\frac{1}{6}}[\hat{\mathbf{x}} - i\hat{\mathbf{y}}]r_v. \tag{15}$$

These three elementary matrix elements govern the actual optical response of III-V semiconductors and have to be used in a twofold sense. At first we need them to describe the *bulk optical response* at the interband transitions onset, where the light and heavy hole band states are degenerate. For the bulk response at the interband transitions onset, Eq. (6) can be used, if we set $F_{hk}=F_{el}=1$, with $k=l=1$ and let h scan both the heavy and light hole bulk states $(m_j=\frac{3}{2},\frac{1}{2},-\frac{1}{2})$. Then all three matrix element contribute equally and Eq. (6) yields effectively a sum of the direct products of the three vectors

$$\sum_{m_j} \mathbf{r}^*_{m_j\uparrow}\mathbf{r}^T_{m_j\uparrow} = r_v^2\left[\frac{2}{3}\hat{\mathbf{x}}\cdot\hat{\mathbf{x}}^T + i\frac{1}{3}\hat{\mathbf{x}}\cdot\hat{\mathbf{y}}^T - i\frac{1}{3}\hat{\mathbf{y}}\cdot\hat{\mathbf{x}}^T + \frac{2}{3}\hat{\mathbf{y}}\cdot\hat{\mathbf{y}}^T + \frac{2}{3}\hat{\mathbf{z}}\cdot\hat{\mathbf{z}}^T\right]. \tag{16}$$

For transitions to the $|s\rangle\downarrow$ state the xy components change sign. Therefore the total sum of direct vector products over both spin orientations becomes

$$\sum_{m_j,m_s} \mathbf{r}^*_{m_j,m_s}\mathbf{r}^T_{m_j,m_s} = r_{\rm ch}^2[\hat{\mathbf{x}}\cdot\hat{\mathbf{x}}^T + \hat{\mathbf{y}}\cdot\hat{\mathbf{y}}^T + \hat{\mathbf{z}}\cdot\hat{\mathbf{z}}^T]$$

$$r_{\rm ch}^2 = \frac{4}{3}r_v^2. \tag{17}$$

This is indeed the isotropic kind of response which the bulk of a III-V semiconductor should yield. The quantity $r_{\rm ch}$ is the bulk real space optical matrix element, as (should be) used elsewhere in the literature.

For the optical response of quantum dots and nanorings the situation is different. The geometry lifts the degeneracy of heavy and light hole states. This means, as mentioned already, that for light hole states the absorption takes place at higher energies than for the heavy hole states. For frequencies being almost at the gap of the nanoring this means that only the first matrix element $(m_j=\frac{3}{2})$ in Eq. (15) contributes and Eq. (16) now becomes

$$\sum_{m_j} \mathbf{r}^*_{m_j\uparrow}\mathbf{r}^T_{m_j\uparrow} = r_v^2\left[\frac{1}{2}\hat{\mathbf{x}}\cdot\hat{\mathbf{x}}^T + i\frac{1}{2}\hat{\mathbf{x}}\cdot\hat{\mathbf{y}}^T - i\frac{1}{2}\hat{\mathbf{y}}\cdot\hat{\mathbf{x}}^T + \frac{1}{2}\hat{\mathbf{y}}\cdot\hat{\mathbf{y}}^T\right] \tag{18}$$

Incorporating the other spin orientation to this result then yields

$$\sum_{m_j} \mathbf{r}^*_{m_j\uparrow}\mathbf{r}^T_{m_j\uparrow} = r_{v\perp}^2[\hat{\mathbf{x}}\cdot\hat{\mathbf{x}}^T + \hat{\mathbf{y}}\cdot\hat{\mathbf{y}}^T]. \tag{19}$$

These findings have to be used in Eq. (6) and we have

$$\vec{\alpha}_G(\omega) = \vec{\alpha}_{GS} + \frac{3}{4}\frac{e^2}{\hbar}r_{\rm ch}^2[\hat{\mathbf{x}}\cdot\hat{\mathbf{x}}^T + \hat{\mathbf{y}}\cdot\hat{\mathbf{y}}^T]\sum_{l=0}^{-2}|\langle F_{hl}|F_{el}\rangle_1|^2 f_{hl,el}(\omega). \tag{20}$$

The damping term γ_{lk} in expression (2) for $\gamma_{lk}(\omega)$ will be chosen to be independent from the indices lk in the near energy gap region. It will be referred to further as γ and its value will be chosen such that the experimentally observed linewidth's will be replicated.

C. Polarizability: Electromagnetism

The polarizability expressions we have derived until here are derived straight by using Ref. 23 and are purely theoretical. As mentioned in that paper all issues related to electromagnetic self interaction have been discarded. To be of use for experimental work these issues need to be addressed here. This holds also for the relationship between continuum and discrete quantities as used in the hybrid approach of this paper. The discussion should start with the response of a *single* quantum dot or nanoring. If we use the theoretical polarizability α_G, exactly as prescribed by Eq. (5), the induced dipole strength $\mathbf{d}$ follows from

$$\mathbf{d} = \vec{\alpha}_G\mathbf{E}_A,$$

$$\mathbf{E}_A = \mathbf{E}_X + \vec{\mathbf{t}}\cdot\mathbf{d}, \tag{21}$$

where $\mathbf{E}_A$ is the average electric field over the volume of the dot or ring. It is by definition different from the external field by an amount controlled by the electromagnetic self-interaction tensor $\mathbf{t}$, as described above. For bodies of revolution with the z axis as axis of revolution this tensor is given in general by

$$\vec{\mathbf{t}} = \vec{\mathbf{t}}_S + \frac{ik^3}{6\pi\epsilon_0}\vec{\mathbf{1}},$$

$$t_{S,vv} = -\frac{N_v(\zeta)}{\epsilon_0 V},$$

$$N_x(\zeta) = N_y(\zeta) = \frac{1 - N_z(\zeta)}{2}, \tag{22}$$

where $v=x,y,z$. Both the static part $\mathbf{t}_S$ and its k^3 dependent dynamic addition have been obtained already by Lorentz. In the electromagnetic literature, they are commonly known as the (static) Lorentz field and radiative damping term. Since only outgoing waves will be considered to be allowed, a change in sign of ω will cause also k to change sign. As a result the self interaction tensor turns into its complex conjugate then.

The self interaction tensor is controlled for bodies of revolution by their volume V and depolarization factor N_z. For ellipsoids with short axis c in the z direction and long axis a in the remaining x, y directions, depolarization factor and volume are given by

$$N_z(\zeta) = \frac{1}{1-\zeta^2}\left(1 - \frac{\zeta\cos^{-1}\zeta}{\sqrt{1-\zeta^2}}\right),$$

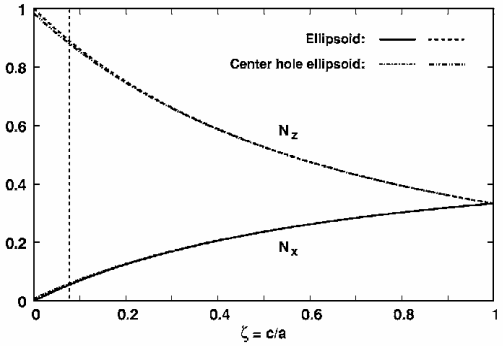

FIG. 4. Depolarization factors $N_{x,z}$ as a function of the aspect ratio $\zeta=c/a$ for normal and center hole ellipsoid. Dashed line at $\zeta=0.081$. Center hole diameter $d=0.257\ a$.

$$V=\frac{4}{3}\pi\zeta a^3, \tag{23}$$

where $\zeta=c/a$ is the aspect ratio of the ellipsoid. The Lorentz factor 1/3 is only obtained for the value of $\zeta=1$, corresponding to a sphere. Notice that $N(\zeta)$ is positive. Since $t_{S,zz}$ is negative then, we see that the (average) field inside a dielectric ellipsoid will always be smaller than the external field applied to the ellipsoid, in agreement with the electromagnetism of dielectrics. Along the main axes of the ellipsoid, the electromagnetic self-interaction tensor is diagonal.

The calculation of the electromagnetic self-interaction for the case of a ring-shaped body is a considerable numerical exercise. In the past attempts have been made to derive it for the case of a torus,[32] but a simple approximate analytical expression can also be obtained by removing a central cylinder with radius d from the ellipsoid treated before. Introducing the angle $\theta_0=\sin^{-1}(d/a)$, we obtain for this case

$$N_\zeta(\zeta)=\frac{1}{2(1-\zeta^2)}\left\{1+\cos\theta_0-\frac{\zeta}{\sqrt{1-\zeta^2}}[\sin^{-1}(\cos\theta_0\sqrt{1-\zeta^2})+\cos^{-1}(\zeta)]\right\},$$

$$V=\frac{4}{3}\pi\zeta a^3\left(1-\frac{d^2}{a^2}\right)^{3/2}. \tag{24}$$

The main assumption, apart from the shape chosen, is that the polarization density inside this open ellipsoid has to be constant. Though this is definitely a regula falsi solution, we do not expect much deviation from the correct result for very oblate ellipsoids. The depolarization factors for both types of ellipsoid are shown in Fig. 4. The depolarization factor hardly depends on the presence of the center hole.

For the case that we want to measure the polarizability of a single dot or ring, we have to proceed differently. For the experimental situation we have to use

$$\mathbf{d}=\vec{\alpha}\mathbf{E}_X, \tag{25}$$

where this experimental polarizability α embodies also the electromagnetic self-interaction. Combining properly the two prescriptions for the induction (21) and (25) leads to

$$\vec{\alpha}^{-1}=\vec{\alpha}_G^{-1}-\vec{\mathbf{t}}. \tag{26}$$

This is a very important relationship, showing that there should be a serious discrepancy between measured and quantum mechanically calculated polarizabilities.

In expression (20) for α_G we need separately an expression for α_{GS}, the quantum-mechanical static polarizability tensor of the dot or ring. For the special case that we represent the dot by an strongly oblate homogeneous dielectric ellipsoid with relative dielectric constant ϵ, this static polarizability is *isotropic* and can easily be obtained. It suffices to introduce for this ellipsoid its α_{GS} as

$$\alpha_{GS,vv}=\alpha_{GS}=\epsilon_0 V(\epsilon-1)=\alpha_0 f_V(\epsilon-1),$$

$$\alpha_0=4\pi\epsilon_0 a_L^3,$$

$$f_V=\frac{\epsilon_0 V}{\alpha_0}=\frac{V}{4\pi a_L^3}, \tag{27}$$

where we introduce the two normalization factors α_0 and f_V. Next we use Eq. (26) to determine the measurable polarizability α_S:

$$\alpha_{S,vv}=\frac{\alpha_{GS}}{1-t_{S,vv}\alpha_{GS}}=\epsilon_0 V\left[\frac{\epsilon-1}{1+N_v(\epsilon-1)}\right]. \tag{28}$$

The same expression has been obtained along a different line of derivation by Avelin.[33] For arbitrary shapes of the dots and rings only a full numerical calculation can be done. The result of such calculation will be $\alpha_{S,vv}$. In Eq. (20) we need $\alpha_{GS,vv}$ and not $\alpha_{S,vv}$. The expression for $\alpha_{GS,vv}$ is simple and given already in Eq. (27). The numerical determination of $\alpha_{S,vv}$ is necessary to obtain the right value for $\mathbf{t}_S$ for arbitrarily shaped bodies from the relation

$$\vec{\mathbf{t}}_S=\vec{\alpha}_{GS}^{-1}-\vec{\alpha}_S^{-1}. \tag{29}$$

This value for $t_{S,vv}$ determines the expression for the applied field in case of arbitrarily shaped bodies.

If we surround this individual dot or ring by a (square) lattice of identical dots and rings, with a_L as lattice spacing, the only difference is that we have to replace the external field $\mathbf{E}_X$ by the local field $\mathbf{E}_L$, given for the single lattice plane by

$$\mathbf{E}_L=\mathbf{E}_X+\vec{\mathbf{f}}'\cdot\mathbf{d},$$

$$\mathbf{E}_A=\mathbf{E}_L+\vec{\mathbf{t}}\cdot\mathbf{d}, \tag{30}$$

where $\mathbf{f}'$ is the intraplanar transfer tensor for the plane. This transfer tensor $\mathbf{f}'$ can be determined numerically to any precision using the Ewald one-fold integral transform.[15] Vlieger, however, has derived, after much effort, a more concise expression:[16]

$$\vec{\mathbf{f}}' = \alpha_0^{-1}\vec{\mathbf{f}}'_S + \frac{i}{2\epsilon_0 a_L^2 k_z}[k^2\vec{\mathbf{i}} - \mathbf{k}_\parallel\mathbf{k}_\parallel^T - k_z^2\hat{\mathbf{z}}\cdot\hat{\mathbf{z}}^T] - \frac{ik^3}{6\pi\epsilon_0}\vec{\mathbf{i}},$$

$$\mathrm{f}'_{S,xx} = \mathrm{f}'_{S,yy} = -4.51681,$$

$$\mathrm{f}'_{S,zz} = -2\,\mathrm{f}'_{S,xx} = 9.03362, \tag{31}$$

where parallel (∥) means parallel to the plane of the dots or rings. The strong aspect of the Vlieger expression is that it gives the intraplanar transfer tensor as a dynamical correction to its static counterpart. This guarantees smooth linkage to the static result, being for a square lattice essentially only the numbers given above. The induction for a dot or ring inside a lattice now becomes

$$\mathbf{d} = \vec{\alpha}_G[\mathbf{E}_X + (\vec{\mathbf{f}}' + \vec{\mathbf{t}})\mathbf{d}],$$

$$(\vec{\mathbf{f}}' + \vec{\mathbf{t}}) = \alpha_0^{-1}(\vec{\mathbf{f}}'_S + \vec{\mathbf{t}}_S) + \frac{i}{2\epsilon_0 a_L^2 k_z}[k^2\vec{\mathbf{i}} - \mathbf{k}_\parallel\mathbf{k}_\parallel^T - k_z^2\hat{\mathbf{z}}\cdot\hat{\mathbf{z}}^T],$$

$$\mathrm{t}_{S,vv} = -\frac{N_v(\zeta)}{f_V}, \tag{32}$$

where, as in the Vlieger derivation, the radiation damping term has disappeared.

D. Electromagnetic response

The electromagnetic response of the layer of dots/rings, has to be determined in two steps. The dipole strength $\mathbf{d}$ induced in the plane is obtained from

$$\mathbf{d} = [\vec{\mathbf{i}} - \vec{\alpha}_G(\vec{\mathbf{f}}' + \vec{\mathbf{t}})]^{-1}\vec{\alpha}_G\mathbf{E}_X. \tag{33}$$

The reflected electric fields at a remote site $\mathbf{R}$ are now given by

$$\mathbf{E}_R(\mathbf{R}) = \vec{\mathbf{f}}_R\mathbf{d},$$

$$\vec{\mathbf{f}}_R = \frac{i\,k^2 e^{i\underline{\mathbf{k}}\cdot\mathbf{R}}}{2\epsilon_0 a_L^2 \beta k_z}[\vec{\mathbf{i}} - \hat{\underline{\mathbf{k}}}\cdot\hat{\underline{\mathbf{k}}}^T],$$

$$\underline{\mathbf{k}} = \mathbf{k}_\parallel - k_z\hat{\mathbf{z}}, \tag{34}$$

where $\mathbf{f}_R$ is the remote interplanar transfer tensor. Physically only those electric fields make sense which go in a direction away from the sources. This means that when the sign of ω is changed also the corresponding wave number or wave vector has to change sign. Therefore it is easily seen that in the above expression when ω is replaced by $-\omega$, both k and k_z have to change sign. Therefore all transfer tensors $\mathbf{t}$, $\mathbf{f}'$, and $\mathbf{f}_R$ will always turn into their complex conjugate when ω changes sign. We have shown already in detail that the same behavior applies also to α_G.[23] This mathematical property guarantees that the dipole strength induced in the plane and the electric field emitted by the plane of dots and rings will be real according to

$$\mathbf{E}(\mathbf{r},t) = \mathrm{Re}[\vec{\mathbf{f}}_R(\omega)\mathbf{d}(\omega)e^{-i\omega t}]. \tag{35}$$

This elementary result and Eqs. (33) and (34) allow the entire electromagnetic derivation to be done using a single complex exponential. Also the following relationship is useful, if not indispensable:

$$\langle AB\rangle = \frac{1}{T}\int_0^T dt\, A(t)B(t) = \frac{1}{T}\int_0^T dt\, \mathrm{Re}[\tilde{A}_0 e^{-i\omega t}]\mathrm{Re}[\tilde{B}_0 e^{-i\omega t}]$$

$$= \frac{1}{2}\mathrm{Re}[\tilde{A}_0^*\tilde{B}_0] \tag{36}$$

for any two harmonic fields $A(t)$, $B(t)$ and further $\omega T = 2\pi$. For electromagnetic derivations, different from the quantum-mechanical derivations treated in Ref. 23, the complex notation is only auxiliary in character and allows for the common smooth usage.

In a further straightforward manner it is easy to show now that only the following reflection and transmission coefficients suffice to describe the full electromagnetic response of a square plane of dots and rings:

$$r_{ss} = \frac{f_k}{A_y\cos\theta_i - f_k},$$

$$r_{pp} = \frac{f_k\cos\theta_i}{A_x - f_k\cos\theta_i} - \frac{f_k\sin^2\theta_i}{A_z\cos\theta_i - f_k\sin^2\theta_i},$$

$$t^{=}_{ss} = 1 + r_{ss},$$

$$t^{=}_{pp} = \frac{f_k\cos\theta_i}{A_x - f_k\cos\theta_i} - \frac{A_z\cos\theta_i}{A_z\cos\theta_i - f_k\sin^2\theta_i}, \tag{37}$$

where θ_i is the angle of incidence. Further use has been made of the notation $t^{=}$ for the transmission coefficient to distinguish it from the self-interaction t and of the following abbreviations to make the expressions more concise:

$$A_v = \alpha_0\alpha_{G,vv}^{-1} - (\mathrm{f}'_{S,vv} + \mathrm{t}_{S,vv}),$$

$$f_k = 2\pi i a_L k \tag{38}$$

with v as defined before. These reflection coefficients are not directly measurable as they are. Measurable are only the reflectances R_{qq} and transmittances T_{qq} defined as

$$R_{qq} = r_{qq}^* r_{qq},$$

$$T_{qq} = t^{=*}_{qq} t^{=}_{qq}, \tag{39}$$

where q stands for the ellipsometric directions s, p. From the energy balance point of view these quantities determine the absorbance A_{qq} in the lattice plane according to

$$A_{qq} = 1 - R_{qq} - T_{qq} = \frac{\omega\mu_0 c}{a_L^2 E_X^2\cos\theta_i}\mathrm{Im}(\mathbf{E}_A^{*T}\mathbf{d}),$$

where E_X is the amplitude of the externally incoming plane wave. Measurable, but less directly, are also the ellipsometric angles Ψ, Δ, which follow from the commonly used definition:

TABLE I. Basic input parameters for lattices of dots and rings. For the meaning of the symbols, see text.

	Quantum dot	Nanoring
a_L	80.0 nm	80.0 nm
a	18.45 nm	18.45 nm
c	1.49 nm	1.49 nm
d	0.00 nm	4.75 nm
$\lvert\langle F_{h0}\rvert F_{c0}\rangle_V\rvert$	0.9454	0.9
$\lvert\langle F_{h,-1}\rvert F_{c,-1}\rangle_V\rvert$	0.9285	0.9
$\lvert\langle F_{h,-2}\rvert F_{c,-2}\rangle_V\rvert$	0.9120	0.9
r_{ch}	0.60 nm	0.60 nm
ϵ	12.2	12.2
$E_G(T=0\,^\circ\mathrm{K})$	0.42 eV	0.42 eV

$$\rho_r = \frac{r_{pp}}{r_{ss}} = \tan\Psi\, e^{i\Delta}$$

In the next section these experimentally accessible quantities will be calculated numerically for the plane of dots and rings.

III. NUMERICAL RESULTS

Using the above expressions for reflection coefficients and related ellipsometric angles Ψ, Δ, we have determined the optical response of a square lattice made from nanorings and, for comparison, from quantum dots. All relevant input material has been collected in Table I.

The optical response for individual dots and rings is completely controlled by the polarizability α_G, given by Eq. (20). The static part of it, α_{GS}, is given by Eq. (27) and is completely determined by the volume V. Volume V is given for the ellipsoid by Eq. (23) and for the center hole ellipsoid by Eq. (24). The geometrical data determining these ellipsoids (see Fig. 1) are a, c, and d and have the values given in Table I. The aspect ratio ζ for both ellipsoids and center hole ellipsoids then becomes

$$\zeta = c/a = 0.081$$

and the corresponding depolarization factors N_z, N_x are for the ellipsoids (dots):

$$N_z = 0.8848, \quad N_x = 0.0576$$

and for the center hole ellipsoids (rings)

$$N_z = 0.8757, \quad N_x = 0.0622.$$

The volume of the ellipsoid (dot) is $V = 2.125 \times 10^{-24}$ m^3 and for the center hole ellipsoid (ring) $V = 1.917 \times 10^{-24}$ m^3. To calculate the static polarizability α_{GS} we need the value of the dielectric constant ϵ for (InAs), the material making up the dot or ring and given in Table I. That number belongs to high-frequency (IR) data at room temperature, since we consider that to be the best choice.

For an single isolated dot or ring, using Eq. (28), we find the following tensor components α_{GS} and α_{vv} for dots:

$$\alpha_{GS} = 3.711 \times 10^{-3}\alpha_0,$$

$$\alpha_{S,xx} = 2.256 \times 10^{-3}\alpha_0,$$

$$\alpha_{S,zz} = 3.401 \times 10^{-4}\alpha_0,$$

and correspondingly for rings

$$\alpha_{GS} = 3.348 \times 10^{-3}\alpha_0,$$

$$\alpha_{S,xx} = 2.188 \times 10^{-3}\alpha_0,$$

$$\alpha_{S,zz} = 3.434 \times 10^{-4}\alpha_0,$$

where $\alpha_0 = 5.69677 \times 10^{-32}$ F m^2. The anisotropy of the static polarizability α_S is entirely due to the electromagnetic self-interaction of the dot or ring. Quantum mechanics plays no role in it.

This will change for frequencies near the energy gap of the dot or ring. Then there is a strong quantum-mechanical contribution to the anisotropy. To determine numerically the dynamic quantum-mechanical part of the polarizability α_G requires knowledge of the overlap matrix elements $\langle F_{hl}\rvert F_{cl}\rangle$. Those were obtained numerically by solving the effective mass Hamiltonian (13) with the Ben Daniel-Duke boundary condition (14). The resulting values are in Table I . There is also the bulk optical matrix element r_{ch}. The transition frequencies ω_{ik} are shown in Fig. 3, but the damping γ can only be used as a free parameter. We have used two values 2 meV and 5 meV for it. If we take $\hbar\omega = 0.86$ eV as a typical energy for the interband transitions of the dots or rings, this corresponds to a wavelength $\lambda = 1459$ nm, well beyond the lattice spacing a_L. This ensures that the Vlieger expressions can be used as they are and that we do not have to bother about possible higher order reflections.

The ellipsometric angles Ψ and Δ are shown for this configuration in Figs. 5 and 6. They are shown in each figure for dots at the left and for rings at the right. The upper panels show results for $\gamma = 2$ meV and the lower panels for $\gamma = 5$ meV. The crucial difference between dots and rings is in the crossing of energy levels. For dots there are no crossings for varying magnetic field strength B, opposite to the behavior of the rings. So the Ψ data display quite monotonous ridgelike patterns for dots but a clear "hill/valley" pattern for rings. This represents a typical manifestation of the optical Aharonov-Bohm effect. This more remarked dependence of the rings upon changes in the magnetic field strength gives them better characteristics for practical use than dots.

This behavior becomes even more manifest for the other ellipsometric angle Δ as shown in Fig. 6. In degrees the peak to peak values for Δ are about five times larger than the corresponding variation in Ψ. Rings in general respond stronger for both angles than dots. This is remarkable, since the volume fraction f_V is smaller for rings than for dots. Yet the understanding of this behavior is quite down to earth: the crossings cause two pairs to contribute in resonance simultaneously and this effectively doubles the response. All values drop by about the same factor as the damping γ is increased for all cases. This is due and in agreement with the general behavior of the frequency dependent functions $f_{ik}(\omega)$, as given by Eq. (1). All values for Ψ and Δ have variations of the order of magnitude of degrees and are therefore easily

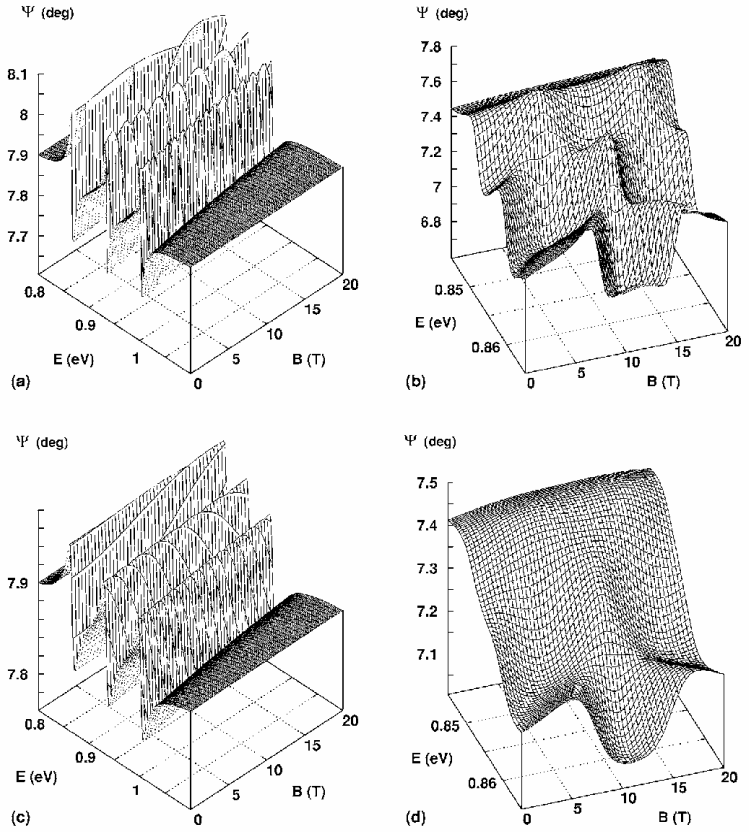

FIG. 5. Ellipsometric angle Ψ for a monolayer of InAs quantum dots and nanorings. (a),(b) Ψ for $\theta_i=60°$ and $\hbar\gamma=2$ meV. (c),(d) Ψ for $\theta_i=60°$ and $\hbar\gamma=5$ meV. Left panels (a),(c): dots, right panels (b),(d): rings.

within range of any modern ellipsometer. Yet it should be mentioned that the variations in Ψ, Δ will reduce drastically, when the embedding is taken into account also, as we hope to show in a forthcoming publication.

The ellipsometric parameters Ψ, Δ are relative quantities and do not contain knowledge about the absolute values of optical response coefficients. Therefore also reflectance and absorbance have been determined for a case where both the ring and the dot lattice have a maximum in the imaginary part of their polarizability (resonance). For both systems we chose a magnetic field strength of $B=7$ T and a damping of $\hbar\gamma=5$ meV. The selected resonance frequencies were $\hbar\omega=0.867$ eV for the dot and $\hbar\omega=0.854$ eV for the ring lattice. The reflectance for those settings is shown in Fig. 7. Typically the values are in the 10^{-5} range, so pretty weak. The ring lattice has a slightly weaker reflectance than the dot lattice, but both systems display the usual angular dependent behavior. The most outspoken aspect is the occurrence for p polarization of the Brewster minimum at about 68°. For bulk InAs the Brewster angle has the value of 74° for comparison.

By means of Eq. (40) we have also calculated the absorbance. This quantity has the most direct connection to the detailed treatment of the microscopic behavior given in this paper, both electromagnetically and quantum mechanically. The results are shown in Fig. 8. The overall picture is that the absorbance in the ring system is stronger than for the dot system. This is the consequence of the enlargement at resonance of the imaginary part of the polarizability due to the crossing of energy levels in the ring system. Indeed the enlargement is about a factor of 2. The most remarkable aspect of the absorbance is the strongly increased dichroism for increasing angles of incidence. For the hypothetical case that the dots or rings would have had an isotropic polarizability, both polarization directions s and p would behave similar to the s components in Fig. 8 . Although the anisotropic behavior of the polarizability of the elements goes back both to electromagnetism (through the electromagnetic self-tensor) and to quantum mechanics (through the expectation value of the position vector), the dichroism is governed in the first place by quantum mechanics. For light components in the z direction the dots and rings will be transparent, for the remaining x, y direction they will be absorbing. So it looks as if research concerning the shape and volume independence of the optical response for isolated levels at resonance, should focus upon absorbance and the dichroism found here.

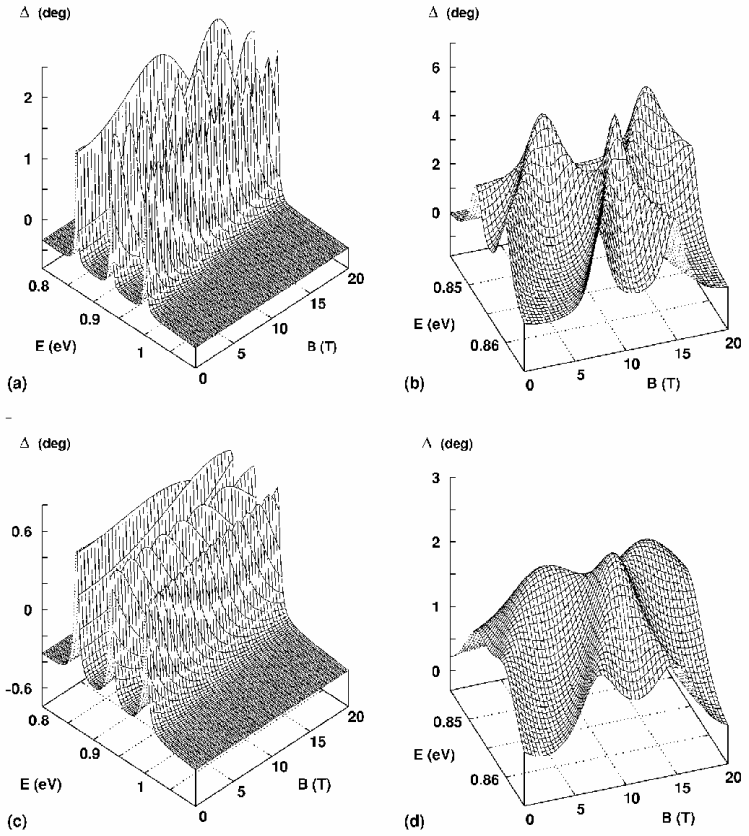

FIG. 6. Ellipsometric angles Δ for a monolayer of InAs quantum dots and nanorings. (a),(b) Δ for $\theta_i=60^\circ$ and $\hbar\gamma=2$ meV. (c),(d) Δ for $\theta_i=60^\circ$ and $\hbar\gamma=5$ meV. Left panels (a),(c): dots, right panels (b),(d): rings.

IV. SUMMARY AND CONCLUSIONS

In this paper we have performed a comparative study of the optical response functions (such as reflectance and absorbance and the ellipsometric angles Ψ, Δ) for quantum dots and nanorings, when they are arranged in a square lattice. We have developed accurate and workable expressions for the response terms of separate quantum dots and nanorings as given by the polarizability. The polarizability is determined

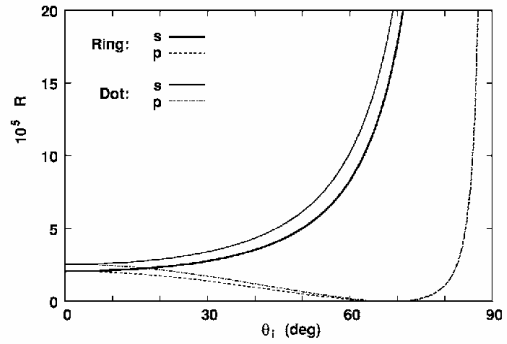

FIG. 7. Reflectance R for a monolayer of InAs quantum dots and nanorings. $B=7$ T. Dots: $\hbar\omega=0.867$ eV, rings: $\hbar\omega=0.854$ eV. Both: $\hbar\gamma=5$ meV.

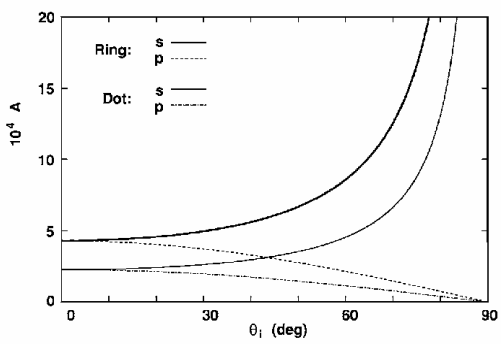

FIG. 8. Absorbance A for a monolayer of InAs quantum dots and nanorings. $B=7$ T. Dots: $\hbar\omega=0.867$ eV, rings: $\hbar\omega=0.854$ eV. Both: $\hbar\gamma=5$ meV.

by both quantum-mechanical and electromagnetic interactions. For nano-objects an outspoken consequence of these two aspects of the polarizability is that far below the energy gap the strength of the polarizability is volume and shape dependent, whereas for separately observable resonant transitions at the absorption edge the strength is volume and shape independent. For the optical response of the square lattices made up from these nano-objects only the electromagnetic interaction needs to be taken into account. The remote response, as represented by reflection and transmission coefficients has been obtained by remote propagators as usual in discrete optics and these coeficients build a key instrument for the quantitative analysis of the magneto-optical response of lattices made from nanosized objects. The calculations clearly show that rings are more effective to exploit the dependence from magnetic fields than dots. Despite a lower volume fraction rings have stronger variation in any of the ellipsometric angles than the dots. The crossing of the transition energies, being characteristic for rings and known as the optical Aharonov-Bohm effect, results in a pronounced variation of the ellipsometric angles for varying magnetic field. The reflectances for both types of lattice are weak, as can be expected from such thin layerlike systems. Remarkable is the strongly increasing dichroism for increasing angles of incidence. Since the origin of this dichroism is in the dynamic part of the anisotropy of the polarizability of the nano-objects, this dichroism can be of use to investigate the size- and shape-dependent behavior of the polarizability. The theoretical findings obtained here, yield also the essential starting point for future work to incorporate the influence of the embedding (capped quantum-dot or nanoring systems). This comparative study shows that use of nano-rings or quantum dots in both the investigation and use of magneto-optical response is in favor of the first.

ACKNOWLEDGMENTS

This work was funded by the National Science Council of Taiwan under Contracts No. NSC-93-2215-E-009-006 and NSC-93-2112-M-009-008.

[1] J. D. Joannopoulos, R. D. Meade, and J. N. Winn, *Photonic Crystals: Molding the Flow of Light* (Princeton University Press, Princeton, 1995).
[2] V. G. Veselago, Sov. Phys. Usp. **10**, 509 (1968).
[3] J. B. Pendry, A. J. Holden D. J. Robbins, and W. J. Stewart, IEEE Trans. Microwave Theory Tech. **47**, 2075 (1999).
[4] O. Voskoboynikov, Yiming. Li, Hsiao-Mei Lu, Cheng-Feng Shih, and C. P. Lee, Phys. Rev. B **66**, 155306 (2002); O. Voskoboynikov and C. P. Lee, Physica E (Amsterdam) **20**, 278 (2004).
[5] D. Bimberg, M. Grundmann, and N. N. Ledentsov, *Quantum Dot Heterostructures* (Wiley Interscience, New York, 1998).
[6] J. M. Garcia, G. Medeiros-Ribeiro, K. Schmidt, T. Ngo, J. L. Feng, A. Lorke, J. Kotthaus, and P. M. Petroff, Appl. Phys. Lett. **71**, 2014 (1997) .
[7] Y. Aharonov and D. Bohm, Phys. Rev. **115**, 485 (1959).
[8] A. O. Govorov, S. E. Ulloa, K. Karrai, and R. J. Warburton, Phys. Rev. B **66**, 081309(R) (2002).
[9] J. I. Climente, J. Planelles, and W Jaskolski, Phys. Rev. B **68**, 075307 (2003); J. Climente, J. Planelles, W. Jaskolski, and J. I. Aliaga, J. Phys.: Condens. Matter **15**, 3593 (2003).
[10] A. Lorke and R. J. Luyken, Physica B **256-B258**, 424(1998); A. Lorke, R. J. Luyken, A. O. Govorov, J. P. Kotthaus, J. M. Garcia, and P. M. Petroff, Phys. Rev. Lett. **84**, 2223 (2000).
[11] J. Planelles, W. Jaskolski, and J. I. Aliaga, Phys. Rev. B **65**, 033306 (2001).
[12] M. Bayer, M. Korkusinski, P. Hawrylak, T. Gutbrod, M. Michel, and A. Forchel, Phys. Rev. Lett. **90**, 186801 (2003).
[13] H. Pettersson, R. J. Warburton, A. Lorke, K. Karrai, J. P. Kotthaus, J. M. Garcia, and P. M. Petroff, Physica E (Amsterdam) **6**, 510 (2000).
[14] G. Y. Slepyan, S. A. Maksimenko, V. P. Kalosha, A. Hoffmann, and D. Bimberg, Phys. Rev. B **64**, 125326 (2001).
[15] G. P. M. Poppe, C. M. J. Wijers and A. van Silfhout, Phys. Rev. B **44**, 7917 (1991).
[16] J. Vlieger, Physica (Amsterdam) **64**, 63 (1973); C. M. J. Wijers and K. M. E. Emmett, Phys. Scr. **38**, 435(1988).
[17] B. C. Lee, O. Voskoboynikov, and C. P. Lee, Physica E (Amsterdam) **24**, 87 (2004).
[18] X. Z. Liao, J. Zou, X. F. Duan, D. J. H. Cockayne, R. Leon, and C. Lobo, Phys. Rev. B **58**, R4235 (1998)
[19] H. A. Kramers and W. Heisenberg, Z. Phys. **31**, 681 (1925).
[20] O. S. Stier, M. G. Grundmann, and D. B. Bimberg, Phys. Rev. B **59**, 5688 (1999).
[21] G. W. Bryant, Phys. Rev. B **37**, 8763 (1988).
[22] P. Enders, A. Bärwolff, M. Woerner, and D. Suisky, Phys. Rev. B **51**, 16 695 (1995).
[23] C. M. J. Wijers, Phys. Rev. A **70**, 063807 (2004).
[24] H. E. van den Brom and J. M. van Ruitenbeek, Phys. Rev. Lett. **82**, 1526 (1999).
[25] G. Bastard, *Wave Mechanics Applied to Semiconductor Heterostructures* (Les Edition de Physique, Les Ulis, 1990).
[26] J. I. Climente, J. Planelles, and J. L. Movilla, Phys. Rev. B **70**, 081301(R) (2004).
[27] E. O. Kane, J. Phys. Chem. Solids **1**, 249 (1957).
[28] M. Asada, A. Kameyama, and Y. Suematsu, IEEE J. Quantum Electron. **20**, 745 (1984); M. Asada and Y. Suematsu, *ibid.* **21**, 434 (1985); M. Asada, Y. Miyamoto, and Y. Suematsu, *ibid.* **22**, 1915 (1986).
[29] L. V. Asryan and R. A. Suris, Semicond. Sci. Technol. **11**, 554 (1996).
[30] S. L. Chuang, *Physics of Optoelectronic Devices* (Wiley, New York, 1995).
[31] P. G. Eliseev, H. Li, A. Stintz, G. T. Liu, T. C. Newell, K. J. Malloy, and L. F. Lester, Appl. Phys. Lett. **77**, 262 (2000).
[32] V. Belevitch and J. Boersma, Philips J. Res. **38**, 79 (1983).
[33] J. Avelin, Ph.D. thesis, Electromagnetics Laboratory, Helsinki University of Technology, 2003.

ELSEVIER

Microelectronics Journal 36 (2005) 564–566

Microelectronics Journal

www.elsevier.com/locate/mejo

Left handed composite materials in the optical range

O. Voskoboynikov[a,*], G. Dyankov[a], C.M.J. Wijers[b]

[a]*Department of Electronics Engineering and Institute of Electronics, National Chiao Tung University, 1001 Ta Hsueh Rd, Hsinchu 300, Taiwan, ROC*
[b]*Faculty of Applied Science, Twente University, P.O.Box 217, 7500 AE Enschede, The Netherlands*

Available online 10 March 2005

Abstract

The purpose of this paper is to show that semiconductor nano-structures built from non-magnetic InAs/GaAs nano-rings can exhibit simultaneously negative effective permittivity and permeability over a certain optical frequency range. The structures are resonant and have this property near the edge of absorption of the nano-rings. This can be particularly interesting in the investigation of the challenging problem of development of left-handed composite materials in the optical range.

Keywords: Left-handed material; Semiconductor nano-rings; Optics

Left handed composite materials (LHCMs) exhibit simultaneously negative permittivity (ε) and permeability (μ) over a certain frequency (ω) range [1–3]. It is acknowledged that LHCMs can have a variety of exciting applications. A particularly important and challenging problem in this field is the realization of LHCMs in the optical frequency range. A negative refractive index was confirmed in the GHz and THz range [3,4] many years after its theoretical prediction [1], but most of magnetic materials at frequencies in the GHz range and above have a magnetic response which is tailing off. That is the reason why it was proposed to realize LHCMs relying upon the idea that inherently nonmagnetic materials can exhibit a magnetic response.

In this work we show theoretically that there is an opportunity to obtain negative permittivity and magnetic permeability simultaneously in the optical range by using nano-structured composite semiconductor materials. Recent advances in the manufacturing of semiconductor nano-rings make it possible to construct arrays of III–V semiconductor nano-scale rings [5]. Just like self-assembled quantum dots, nano-rings posses atom-like optical properties, but at the same time nano-rings are non-simply connected quantum systems, exhibiting unusual magnetic [6–8] and magneto-optical properties [5,9,10]. One of the problems arising in LHCMs for the optical range is that the size of the structural elements has to be of nanometer scale. Another problem is that the use of conductive elements is inappropriate because of the high losses [11]. Semiconductor nano-rings are ideal building blocks and could meet the requirements mentioned. It is necessary to emphasize that structural elements possessing magnetic response, have sizes much smaller than the operating wavelength and the composite materials made from them can be characterized by effective permittivity $\varepsilon(\omega)$ and magnetic permeability $\mu(\omega)$ only [1,2,11].

In this study we show that for three-dimensional photonic structures based on an artificial lattice of InAs/GaAS nano-rings [5] the effective permittivity can be negative in the optical range. At the same time the frequency domain with $\mu(\omega)<0$ can be tuned by changing the individual capacity of the rings.

To demonstrate theoretically a nano-structured composite material with negative permittivity and permeability in the optical range, we first consider a basic cell of a material made from semiconductor nano-rings (see insert in Fig. 1). Two-dimensional square arrays of these cells (with characteristic lattice constant a) then are stacked as a layered meta-structure (with distance between layers l) (Fig. 1). This establishes magnetic activity along the direction of stacking (z-axis in Fig. 1). In this work we consider only TE-polarized light, with the magnetic field parallel to this z-axis.

* Corresponding author. Tel.: +886 3 5612121x54174; +886 3 5724361.
E-mail address: vam@faculty.nctu.edu.tw (O. Voskoboynikov).

0026-2692/$ - see front matter © 2005 Elsevier Ltd. All rights reserved.
doi:10.1016/j.mejo.2005.02.070

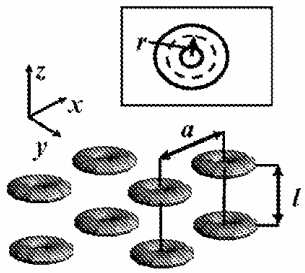

Fig. 1. Schematic diagram of a composite material built from nano-rings. In insert: in-plane cross-section of a single ring with the perimeter determining the effective resistance.

To evaluate the dielectric and magnetic properties of this structure, we first calculate the polarizability tensor $\hat{\alpha}$ of a single ring. For frequencies close to the energy gap of the nano-ring, the size of the ring is smaller as compared to the wavelength. One can use then the dipole approximation and the Kramers–Heisenberg expression for $\hat{\alpha}(\omega)$ [12]:

$$\hat{\alpha}(\omega) = \hat{\alpha}_s + \frac{2e^2}{\hbar}\sum_{i,f}\left(\frac{\omega_{fi}}{\omega}\right)\left[\frac{\langle i|\mathbf{r}|f\rangle\langle f|\mathbf{r}|i\rangle^{\mathrm{T}}}{\omega_{fi}-\omega-i\Gamma}\right] \tag{1}$$

Γ is the damping factor chosen to be independent from frequency near the resonance region. The possible transition energies $\hbar\omega_{fi} = E_f^h - E_i^e$ are determined by the discrete energies E_f^h, E_i^e for the electron and hole states respectively. The dynamic part of the polarizability is determined by the optical matrix elements $\langle i|\mathbf{r}|f\rangle$, the expectation value of the position vector $\mathbf{r}=(x,y,z)$ taken over the volume of the nano-ring. The sum over states in (1) is limited to transitions with the lowest $\hbar\omega_{fi}$, being near the absorption edge of the system.Using the approach proposed in [6,10] and taken into account the cylindrical symmetry of the ring, we obtain for the optical transition elements [10]

$$\langle i|z|f\rangle = 0 \quad |\langle i|x|f\rangle| = \langle i|y|f\rangle| = \left|\frac{\langle S|x|X\rangle}{\sqrt{2}} I_{\mathrm{eh}}\right|,$$

where $I_{\mathrm{eh}} = V_{\mathrm{u}}^{-1}\int \rho d\rho dz \Phi_{\mathrm{e}}(\boldsymbol{\rho},z)\Phi_{\mathrm{h}}(\boldsymbol{\rho},z)$ is the electron-hole overlap integral for the envelope wave functions, V_{u} is the volume of the conventional bulk unit cell, and $\boldsymbol{\rho}=(x,y)$. The matrix elements $\langle S|x|X\rangle$ can be presented in the conventional notation of the Kane parameter P

$$\langle S|x|X\rangle = \frac{P}{\hbar\omega_{fi}}$$

Previously we have calculated the energy levels and wave functions for electrons and holes confined in InAs/GaAs nano-rings of different sizes and shapes [6] and the static polarizability of these rings. Based on this calculation, we can reconstruct the polarizability tensor and using the Clausius-Mossotti relation we obtain an effective permittivity for TE-polarized light in the structure

$$\varepsilon(\omega) = \varepsilon^s \frac{1+\frac{2}{3\varepsilon_0\varepsilon^s}N\alpha_{xx}(\omega)}{1-\frac{1}{3\varepsilon_0}N\alpha_{xx}(\omega)}, \tag{2}$$

where $\varepsilon^s = (1-x)\varepsilon_{GaAs} + x$ is the effective static permittivity of the system, x is the relative volume occupied by the rings in this structure, $\varepsilon_{\mathrm{GaAs}}$ is the optical dielectric constant of GaAs, N is the density of the rings in the structure, and ε_0 is the permittivity of free space.

We use this effective permittivity of the system to obtain in turn its magnetic permeability. To describe the effective magnetic response of the structure, we follow the approach of [11] and assume that for electromagnetic fields with frequency near the absorption edge of nano-rings, a circular current flow is induced inside the rings. Following [11], we define the effective permeability of this structure in the optical range near the adsorption edge

$$\mu(\omega) = 1 - \frac{F}{1+\frac{l}{\mu_0\pi r^2\omega^2}\left[iR_{\mathrm{eff}}\omega - \frac{1}{C_{\mathrm{eff}}}\right]}, \tag{3}$$

where $F = \pi(r_{\mathrm{out}})^2/a^2$ is the geometrical filling-factor of the basic cell, r_{out} is the outer radius of the ring, R_{eff} is the resistance of the ring measured over the perimeter of a circle with radius r (see insert in Fig. 1), C_{eff} is the effective capacitance of the ring, and μ_0 is the permeability of free space. The resistance of the ring we can calculate by the following assumptions

$$R_{\mathrm{eff}} = \frac{1}{\sigma_{\mathrm{eff}}}\frac{2\pi r}{S}, \tag{4}$$

where σ_{eff} is the effective conductance of the system (note: in [11] σ refers to the resistivity, not to conductance) and S is the area of the ring cross-section. The conductance is connected to the effective permittivity (2) as follows [13]

$$\varepsilon(\omega) = \varepsilon(0) + i\frac{\sigma_{\mathrm{eff}}}{\varepsilon_0\omega}. \tag{5}$$

Combining (3)–(5) one can find the effective magnetic permeability of the structure in generic form. Detailed calculations give

$$\mu(\omega) \approx 1 - \frac{F\omega^2}{\omega^2 - \omega_0^2 + i\gamma^2}, \tag{6}$$

where ω_0 is the effective resonance frequency, which is a solution of the following equation

$$\omega^2 = \frac{2lc_0^2}{rS}\left\{\frac{[\varepsilon_r(\omega)-\varepsilon(0)]}{[\varepsilon_r(\omega)-\varepsilon(0)]^2+[\varepsilon_i(\omega)]^2} + \frac{\varepsilon_0 S}{2\pi r C_{\mathrm{eff}}}\right\}, \tag{7}$$

Table 1
Dependence of the effective resonance frequency ω_0 on the capacitance of the structure with S_{u}

C_{eff} (10^{-17} F)	30	3	0.3	0.03
ω_0 (10^{15} Hz)	1.86	1.87	1.92	3.13

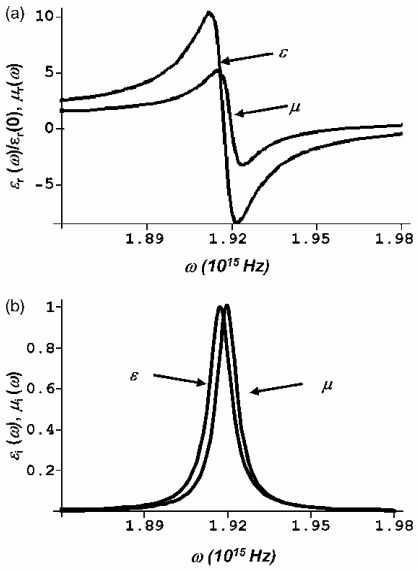

Fig. 2. Effective permittivity and permeability of the system from Fig. 1 with $S_u = \{33, 5, 10, 4.5, 1\ \text{nm}\}$ and $C_{\text{eff}} = 0.3 \times 10^{-17}$ F: (a) Real parts of $\varepsilon(\omega)$ and $\mu(\omega)$; (b) normalized imaginary parts of $\varepsilon(\omega)$ and $\mu(\omega)$.

and

$$\gamma = \sqrt{\frac{2lc_0^2}{rS}\frac{\varepsilon_i(\omega_0)}{[\varepsilon_r(\omega_0) - \varepsilon(0)]^2 + [\varepsilon_i(\omega_0)]^2}} \tag{8}$$

is the effective damping factor (c_0 is the speed of light in free space), $\varepsilon_r(\omega)$ and $\varepsilon_i(\omega)$ are correspondingly the real and imaginary parts of the effective permittivity.

We will now calculate the dispersion of $\varepsilon(\omega)$ and $\mu(\omega)$ for the structures built from the InAs/GaAs nano-rings. The nano-ring shape is generated by an ellipsoidal contour [6]: the cross-section of the ring shows an ellipse with semi-major axis r_0 and semi-minor axis z_0 (semi-height of the ring). We use the values of $\hat{\alpha}(\omega)$as calculated previously by us for the nano-rings. Then almost all parameters in (2) and (3) for a structure built from the rings can be easily computed for a certain set of parameters $S = \{a, l, r, r_0, z_0\}$. Only the capacitance of the rings remains unknown and should be taken from experiments. But, from literature [9] it is known that the capacitance of semiconductor nano-objects (quantum dots and nano-rings) is in the range from 10^{-16}–10^{-18} F. In Table 1 we present results of our calculations of ω_0 for a few possible values of the capacitance using Eq. (7) and $S_u = \{33, 5, 10, 4.5, 1\ \text{nm}\}$. Obviously the resonance frequency for the effective permeability turns out to be in the range of interest. The capacitance of the ring plays the role of a tuning parameter for the frequency.

The resulting dispersion for the effective permittivity $\varepsilon(\omega)$ and permeability μ (ω) is presented in Fig. 2. A negative permeability is possible for the system in the same region where the effective permittivity is negative. The region is rather narrow but quite visible. There is a possibility to tune the size of the region and position by varying the ring capacitance like it is shown in Table 1.

We stress that the negative permeability can be obtained only under rigid requirements. One needs to keep the deviations from the dimensions of Fig. 2 lower than about 10%. Larger deviations can crush the frequency region where the permeability is negative. But a strong dispersion (without obtaining negative values) remains for effective permittivity and permeability within a wide range of possible sets S.

In conclusion, we have demonstrated that dense nano-composite materials built from small nano-rings can exhibit simultaneously negative permittivity and permeability in the optical range. The range is wide enough to be scanned conveniently with lasers having typical spectral width of $\Delta\nu \approx 10^{13}$ Hz. The range can be tuned by changing the ring's capacity. These results could be particularly useful for design of a new class of LHCMs in the optical range.

This work was funded by the National Science Council of Taiwan under Contracts No. NSC 93-2112-M-009-008 and NSC 93-2215-E-009-006.

References

[1] V.G. Veselago, Sov. Phys. Usp. 10 (1968) 509.
[2] J.B. Pendry, Phys. Rev. Lett. 85 (2000) 3966.
[3] R.A. Shelby, D.R. Smith, S. Schulz, Science 292 (2001) 79.
[4] T.J. Yen, W.J. Padilla, N. Fang, D.C. Vier, D.R. Smith, J.B. Pendry, D.N. Basov, Z. Zhang, Science 303 (2004) 1494.
[5] J.M. Garcia, G. Mneiros-Ribeiro, K. Schimidt, T. Ngo, J.L. Feng, A. Lorke, J. Kotthaus, P.M. Petroff, Appl. Phys. Lett. 71 (1997) 2014.
[6] O. Voskobyonikov, Y. Li, H.M. Lu, C.F. Shih, C.P. Lee, Phys. Rev. B 66 (2002) 155306.
[7] O. Voskobyonikov, C.P. Lee, Physica E 20 (2004) 278.
[8] J.I. Climente, J. Planelles, J.L. Movila, Phys. Rev. 70 (2004) 081301.
[9] A. Emperador, M. Pi, M. Barraco, A. Lorke, Phys. Rev. B 62 (2000) 4573.
[10] J.I. Climente, J. Planelles, W. Jaskolski, Phys. Rev. 68 (2003) 075307.
[11] J.B. Pendry, A.J. Holden, D.J. Robbins, W.J. Stewart, IEEE Trans. Microw. Theory Tech. 47 (1999) 2075.
[12] C.M.J. Wijers, Phys. Rev. A 70 (6) (2004).
[13] L.D. Landau, E.M. Lifshitz, Electrodynamics of Continues Media, Pergamon, Oxford, 1960.

5.3 Main results and discussion

We studied theoretically the magneto-optical response functions (like polarizability and absorbance) for semiconductor quantum dots and nano-rings, when they are arranged in a square lattice. The calculations clearly show that rings are more effective to exploit the response from magnetic fields than dots. Despite a lower volume fraction ring structures have stronger variation of absorbance when the magnetic field changes than the dots. We have shown that layers of InAs/GaAs self-assembled nano-rings exhibit the optical AB effect particularly in reflectance mode. While AB effects are discussed in the literature for the cases of infrared absorption and photoluminescent emission, we can expect this behavior to be observable in ellipsometric measurements with good resolution. The calculated results suggest large polarization anisotropy for absorbance at large angles of incidence. This can be measured and should display the new optical AB effects for low temperature and moderate magnetic field regimes. Actual magnitude of the effect should be verified both by experiment and by more sophisticated calculations.

Left handed composite materials (LHCMs) exhibit simultaneously negative permittivity and permeability over a certain frequency range. It is acknowledged that LHCMs can have a variety of exciting applications. A particularly important and challenging problem in this field is the realization of LHCMs in the optical frequency range. A negative refractive index was confirmed in the GHz and THz range many years after its theoretical prediction, but most of magnetic materials at frequencies in the GHz range and above have a magnetic response which is tailing off.

In this our work we show theoretically that there is an opportunity to obtain negative permittivity and magnetic permeability simultaneously in the optical range by using nano-structured composite semiconductor materials. One of the problems arising in LHCMs for the optical range is that the size of the structural elements has to be of nanometer scale. Another problem is that the use of conductive elements is inappropriate because of the high losses. Semiconductor nano-rings are ideal building blocks and could meet the requirements mentioned. It is necessary to emphasize that structural elements possessing magnetic response, have sizes much smaller than the operating wavelength and the composite materials made from them can be characterized by effective permittivity and magnetic permeability only.

In this study we have shown that for three-dimensional photonic structures based on an artificial lattice of InAs/GaAS nano-rings the effective permittivity can be negative in the optical range. At the same time the frequency domain with the negative permittivity and magnetic permeability can be tuned by changing the individual capacity of the rings. These results could be particularly useful for design of a new class of left handed composite materials in the optical range.

6. Self-evaluation

In the project which results reported we investigated deploying of the spin-orbit interaction in conventional non-magnetic III-V semiconductor nano-structures to build elements of spintronic devices. The semiconductor approach has the advantage of being compatible with conventional semiconductor technology. It has been demonstrated theoretically that the structures can be efficiently used to polarize, inject, transport, manipulate, store, and detect electron spins. Our results suggest to exploit spin-orbit interaction in semiconductor nano-structures for spintronics needs.

#1. It has been proposed that in tunnel barrier structures the spin-orbit interaction can lead to the spin-filtering. In resonant tunnel heterostructures (due to the strict resonant tunnel conditions) the spin-filtering can gain a higher level without an additional magnetic field and can be controlled by external electric fields even in symmetrical structures. This idea attracted much interest in publications of other authors and it is an important enhancement of or previous pioneering works in a new branch of spin-dependent investigation in all semiconductor structures – spin-filtering without magnetic elements. Those results are published in the leading international journals, appreciated by the scientific society and citied.

#2. We introduced a model of the spin dependent electron scattering from an array of nano-scale all semiconductor quantum dots (antidots) - “artificial defects”. We found theoretically for the first time that the differential cross-section for InAs/GaAs antidots demonstrates a relatively large left-right asymmetry in scattering cross-section. We described theoretically the Anomalous Hall effect appeared in three-dimensional random arrays of small semiconductor quantum dots and due to spin-dependent scattering from impurities in two-dimensional channels as well. In semiconductor quantum wells the effect of the spin-orbit interaction on the processes of electron’s scattering appears to more stronger that in the bulk. This is a result of the localization of electrons' wave-functions in the conduction channel. The one-electronic-band effective Hamiltonian and spin-orbit coupling potential of the impurities allowed us to formulate and solve for the first time the 2-D spin-dependent Boltzmann equation and to calculate the spin-dependent Hall angle at zero magnetic field. We have found large spin-dependent Hall angles for AlInAs/InGaAsAs/AlInAs and CdTe/InSb/CdTe symmetrical quantum wells. This could be detected in the measurements of the Hall effect at low temperatures and this is potentially useful in integrated electron spin-polarization devices based on all-semiconductor heterostructures. It also can be used as a tool of determination of spin coupling parameters in III-V narrow gap semiconductor heterostructures. We suggest that experimental investigations should be conducted to verify our theory predictions. Several publications in leading international journals were performed based on the results. The publications are appreciated by the scientific society and citied.

.

#3. We found that a significant spin-splitting in the electron energy spectrum in semiconductor quantum dots and nano-rings at zero magnetic field and the state crossing with external magnetic. The crossing of electron energy levels with different spins leads to unusual magnetic properties of quantum dots and an additional degree of freedom for the electron spin state (qubit) manipulation in quantum dots. We calculated the magnetization and susceptibility of a cylindrical quantum dot with the parabolic confinement potential for electrons when the spin-orbit interaction is included into consideration. Application of a magnetic field along the dot axes generates a complicated structure of the electron energy levels and the theoretical analysis of the parabolic quantum dots in magnetic fields achieves a rich physics. The well pronounced spin-splitting was found by us for the parabolic confinement potential model of semiconductor quantum dots with parameters of InSb and InAs. The spin-splitting at zero magnetic field leads to a crossing of the energy levels in weak external magnetic fields (similarly to the general

Paschen-Back effect) and can provide unusual magnetic properties of the quantum dots. Results of those works are also appreciated and citied.

#4. In view of possible nano-scale semiconductor spintronic device and quantum computing implementations, we investigated in detail the quantized energy structures and magnetic properties of a new semiconductor nano-object - quantum nano-ring. We have shown that layers of InAs/GaAs self-assembled nano-rings exhibit a new types of the optical Aharonow-Bohm effect particularly in reflectance mode. While AB effects are discussed in the literature for the cases of infrared absorption and photoluminescent emission, we predicted this behavior to be observable in ellipsometric measurements with good resolution. The calculated results suggest large polarization anisotropy for absorbance at large angles of incidence. This can be measured and should display the new optical AB effects for low temperature and moderate magnetic field regimes. We have shown for the first time that for three-dimensional photonic structures based on an artificial lattice of InAs/GaAS nano-rings the effective permittivity can be negative in the optical range. At the same time the frequency domain with the negative permittivity and permeability can be tuned by changing the individual capacity of the rings. These results could be particularly useful for design of a new class of left handed composite materials in the optical range.

7. List of publications

Referred papers:

1. Edward Chen, O.Voskoboynikov, C. P. Lee, “Spin-dependent electron single and double scattering from quantum dots and antidotes”, Solid state communications, vol. 125, no. 7-8, pp. 381-385, Feb. 2003.(SCI)

2. H. C. Huang, O.Voskoboynikov, and C. P. Lee, “Spin-orbit interaction and electron elastic scattering from impurities in quantum wells”, Physical Review B, vol. 67, no.19, pp. 195337-1-8, May 2003.(SCI)

3. H. C. Huang, O.Voskoboynikov, and C. P. Lee, “Role of the spin-orbit interaction in elastic scattering of electrons in quantum wells”, Microelectronics Journal, vol. 34, no. 5-8, pp. 687-690, Aug. 2003.(SCI)

4. O.Voskoboynikov, O. Bauga, C. P. Lee, and O. Tretyak, “Magnetic properties of parabolic quantum dots in the presence of the spin-orbit interaction”, Journal of Applied Physics, vol. 94, no. 9, pp. 5891-5895, Nov. 2003.(SCI)

5. H. C. Huang, O.Voskoboynikov, and C. P. Lee, “Spin-dependent Hall effect in semiconductor quantum wells”, Journal of Applied Physics, vol. 95, no. 4, pp. 1918-1923, Feb. 2004.(SCI)

6. Leo Yu and O.Voskoboynikov, “Electron spin filtering in all-semiconductor tunneling”, Superlattices and Microstructure, vol. 34, no. 1-2 , pp. 547-552, Aug. 2004. (SCI)

7. O.Voskoboynikov, G. Dyankov, C. M. J. Wijers, “Left Handed Composite Materials in the Optical Range”, Microelectronics Journal, vol. 36, no. 1, pp. 564-566, May. 2005. (SCI).

8. O.Voskoboynikov, C. M. J. Wijers, J.J. Liu, and C.P. Lee, “Interband magneto-optical transitions in a layer of semi-conductor nano-rings”, Europhysical Letter, vol. 70, no. 5, pp. 656-662, Jun. 2005. (SCI).

9. O.Voskoboynikov, C. M. J. Wijers, J.J. Liu, and C.P. Lee, “The Magneto-Optical Response of Layers of Semiconductor Quantum Dots and Nano-Rings”, Physical Review B, vol. 71, no. 24, pp. 245332-1-12, Jun. 2005. (SCI).

10. Leo Yu and O. Voskoboynikov, “Time resolved spin-filtering in semiconductor symmetric resonant barrier structures”, Journal of Apply Physics, vol. 98, no. 2, pp. 023716-1-5, Jul. 2005. (SCI).

11. O.Voskoboynikov, C. M. J. Wijers, J.J. Liu, and C.P. Lee, “Magneto-optics of layers of semiconductor quantum dots and nano-rings”,Brazlian Physical Journal, accepted, to appear in August 2005.

12. O. Bauzha, O.Voskoboynikov, O. Tretyak, “Influence of spin-orbit interaction on magnetization of quantum dots”, accepted to appear in Bulletin of the University of Kiev. Series Physics and mathematics (2005).

13. O. Bauzha, O.Voskoboynikov, O. Tretyak, O. Synyavski, “Magnetic properties of

quantum rings with spin-orbit interaction", submitted to Ukrainian Physical Journal (2005).

Conference abstracts:

1. O.Voskoboynikov, and C. P. Lee, "Electron spin filtering in all-semiconductor tunnel structures", International conference on narrow gap semiconductors (NSG-11), Buffalo, USA, June 16-20, 2003.

2. Leo Yu, H. C. Huang and O.Voskoboynikov, "The Dresselhause and Rashba Spin-Orbit Interactions and Spin Filtering", The International Symposium on Functional Semiconductor Nanosystems (FSNS2003), Atsugi, Japan, November 12-14, 2003.

3. Leo Yu and O.Voskoboynikov "Electron spin filtering in all-semiconductor tunneling", Sixth International Conference on New Phenomena in Mesoscopic Structures and Fourth International Conference on Surfaces and Interfaces of Mesoscopic Devices, Maui, Hawaii, U.S.A., November 30-December 5, 2003.

4. H. C. Huang and O.Voskoboynikov, "Spin-dependent Hall effect in semiconductor quantum well and two-dimensional electron polirazer", Sixth International Conference on New Phenomena in Mesoscopic Structures and Fourth International Conference on Surfaces and Interfaces of Mesoscopic Devices, Maui, Hawaii, U.S.A., November 30-December 5, 2003.

5. O.Voskoboynikov, C.M.J. Wijers, J.L. Liu, and C. P. Lee, "Magneto-optical response by a layer of semiconductor nano-rings", Proceedings of the 20th General Conference of the Condensed Matter Division of the European Physical Society, Prague (The Czech Republic), July 19-23, 2004.

6. O. Voskoboynikov, G. Dykonov, C. M. J. Wijers, "Left handed composite materials in optical range", Book of Abstracts, The Fifth International Conference on Low Dimensional Structures and Devices, Cancun (Mexico), December 12-17,2004.

7. O. Bauzha, O.Voskoboynikov, O. Tretyak, C. P. Lee, "Spin orbit interaction impact on magnetization of quantum dots" II Ukranian Scientific Conference on Semiconductor Physics, Chernovtsy (Ukraine), September 20-24, 2004.

8. List of thesis's of graduated students

1. Hua-Chiang Huang, "Electron Spin-Dependent Transport in Semiconductor Heterostructures", M.S. thesis, NCTU, Hsinchu, May 2003.

2. Leo Yu, "Electron Spin Filtering in All-Semiconductor Tunneling Structures", M.S. thesis, NCTU, Hsinchu, June 2004.

3. Chi-Huei Chen, "Spin Orbit Splitting of Energy Levels in Semiconductor Asymmetric Double Well Structure", M.S. thesis, NCTU, Hsinchu, June 2005.